MAX-PLANCK-INSTITUT FÜR QUANTENOPTIK

Single photons from a single atom trapped in a high-finesse optical cavity

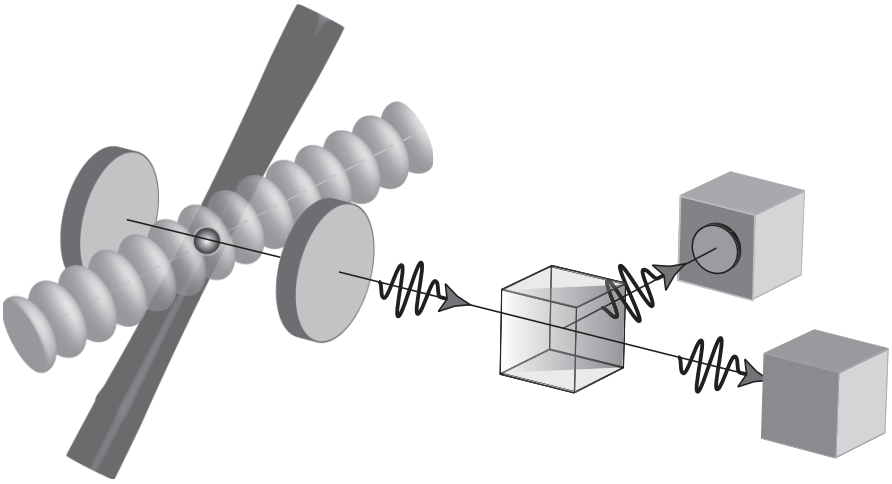

Markus Hijlkema

MPQ 312 Juli 2007

Zusammenfassung

Eines der interessantesten skalierbaren Systeme für die deterministische Verarbeitung von Quanteninformation sieht ein Netzwerk von in Resonatoren gespeicherten Atomen vor, wobei die Informationsübertragung über einzelne Photonen stattfinden soll. Neutrale Atome bieten folgende Vorteile: Zum einen haben Atome eine diskrete Niveaustruktur, in der Quantenbits gut implementiert werden können. Zum anderen ist ein neutrales Atom, im Hochvakuum in einer optischen Dipolfalle gespeichert, gut von seiner Umgebung abgeschirmt, so daß die Dekohärenz minimal ist. Die Speicherzeit eines Atoms im Resonator war bisher aber immer der limitierende Faktor und stand der Anwendung des Systems für viele Experimente im Weg.

In dieser Doktorarbeit wird ein Experiment vorgestellt, in dem ein einzelnes Atom bis zu einer Minute in der Mode eines Resonators gespeichert werden kann,und dazu verwendet wird, kontrolliert einzelne Photonen zu erzeugen. Mit Hilfe von Resonator-Kühlkräften konnten sehr lange Wechselwirkungszeiten zwischen Atom und Resonator erreicht und dabei lange Einzel-Photonen-Ströme von ein und demselben Atom emittiert werden [1]. Zum ersten Mal konnte die Quantisierung des electromagnetischen Feldes im abgestrahlten Licht von einem einzelnen Atom nachgewiesen werden, ohne über viele Einzel-Atom-Ereignisse zu mitteln. Wie in vorangegangenen Experimenten gezeigt wurde, besitzen die auf diese Weise erzeugten Photonen Eigenschaften, die für die Verarbeitung von Quanteninformation notwendig sind. Die Apparatur, wie sie in Abbildung 1 dargestellt ist, eignet sich deshalb als Einzel-Photonen-Server für Quanteninformationsexperimente basierend auf einzelnen Photonen und linearer Optik.

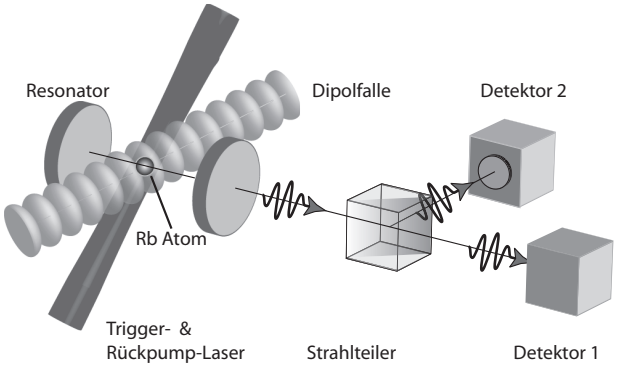

Abbildung 1 Schematische Darstellung des Experiments. Ein einzelnes Atom gespeichert in einem Resonator wird von Laserpulsen zur Emmision von einzelne Photonen angeregt.

Initialisiert wird das System durch das Laden von ^{85}Rb Atomen in eine magneto-optische Falle. Anschließend werden die auf tiefste Temperaturen abgekühlten Atome mit Hilfe einer von einem Laserstrahl realisierten optischen Dipolfalle in den Resonator befördert. Dort wird die Geometrie dieser Lichtfalle geändert und die Atome werden in einer tiefen Lichtfalle mit Stehwellengeometrie gespeichert. Die Atome werden von einem Pumplaser

angeregt, der senkrecht zur Resonatorachse und unter einem Winkel von 45° bezüglich die Lichtfalle eingestrahlt wird. Um den vom Pumplaser erzeugten Strahlungsdruck auszugleichen wird der Pumpstrahl zurückreflektiert, wobei die Polarisation des reflektierten Lichtes um 90° gedreht wird, um eine Stehwellenstruktur zu vermeiden. Wie in diesem Experiment gezeigt wurde, führt diese Anordnung von Resonator und Laserstrahlen zu Kühlkraften, die genutzt werden können um die durchschnittliche Wechselwirkungzeit eines einzelnes Atoms mit dem Resonator auf mehr als 10 s zu erhöhen [1].

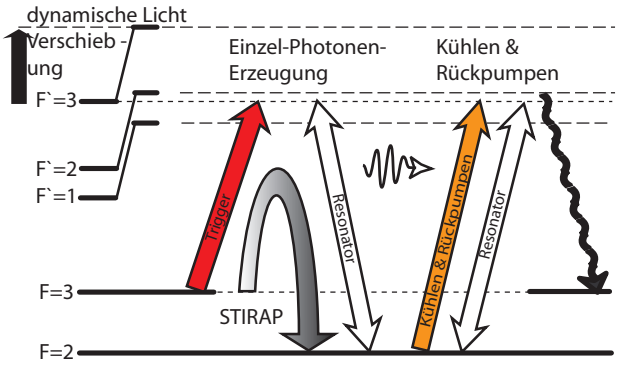

Abbildung 2 Das Erzeugungsschema für einzelne Photonen.

Um kontrolliert einzelne Photonen zu erzeugen, wird ein präpariertes Atom mit einer Sequenz von Laserpulsen angestrahlt. Ein schematischer Ablauf ist in Abbildung 2 dargestellt. Zunächst befindet sich das Atom im $|5S_{1/2}$ F=3$\rangle$ Zustand. In einem sogenannten Vakuumstimulierten adiabatischen Raman Übergang wird jetzt durch Einstrahlen eines mit dem Übergang $|5S_{1/2}F = 3\rangle \rightarrow |5P_{3/2}F' = 3\rangle$ resonanten Triggerpulses das Atom in den $|5S_{1/2}F = 2\rangle$ Zustand transferiert. Gleichzeitig wird in diesem Prozess ein einzelnes Photon in den mit dem Übergang $|5S_{1/2}F = 2\rangle \rightarrow |5P_{3/2}F' = 3\rangle$ resonanten Resonator emittiert. Danach muss das System wieder in den Ausgangszustand gebracht werden, was mit einem mit dem Resonator resonanten Rückpumppuls und anschließenden spontanen Zerfall erreicht wird. Gleichzeitig wird das Atom während des Rückpumppulses durch einen dem Sisyphus-kühlen ähnlichen Mechanismus gekühlt [1]. Bis zu 30 s lang konnte ein einzelnes Atom auf diese Weise zur Emission einzelner Photonen initiiert werden, und das bei einer Sequenz-Wiederholungsrate von 100 kHz. Die Wahrscheinlichkeit, ein einzelnes Photon in einem Puls zu erzeugen, lag bei 9%; Es konnten also bis zu 3×10^5 Photonen vom selben Atom erzeugt werden.

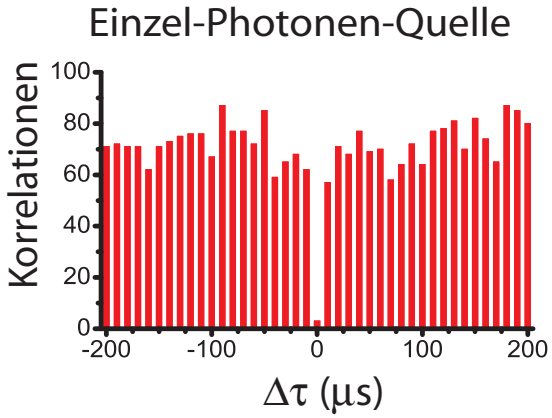

Abbildung 3 Korrelationen zwischen Detektor-Ereignisse als Funktion der zeitliche Abstand dieser Detektionen, für das aus dem Resonator emittierte Licht. Das einzelne Atom war über 28s gespeichert. Das Fehlen von koinzidenten Korrelationen ($\Delta\tau = 0$) beweist, dass einzelne Photonen produziert wurden.

Abbildung 3 zeigt die Anzahl von Korrelationen zwischen Photon-Detektionen der beiden Detektoren als Funktion der zeitliche Abstand dieser Detektionen. Die Figur ist das Ergebnis für den Photonenfluss erzeugt mit einem über 28 s im Resonator gespeicherten Atom. Wird während des Triggerpulses nur jeweils ein einzelnes Photon in den Resonator emittiert, so sollte es keine koinzidenten Detektionen von den Photodioden geben. Wie man in Abbildung 3 ablesen kann, fehlen diese Korrelationen für $\Delta\tau = 0$. Die im Vergleich zu den zeitverschobenen Korrelationen niedrige Anzahl von restlichen koinzidenten Korrelationen werden vom Detektorrauschen und von Streulicht verursacht. Nach 1.5 s Photonenerzeugung ist die Statistik ausreichend, um eindeutig zwischen ein oder zwei Atomen im Resonator zu unterscheiden. Hat man auf diese Weise festgestellt, dass einzelne Photonen produziert werden, können die nachfolgenden Photonen einem Anwender zur Verfügung gestellt werden. Die Präsenz des Atoms kann über das während des Rückpumppulses emittierten Lichtes überwacht werden. Der Verlust eines Atoms kann so mit 98% Wahrscheinlichkeit innerhalb von 30 ms festgestellt werden, wonach ein neues Atom nachgeladen werden kann. Auf diese Weise ist es möglich, einen effizienten Photonenserver bereit zu stellen.

[1] S. Nußmann, K. Murr, M. Hijlkema, B. Weber, A. Kuhn and G. Rempe. Vacuum-stimulated cooling of single atoms in three dimensions. *Nature Physics* **1**, 122–125 (2005).

[2] M. Hijlkema, B. Weber, H.P. Specht, S.C. Webster, A. Kuhn, G. Rempe. A Single-Photon Server with Just One Atom. *Nature Physics*. **3**, 253-255 (2007).

Abstract

One of the most promising platforms for scalable deterministic quantum information processing is formed by a network of single atoms in cavities interconnected via photon exchange. Using neutral atoms has several advantages: First, the advantage of a two-level system to encode the quantum information in. Second, as the neutral atom is trapped in a laser beam in vacuum, it is relatively immune to pertubations originating from the environment. A limitation, however, has always been the time a single atom can be observed. Using state of the art trapping techniques and devising new cavity cooling schemes [1], the time during which a single neutral atom can be trapped in the cavity has been extended up to a minute.

In this thesis an experiment is presented in which a single neutral atom trapped in a cavity is used to generate single photons in a controlled way [2]. For the first time, the quantized nature of the electromagnetic field could be observed directly in the light emitted by a single neutral atom, without any averaging over multiple single-atom measurements. It has been shown that photons produced with an atom-cavity system are of such a quality that they could be used for quantum information processing. The setup, shown in figure 1, could therefore operate as a single-photon server for such experiments, by distributing a stream of single photons to an independent user.

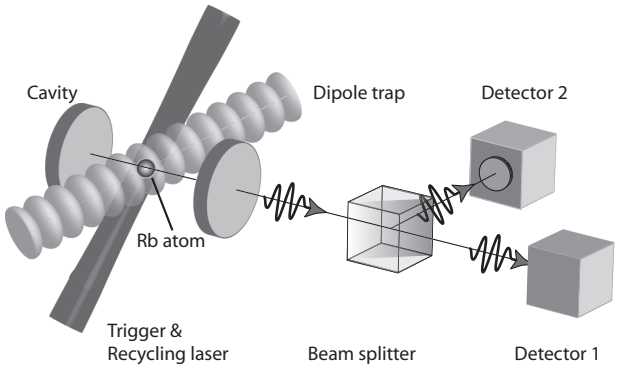

Fig.1 A schematic of the experiment is depicted. A single atom trapped inside a cavity is excited by laser pulses, as a result, single photons are emitted.

The system is prepared by loading ^{85}Rb atoms into a magneto-optical trap. From here, the atoms are transported by a dipole trap into a high-finesse optical cavity. There, the atoms are trapped in a standing wave dipole trap. A pump laser is aligned perpendicular to the cavity axis and under 45° to the dipole trap, it is retroreflected to balance the radiation pressure and the polarization of the reflected beam is rotated by 90° to avoid a standing-wave geometry. With this configuration of lasers and cavity it is possible to store the atom in the cavity for several 10 seconds, making use of cavity cooling forces [1].

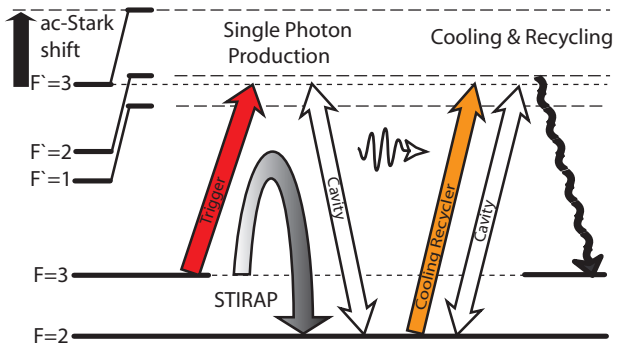

Fig.2 The single-photon production scheme.

After an initial cavity cooling phase, where the pump beam is on continously, pulsed single-photon generation is started. As one can see in figure 2, the atom, initially in the $|5S_{1/2}F = 3\rangle$ state undergoes a vacuum-stimulated Raman adiabatic passage into the $|5S_{1/2}F = 2\rangle$ state by exciting with a trigger laser pulse resonant with the $|5S_{1/2}$ $F = 3\rangle \rightarrow |5P_{3/2}F' = 3\rangle$ transition. In this process, a single photon is emitted into the cavity, which is resonant with the $|5S_{1/2}\ F = 2\rangle \rightarrow |5P_{3/2}F' = 3\rangle$ transition. To recycle the atom back to the $|5S_{1/2}F = 3\rangle$ state, the atom is subsequently excited by a laser pulse resonant with the $|5S_{1/2}F = 2\rangle \rightarrow |5P_{3/2}F' = 3\rangle$ transition, a process which at the same time cools the atom by a Sisyphus-like cooling mechanism [1]. The atom is subject to a stream of trigger and recycle pulses, with a repetition rate of 100 kHz. Single photons from one-and the same atom have been generated for more than 30 s, with the probability of 9% that a single photon is emitted from the cavity during a trigger pulse, this amounts to 3×10^5 single photons from the same atom. In figure 3 the number of correlations between photon clicks by both detectors versus the time interval between these events is plotted for the cavity output during trigger pulses. The graph shows this data for an atom that was available for 28 s of single-photon production.

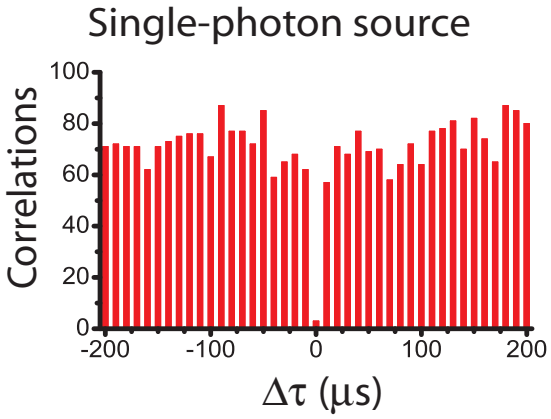

Fig.3 The graph shows the number correlations between photon clicks of both detectors as a function of the time interval between these events. The data shown are the correlations found in the light emitted during 28 s by just one atom. The absence of correlations at $\Delta\tau$=0 indicates that our source produces single photons.

For single photons no equal-time ($\Delta\tau = 0$) coincidences are expected, and one does indeed see an almost complete absence of correlations. The remaining correlations can be explained from the background count rate. 1.5 s of photon production is enough to unambiguously determine that a single atom is emitting single photons, by calculating the photon statistics. The photons that are produced following such a test can then be distributed to a user. In the mean time the cavity output can be monitored during the recycling pulses for the presence of the atom. The loss of an atom can be detected within 30 ms with 98% probability, and the atom loading sequence can be started again. In this way a high duty cycle of photon production should be possible, and the user can be notified when the photon server is online. Single-photon production with a neutral atom in a cavity has therefore progressed from a proof-of-principle experiment to a useful device whose performance is specified during operation.

[1] S. Nußmann, K. Murr, M. Hijlkema, B. Weber, A. Kuhn and G. Rempe. Vacuum-stimulated cooling of single atoms in three dimensions. *Nature Physics* **1**, 122–125 (2005).

[2] M. Hijlkema, B. Weber, H.P. Specht, S.C. Webster, A. Kuhn, G. Rempe. *et al.* A Single-Photon Server with Just One Atom. *Nature Physics*. **3**, 253-255 (2007).

Contents

Chapter 1

Introduction

A neutral atom, which is placed between two mirrors. As simple as it may sound, the study of this system has involved many scientists over many decades. From the first nuclear magnetic resonance experiments to the technology driven quest for the quantum computer, the atom-cavity system has provided insight into the strangeness of the quantum world.

Nowadays a classic problem in textbooks on quantum mechanics, the interaction of an atom with the electromagnetic field is described quantum-mechanically using two discrete atomic energy levels. The presence of a resonant external electromagnetic field couples both levels so that the atom can cycle back and forth between the ground state and the excited state by the processes of stimulated emission and absorption. An atom in the excited state will eventually fall back to the ground state, even without an external field present. This so called spontaneous emission was described phenomenologically by Albert **?**. He described this process as the emission of a photon, the elementary particle of the electromagnetic field, in an arbitrary direction. He used a statistical argument to connect the rate for spontaneous emission to those for absorption and stimulated emission. A quantum-mechanical description of the electromagnetic field was then developed by others which allowed for a fully quantum-mechanical description of the interaction of a two-level atom with the radiation field. In this framework of quantum electrodynamics spontaneous emission could be understood as stimulated emission induced by vacuum fluctuations of the electromagnetic field. Some time later it was realized that the rate of spontaneous emission is not a fixed property of the atom, but can instead be influenced by changing the density of electromagnetic modes surrounding the atom. This effect was first described by **?** in the context of nuclear magnetic resonances, where he proposed to couple a system of nuclear spins to a resonant electrical circuit to increase the rate of spontaneous emission. **?** were the first to predict that the use of a resonant microwave cavity could enhance the rate of spontaneous emission. In the same year the maser was invented by **?**, which consisted of a beam of ammonia molecules sent through such a cavity. The theory of an atom coupled to a single quantized mode of the electromagnetic field was described by **?**. Not only the Purcell effect was described, it was also recognized that if the coupling of an atom to a cavity is stronger than the coupling of the atom and the mode to the environment, a

photon emitted into the cavity by the atom remains in the cavity long enough to re-excite the atom again. This regime is referred to as strong coupling. Experimental observations based on these theoretical predictions have been plenty and the reader is referred to the review articles of **?** and **?** for an overview of the field of *cavity quantum electrodynamics*.

In 1995 a paper was published by **?** that proposed to use a string of trapped ions to implement a quantum gate. Such a gate would form a building block for a future quantum computer, where the use of superposition states for computation promises a large gain in computational power for certain tasks compared to a classical computer, see **?** for an overview of the requirements. The proposal was met with great enthusiasm by the physics community and since then similar proposals have emerged based on the controlled coupling of a single atom with a high-finesse cavity. [**??**] Other schemes were proposed that were based on the usage of single photons. Here the quantum bit can be implemented in the polarization degrees of freedom of the photon. In this way single photons are ideal carriers of quantum information. Using linear optical elements, i.e. beam splitters and wave plates, it should be possible to implement all the logic operations necessary for quantum computation, see for instance **?**. Single photons can be generated using a single quantum emitter, for instance a neutral atom. Because this emission can be directed if one places the quantum emitter in a cavity, one successful application of the atom-cavity system for quantum information purposes has been its operation as a single-photon generator. Experiments with neutral atoms and cavities on this subject in the Rempe group [**???**] were successful but the number of single photons from the same atom was severely limited by the fact that the atom was not trapped in the cavity, but instead moved through the cavity mode due to the gravitational field. The various approaches of other groups to atom trapping have resulted in larger atom-cavity interaction times and longer single-photon streams. **?** have made use of an optical dipole trap along the cavity axis, **?** used an ion in an electric trap and **?** used an optical dipole trap but used a lens with a high numerical aperture instead of a cavity.

In this thesis an experiment is presented that consists of a single Rubidium atom trapped in the mode of a high-finesse optical cavity by a transverse optical dipole trap, in order to increase the atom-cavity interaction time. This has led to a big increase in the number of photons that can be generated from the same atom. As was first predicted by **?**, forces mediated by the cavity itself can be used to cool the motion of the atom in the trap. These forces were observed and used successfully to increase the interaction time of a single atom with the cavity mode.[**??**] In addition, the use of a standing wave geometry for the dipole trap allowed for the control of the atom-cavity coupling strength. [**?**] Based on the experience of prior experiments performed in the Rempe group on single-photon production, generation of single photons was then implemented for a trapped atom. [**?**]

The manifestation of antibunching of photoelectric detector clicks when probing a light source is only understandable under the assumption of a quantized electromagnetic field. Observations of photon antibunching were first reported by **?**, in resonance fluorescence experiments using a thermal beam of sodium atoms. Since then, similar experiments have been performed with many different improved experimental systems. With the advances in laser cooling techniques and the construction of high-finesse optical cavities, the brightness

of atom sources, the single atom observation time and the collection efficiency of the emitted photons has been increased. At the same time, one still has had to combine the signal of many experimental runs or many atoms in order to observe an antibunching in the detected photon arrival times. **?** observed antibunching in the fluorescence of a single ion trapped in a cavity, but to our knowledge, the antibunching in the photon signal generated by one and the same neutral atom trapped in the cavity presented in this thesis is the first observation of antibunching without combining the respective signal of many single neutral atoms. In this sense this thesis reports on the first experiment in quantum optics based on a single neutral atom. The high visibility of the antibunching in combination with the large signal from the same atom permits the reversal of the argument: Because one sees antibunching, only a single atom is trapped. This turns out to be useful if one wants to distribute the generated single photons to an independent user.

The thesis is structured in the following way:

Chapter 2: Here the experimental apparatus is presented.

Chapter 3: Results are presented on cavity cooling experiments. It will be shown that the configuration of trapping and cooling lasers in combination with the cavity enables the trapping of a single atom inside the cavity for more than 60s, and that the cavity cooling forces can be used with the cavity resonant to different transitions.

Chapter 4: It will be shown that after the preparation of single atoms in the cavity by cavity-mediated cooling, these atoms can be moved in and out of the cavity with a high repeatability. This allows for a precise adjustment of the coupling of a single atom to a cavity.

Chapter 5: Results will be presented on the generation of single photons by applying laser pulses to a single atom trapped in the cavity. The atom is cooled in the process, leading to a stream of single photons large enough to be distributed. The atom-cavity system can therefore operate as a single-photon server.

Chapter 6: An outlook on ongoing and future experiments with the experimental setup is presented.

Chapter 2

The Experimental Setup

In 2001, construction of the experimental setup described in this chapter was started. Being the third cavity-based setup in the group of professor Rempe at the Max-Planck-Institut für Quantenoptik, the design goals were to increase the atom-cavity interaction time compared to the older experiments, gain more control over the atom-cavity coupling and make use of the latest technology and know-how to create a stable and robust machine. In the next sections, the various parts of the setup are introduced and described. Apart from short data-taking intervals, building and expanding the apparatus has been an ongoing effort, already consuming more than 16 man-years to be able to do the measurements in this thesis. It is thus beyond the scope of this thesis to describe all the details of the experiment. Instead, the description aims to provide a basis for understanding the experiments in the next chapters. For more details, the reader is referred to the PhD-thesis of Stefan **?**.

2.1 Concept

After the first optical cavity experiments that coupled atoms from a thermal beam to the resonator, various groups started employing magneto-optical traps to prepare ultracold atoms, thereby increasing the interaction times of the atoms with the cavity. Twenty years after the first realization of such a magneto-optical trap (MOT) by **?**, and ten years after the Nobel prize was awarded to Steve Chu, Claude Cohen-Tannoudji and William D. Phillips, three pioneers in the field of laser cooling of atoms, the MOT has become a widely used workhorse in the quantum optics community. Because cavities designed for strong coupling inherently have a small mode volume, and thus a limited optical acces from the side, it has so far not been possible to create a MOT that overlaps with the mode of such a cavity. Instead a MOT is created in the vicinity of the cavity and the atoms are transported from there into the cavity. Older experiments either drop the atoms from above the cavity, which is situated below the MOT, see for instance **?**, or alternatively launch the atoms from a MOT below the cavity in a *moving molasses*, with the cavity at

the turning point (see for instance **?**). The atoms can also be guided and trapped in an optical dipole force trap, which is the method applied here. With such a trap, especially in a standing wave geometry, the position of the atom can be controlled with great accuracy, as was impressively demonstrated by **?**. The challenge here is to combine such a trap with the cavity, which has only limited optical access.

In figure 2.1 the main ingredients of the setup are depicted in a schematic way. First, neutral ^{85}Rb atoms are loaded into a MOT, where they are cooled down to temperatures below 100 μK. Second, the atoms are transferred into a running wave optical dipole force trap. This trap is formed by a laser beam, its focus is located between the MOT-region and the cavity. These are located 14 mm apart. As this laser is far detuned from the atomic resonance, the trap potential is approximately conservative, with its potential minimum in the focus of the laser beam. The atoms therefore start to oscillate in the trap. With appropriate timing, the atoms can be loaded into another dipole trap as soon as they arrive in the cavity. The latter trap is formed by a tightly focussed laser beam, which, in addition, is retroreflected to create a standing wave pattern. Atoms can be stored in each of the antinodes. As a fourth step, the atoms can be detected by observing the output of the cavity while the atom is excited by a laser which is arranged perpendicular to the cavity axis and under an angle of 45° to the dipole trap axis. In order to balance any possible radiation pressure felt by the atom from the laser beam, it is also retroreflected. The two mirrors of the cavity have different transmission coefficients, one is fifty times more transmissive than the other. Most of the generated photons therefore leave the cavity through this mirror. These photons can then be detected by avalanche photodiodes with single-photon counting capabilities.

2.2 Design of the apparatus

In order to create a MOT, several dipole traps and a cavity system that can be actively stabilized and addressed, more than 10 separate laser beams have to be prepared and subsequently brought into the vacuum chamber where the atoms will be trapped in the MOT and transported into the cavity. All of these beams have to be precisely tuned in shape, frequency and intensity and need to be switched on and off with microsecond time resolution. The optics needed to enable this fill an entire 4.80×1.50 m optical table, and it is convenient to place the cavity in a vacuum chamber as small as possible so that it can directly be placed on the optical table. The vacuum chamber is depicted in figure 2.2, the octagonal shape provides a good optical acces from all directions. The large top and bottom viewport are constructed in such a way that the distance between the top viewport and the cavity is only 22 mm, which becomes important if one wants to image the atoms that are trapped in the cavity with a CCD camera. The beam paths of the various laser beams are indicated. The MOT is loaded with atoms from a rubidium dispenser. This is a metal filament which contains a rubidium-chromate, which sets free atomic rubidium in a redux reaction if the filament is heated by applying a current through it. By directly loading atoms from this dispenser, the background pressure of the vacuum chamber can be kept at $2 \cdot 10^{-11}$ mbar, compared to a background pressure of 10^{-9} mbar if the MOT were

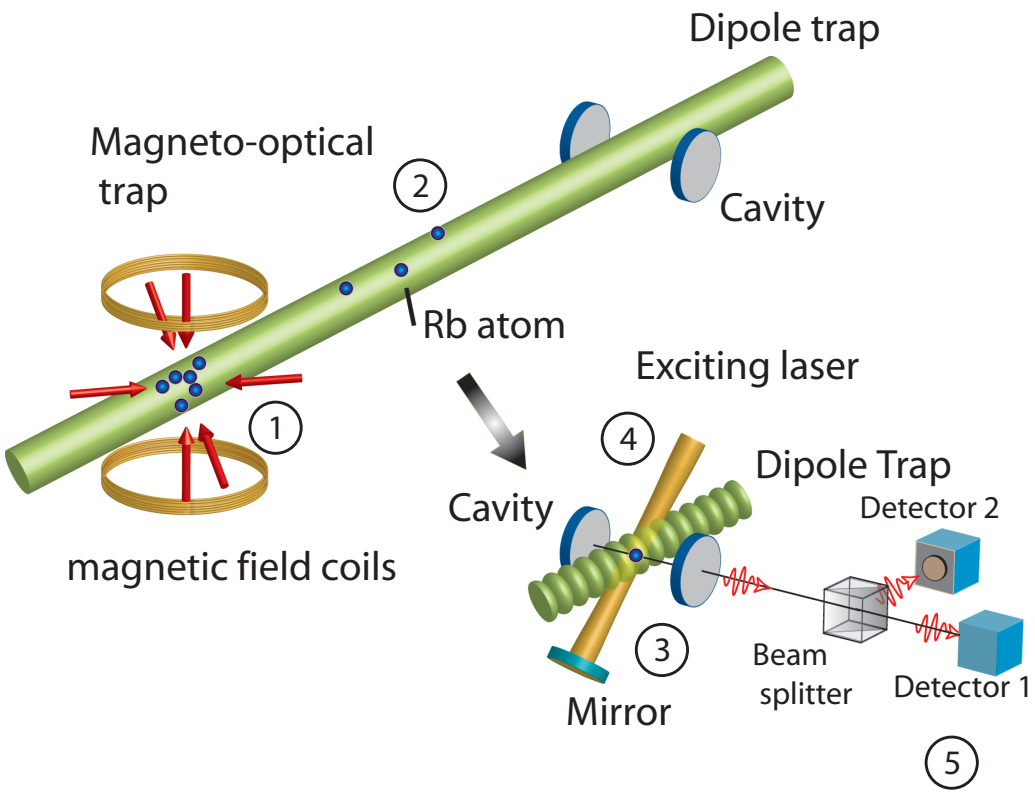

Figure 2.1: **Schematic overview** *of the experimental setup.* **1.** *A combination of six laser beams and two magnetic field coils in an anti-Helmholtz configuration form a magneto-optical trap (MOT) where* ^{85}Rb *atoms can be trapped and cooled down to temperatures of several* $10\,\mu K$. **2.** *These atoms are then loaded into an optical dipole force potential generated by a red-detuned laser beam focussed between MOT and cavity. The atoms start to oscillate in the trap.* **3.** *As soon as the atoms reach the cavity, the dipole trap geometry is changed to a standing wave trapping potential with the focus in the cavity. One of the mirrors has a higher transmission and acts as an output mirror.* **4.** *In order to observe the atoms in the cavity the atoms are excited by a laser beam aligned under an angle of* $45°$ *to the dipole trap and perpendicular to the cavity axis.* **5.** *To observe the photon signal leaking out of the cavity, a set of two avalanche photodetectors is used in combination with a non-polarizing beamsplitter that randomly directs the photons onto one of the detectors.*

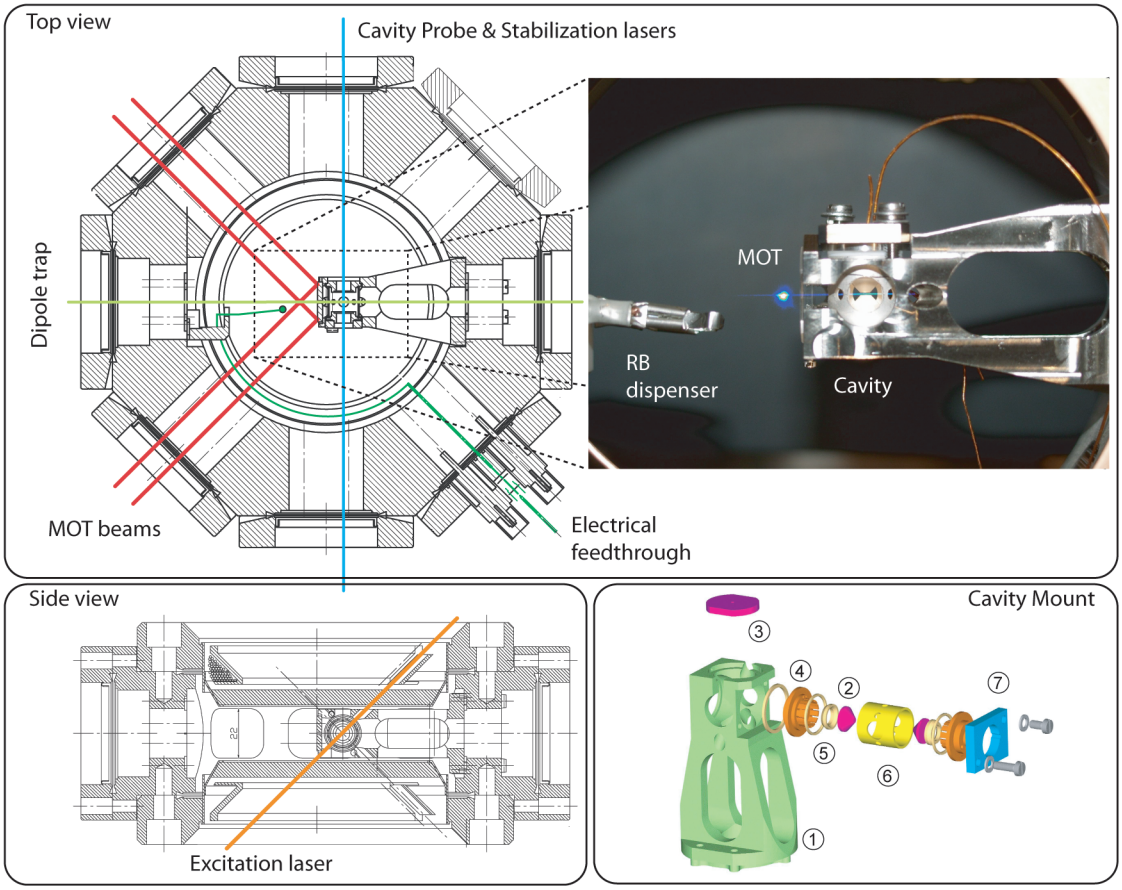

Figure 2.2: **The Vacuum Chamber. Top view:** *A CAD-drawing of the octagon-shaped vacuum chamber with the cavity mount and a photograph taken through the top viewport are depicted. Indicated are the MOT-laser beams(red laser beams), the cavity probe & stabilization lasers (blue laser beams), the dipole trap (green laser beams), and the electrical wiring to heat the rubidium dispenser (darkgreen).* **Top view of the cavity:** *An absorption image of the MOT and dipole trap is overlapped with a photograph of the actual setup. In the middle the two coned mirror substrates are visible.* **Side view of the cavity:** *The optical path of the excitation laser is plotted in orange.* **Exploded view of the cavity mount:** 1 *The cavity mount.* 2 *The cavity mirrors.* 3 *The MOT mirror* 4 *The glueless mirror holder.* 5 *Spacer rings.* 6 *The piezo-ceramic spacer with which the length of the cavity can be tuned.*

loaded from the background gas. A lower background pressure means that the collisions of cold atoms with the thermal background gas occur less frequently, and thus the lifetime of the atoms in the trap is expected to be several minutes, if there are no other loss mechanisms. A drawback of a direct loading from the dispenser by applying a pulsed current through the filament is that it does not work well if the trapping times become too long. The current is used to heat the rubidiumchromate, but this becomes impractical,

because the system takes a long time to reach a regime where the number of atoms in the MOT is constant from shot to shot. This repeatability is vital for parameter scans, and therefore a different scheme to load the MOT was implemented. Using a technique called *light induced atom desorption*[?], rubidium atoms adsorbed by the walls of the vacuum chamber can be quickly desorbed by illumination of the walls by ultraviolet light from a light-emitting diode. In this way, the loading rate of the MOT becomes independent of the time interval since the last MOT was created. This method was first implemented in experiments resulting in the data found in section 5.4.

The cavity mount protrudes into the vacuum chamber. A mirror is mounted on its end, which is used to create a MOT in the vicinity of the cavity. Through a $1 \times 1\,\mathrm{mm}^2$ hole in the mirror the atoms can be transported over a distance of 14 mm into the cavity. The cavity mirrors are spaced by a piezo-ceramic tube, as can be seen from the *exploded view* schematic of the cavity mount in figure 2.2. By applying a voltage to the piezoceramic, its length can be tuned, and thus the resonance frequency of the cavity.

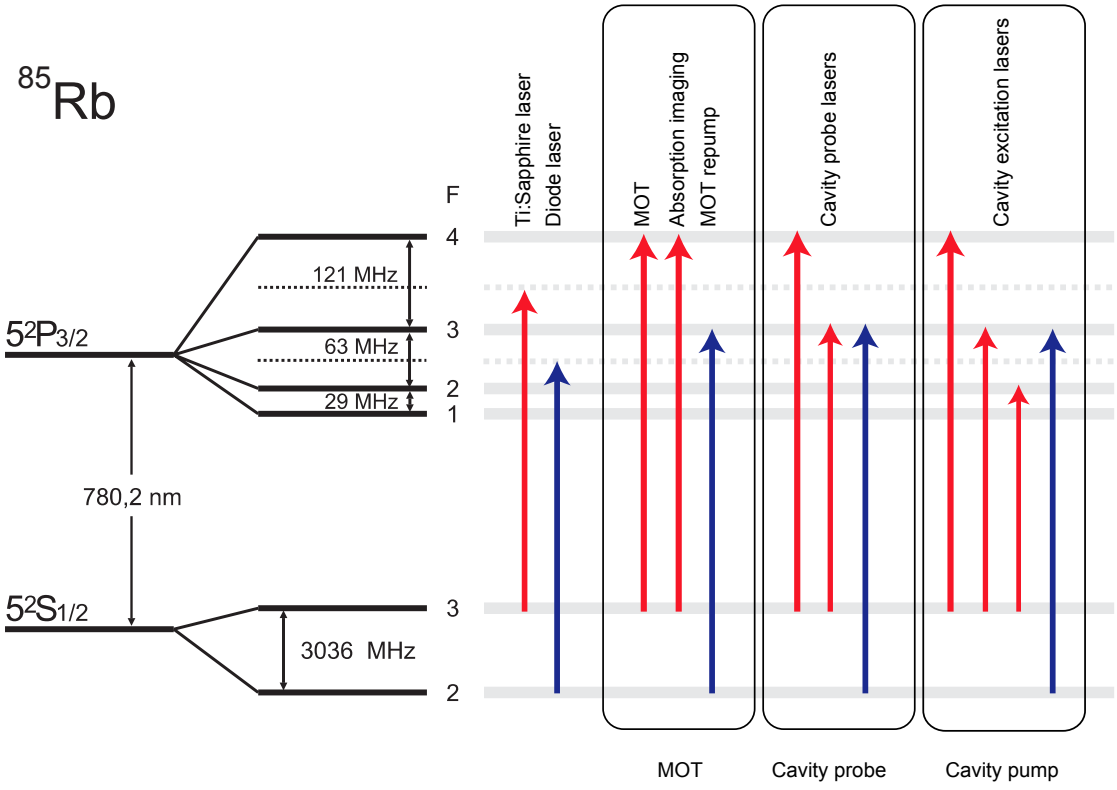

Figure 2.3: *All the resonant laser beams are derived from a Ti:sapphire laser and a diode laser system by shifting the frequencies by an AOM. There are three main applications:* 1 *the MOT.* 2 *The cavity probe lasers.* 3 *The cavity excitation lasers.*

2.3 The laser system

To address the relevant transitions of the rubidium atom, which in this case all belong to the D_2-line ($5^2S_{1/2} \rightarrow 5^2P_{3/2}$), several laser beams are derived from two laser systems. The first system, a *Coherent MBR110* titanium-sapphire laser pumped by a *Coherent VERDI V-10*, a frequency doubled Nd:YAG laser at 532 nm, delivers 800 mW of optical power. It is stabilized on the cross-over line $|F = 3\rangle \rightarrow |F' = 3-4\rangle$, which is the strongest line in a Doppler-free saturation spectroscopy on a rubidium vapor cell. This laser light is then used to derive 7 independent laser beams driving three different transitions by use of *acousto-optic modulators* (AOM) to shift the frequency of the respective beams into resonance with the target transition. In figure 2.3 the energy level diagram of ^{85}Rb is depicted with the transitions that can be driven with the laser beams.

The second system, a *Toptica DL100* diode laser system with 30 mW of optical power is stabilized on the $|F = 2\rangle \rightarrow |F' = 2-3\rangle$ cross-over line and is used to address the $|F = 2\rangle \rightarrow |F' = 3\rangle$ transition. From it derive three laser beams. The laser beams can be divided into three groups based on their function, namely the MOT, cavity probe, and cavity excitation lasers. The linewidth of the Ti:sapphire laser is 30 kHz, the linewidth of the diode laser 300 kHz, which both are small compared to the 6 MHz linewidth of the rubidium D_2 line.

2.4 The magneto-optical trap

Every time an atom absorbs a photon, the atom acquires $\hbar\vec{k}$ momentum. The atom decays, the photon is emitted and momentum is transferred back to a photon. Because spontaneous emission has no preferred direction, the momentum kicks to the atom upon emission will average out when this process is repeated many times. The momentum kick upon absorption will not, and thus the atom will feel a net force. If one now illuminates the atom from all directions with light slightly detuned below the atomic transition frequency (i.e. red detuned), the atom can be cooled due to the Doppler shift. The atom will be more resonant with counter-propagating photons than with co-propagating photons, so that the atom experiences a nett force in the opposite direction. The atomic position will undergo a random walk but if one now applies an external position-dependent quadrupole magnetic field in combination with circular-polarised light, a stable trap can be generated. The magnetic field creates a position-dependent Zeeman-shift of the atomic transition. The sign of this shift depends on the Zeeman state the atom occupies. An atom is more resonant with the laserlight whose direction pushes the atom to the zero magnetic field position, if the polarization of the laser beams is chosen suitably. The center of the trap is situated at the position with zero magnetic field.. The MOT beams have a diameter of 7 mm, and in total 9 mW of laser light is used. In the MOT created in the present apparatus, up to 10^7 atoms can be trapped with temperatures ranging between $60 - 100\,\mu$K, depending on the number of particles. The temperature was determined by taking absorption images of

an expanding cloud in order to determine the temperature and observing the fluorescence of the MOT to determine the number of atoms.

2.5 The optical dipole trap configuration

In an electric field E, a particle with polarisability α has a dipole moment $\alpha \cdot E$ and a potential energy $-\alpha \cdot E^2$. If the field is position-dependent, the particle experiences a force, which, in the case of $\alpha > 0$, attracts the particle to the position with the highest E field. Such a dipole force can also be applied to a particle by laser light. In the optical domain, the frequency of the electromagnetic radiation is on the order of several hundred THz. The particle cannot follow this extremely fast oscillation, instead, it will 'see' the average intensity of the electric field component of the light. The polarisability of an atom in the ground state is positive if the laser frequency is red detuned from the atomic transition. As was originally proposed by **?**, it is thus possible to trap atoms in a focussed red detuned laser beam. The dipole potential that can be generated with laser light is rather small, the temperature of the atom cannot be larger than a few mK, otherwise it escapes from the trap. Only with the advance of laser cooling of atoms has it become possible to trap them using the optical dipole force. In a quantum-mechanical description, the effect of such a trapping laser on the atomic levels can be treated as a pertubation of second order in the electric field, i.e. linear in the field intensity I. Applying second-order time-independent pertubation theory for non-degenerate states, the atom-field interaction will shift the energy of the atomic levels by Δ_s, the so-called ac-Stark shift. This shift of the 'dressed' ground state exactly corresponds to the dipole potential for the atom. For laser light red detuned with respect to the atomic transition, the shift is negative, and the atom is attracted to an intensity maximum. For blue detuning, the atom is repelled from it. The dipole potential scales with I/Δ_{as}, with $\Delta_{as} = \omega_a - \omega_s$, wheras the rate the atom scatters light upon illumination with the far detuned laser light scales as I/Δ_{as}^2. Scattering is unwanted, because it can lead to heating, and for this reason often a laser with large detuning in combination with a high laser intensity is used. In order to calculate the trap depth as a function of the intensity used, the multilevel structure of the atom has to be taken into account. Both the $D_1 : 5^2S_{1/2} \rightarrow 5^2P_{1/2}$ and the $D_2 : 5^2S_{1/2} \rightarrow 5^2P_{3/2}$ lines contribute, and in the case of linearly polarised light the dipole potential is given by [**?**]:

$$U_{dip}(\vec{r}) \;=\; \frac{\pi c^2 \Gamma}{2\omega_a^3} \left(\frac{2}{\omega_s - \omega_{D2}} \;+\; \frac{2}{\omega_s + \omega_{D2}} \;+\; \frac{1}{\omega_s - \omega_{D1}} \;+\; \frac{1}{\omega_s + \omega_{D1}} \right) I(\vec{r}) \;. \quad (2.1)$$

where $\Gamma = 2\pi \times 6\,\mathrm{MHz}$ is the natural linewidth, ω_a the frequency of the atomic resonance and ω_s the laser frequency. The corresponding ac-Stark shift is given by $\Delta_s = 2U_{dip}/h$, because both the ground and excited level are shifted by the laser.

In the experiment the dipole traps are derived from an *ELS Versadisk Yb:YAG* laser with an output power of 9 W at 1030 nm. With the relevant ^{85}Rb transitions at 780 nm, the laser is very far detuned in the red, and due to the different scaling with intensity

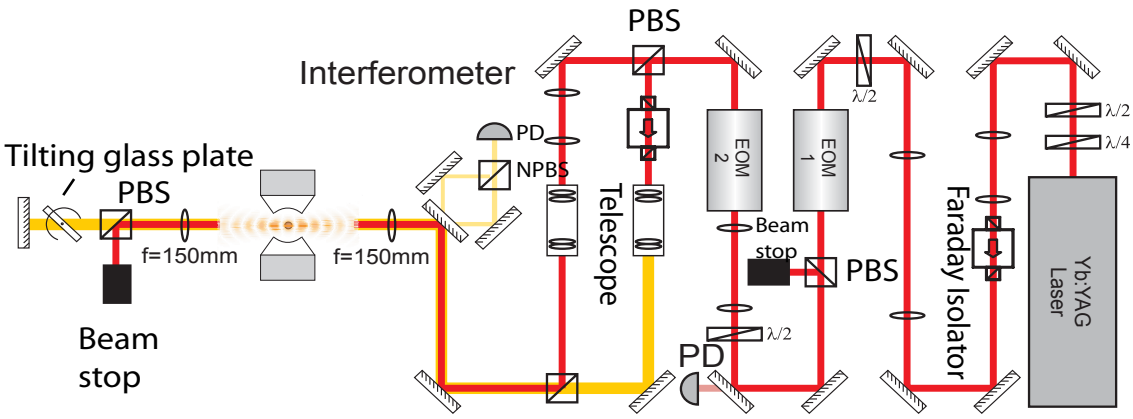

Figure 2.4: **The dipole laser setup.** *The laser intensity is stabilized by an EOM in combination with a polarizing beam splitter, by changing the polarization of the laser with a second EOM the intensity of the light in two optical paths can be set. The lasers propagating through different telescopes form the transport dipole trap and the standing wave trap respectively.*

of dipole force and scattering rate, the dipole potential generated with this laser can be considered quasi-conservative, often called a *Far Off Resonant Trap* (**FORT**). In figure 2.4 the configuration of optical elements needed to deliver the dipole trap beams to the vacuum chamber are depicted. By changing the polarization of the light from the laser using an *Electro-Optic Modulator* (**EOM**), it is possible to send it along different paths, passing through a different array of lenses before entering the vacuum chamber. In this way two trapping geometries are created. The first geometry is that of the transfer trap. The focus of this beam is situated between cavity and MOT. After the atoms have been loaded from the MOT into this dipole laser, the atoms move down the potential towards the focus and move further to the cavity. As soon as the atoms arrive there, the EOM is switched, creating a new trap geometry. The focus overlaps with the cavity mode. This laser beam is also retroreflected by a mirror, and it interferes with itself to create a standing wave pattern. In the following table the parameters of both traps are listed:

		Standing Wave:	Transport trap:		
	Parameter	2 W	Distance from focus		4 W
			0 mm	2 mm	7 mm
beam waist	w_0 , (w(z))	16 μm	41 μm	(44.1 μm)	(72.0 μm)
Rayleigh length	$z_0 = \pi w_0^2/\lambda_s$	0.6 mm	4.8 mm		
Trap depth	U_0/k_B	2.5 mK	188 μK	(160 μK)	(60 μK)
ac-Stark shift	$\Delta_s/2\pi$	103 MHz	9 MHz	7.7 MHz	2.9 MHz
radial trap frequency	ν_{rad}	9.8 kHz	1.1 kHz		
axial trap frequency	ν_{ax}	0.68 MHz	(6.0 Hz)		
radial wavepacket size	$\overline{x}_{rad}/\lambda_s$	0.11	0.33		
axial wavepacket size	$\overline{x}_{ax}/\lambda_s$	0.013	(4.3)		

The standing wave trap has a tighter focus, which leads to a deeper trap potential. Also depicted in figure 2.4 is the rotatable glass plate in the beam path of the standing wave that enables moving the atoms in and out of the cavity once they are trapped.

The transport of the atoms from the MOT into the cavity was first tested without a cavity. By making absorption images of the atomic clouds at different stages of the transport this process can be visualized, see figure 2.5.

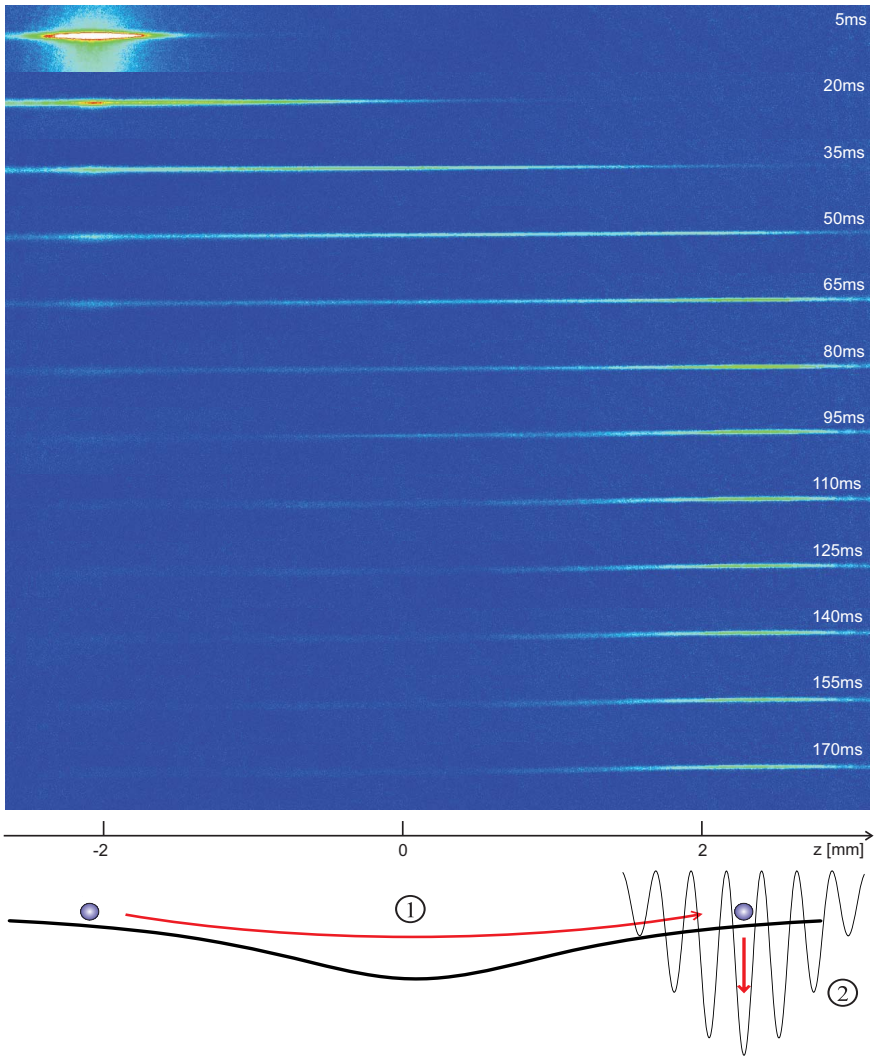

Figure 2.5: **The transport of atoms from the MOT into the Cavity** *is illustrated here by a series of absorption pictures taken for increasing interval length after the initial loading of the atom in the dipole trap. After approximately* 90 *ms the atomic cloud has moved into the cavity region where it has been trapped in the standing wave dipole potential.*

In the first image, the transport dipole trap is overlapped with the MOT, which one can see by the elongated distortion in what was a spherical MOT. Analysis shows that

approximately $57 \pm 8\%$ of the atoms in the MOT can be transferred into the dipole trap. [?] In the next 80 ms the atoms spread in the dipole trap and start moving in the potential that is sketched below the images. Upon arrival at the other turning point, the standing wave trap is turned on and the atoms remain trapped in what will be the center of the cavity.

2.6 The Cavity

In a widely used description of cavity quantum-electrodynamics (**cavity-QED**) a central role is played by the cooperitivity parameter $C = g^2/2\kappa\gamma$. It is a measure of the atom-cavity interaction strength g with respect to the cavity decay κ and the atomic decay γ. If $C \ll 1$ this is referred to as the 'bad cavity' limit, where the main effect of the cavity is enhanced spontaneous emission, which is known as the Purcell effect. [?] In the limit $C \gg 1$ the system is said to be in the 'strong coupling' regime, where the atom-cavity system can evolve coherently by exchange of photons. The present cavity was designed with single-photon generation in mind. On the one hand this needs a strong interaction, as a Raman adiabatic passage scheme is used that relies on a strong g. On the other hand, a generated photon must leave the cavity fast enough to be able to repeat the process at an acceptable rate. The cavity decay rate κ should therefore be not too small. Therefore a cavity configuration was chosen that is in the intermediate regime, $C = 1.7$. The atom-cavity interaction strength is a function of the volume V of the cavity mode:

$$g_0 = \sqrt{\frac{\omega_c}{2\epsilon_0 V \hbar}} \cdot \mu_{ge}, \tag{2.2}$$

Here μ_{ge} is the dipole matrix element of the atomic transition, see appendix A. For this reason coned mirrors are used that are brought together closer than a millimeter. The design length of the cavity was 0.5 mm, which is a compromise between high g and optical accessability for the optical dipole trap. Because the curvature of the mirrors was 5 cm, much larger than the cavity length, the cavity mode envelope is approximately cylindrical. The mode itself is modulated sinusoidally along the cavity axis due to the standing wave pattern. The cavity decay rate κ is a function of the reflectivity of the mirrors. It can be expressed as

$$2\pi\delta\nu = 2\kappa \tag{2.3}$$

with $\delta\nu$ the linewidth of the cavity. The reflectivity $\mathcal{R}$ of the mirrors is limited by the losses $\mathcal{L}$ and the transmission $\mathcal{T}$, with $\mathcal{R} + \mathcal{T} + \mathcal{L} = 1$. The cavity linewidth is linearly dependent on the inverse length of the cavity, which was chosen to be short. One does no longer have to worry that κ will be too small, instead one has to use ultra-clean state-of-the-art ultra high reflective dielectric mirrors (provided by *Research-Electro-Optics*) to decrease the cavity decay rate to an order of magnitude comparable or lower than g and γ. Light that is transmitted through a cavity mirror provides a means to observe the dynamics of the atom-cavity system, the measurements rely on the observability of this signal. The challenge is to build a cavity with mirrors with a small, but useful transmission $\mathcal{T}$, and minimize the losses $\mathcal{L}$. A cavity assymmetric in the transmission $\mathcal{T}_{1,2}$

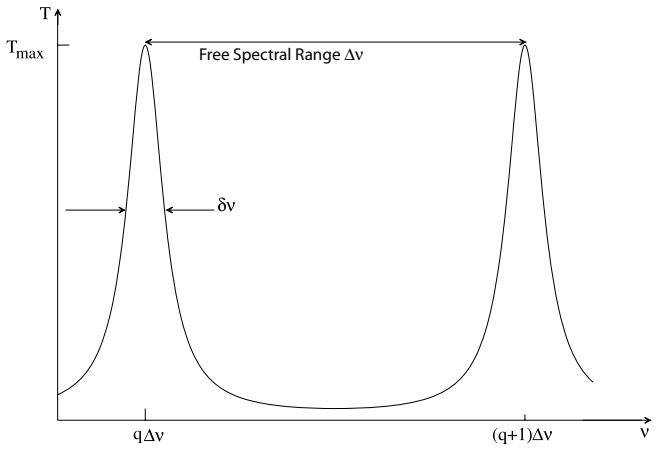

Figure 2.6: *The* free spectral range *is defined as the frequency difference between adjacent cavity modes. A cavity resonance occurs every time a discrete number of half- wavelengths fits inside the cavity. The linewidth of this resonance depends on the number of roundtrips the light wave oscillates. More roundtrips means that the frequency of the laser must be closer to the center frequency of the cavity if it is to remain resonant. Therefore the linewidth of the cavity is directly related to the lossyness of the cavity.*

was chosen to make sure that most of the photons in the cavity will leave through the 'output' mirror. One of the mirrors therefore has a 'design' transmittivity $\mathcal{T} = 4$ ppm, wheras the other has transmittivity $\mathcal{T} = 100$ ppm. The cavity can be characterized by measuring the linewidth of the cavity and its free spectral range $\Delta\nu$, which is the frequency spacing between adjacent cavity modes, see figure 2.6. These quantities can be measured directly by scanning the frequency of a laser beam coupled into the cavity and monitor the transmitted signal. For the cavity at hand the following values were found:

$$\delta\nu = 4.8\,\mathrm{MHz} \qquad \Delta\nu = 304.4 \pm 0.2\,\mathrm{GHz} \tag{2.4}$$

Now κ is known and via the relation $\Delta\nu = \frac{c}{2d}$ the length d of the cavity is determined which is used to calculate g:

$$d = 492.8 \pm 0.3\,\mu\mathrm{m} \rightarrow g^{max} = 2\pi \cdot 5.3\,\mathrm{MHz}, \kappa = 2\pi \cdot 2.4\,\mathrm{MHz} \tag{2.5}$$

In this case the μ_{eg} of the $|F = 2, m_F = 2\rangle \rightarrow |F' = 3, m_F = 3\rangle$ transition was used.

The finesse of the cavity is defined as:

$$\mathcal{F} \equiv \frac{\Delta\nu}{\delta\nu} = \frac{\pi\sqrt{\sqrt{R_1 R_2}}}{1 - \sqrt{R_1 R_2}} = 62250 \pm 734 \tag{2.6}$$

Following the measurement procedure described in **?** one finds the respective transmittivities of the mirrors to be:[**?**]

$$T_1 = 1.96 \pm 0.03\,\text{ppm} \quad (2.7)$$
$$T_2 = 92.4 \pm 0.2\,\text{ppm} \quad (2.8)$$
$$L_1 + L_2 = 6.57 \pm 0.20\,\text{ppm} \quad (2.9)$$

Unfortunately, six months after the cavity was placed in the vacuum chamber, a change in the cavity linewidth was observed, but strangely enough only for the TEM_{00} mode. An investigation showed that a dust particle adhering to one of the mirrors had slipped into the cavity mode thus increasing the losses $\mathcal{L}$, leading to a larger $\kappa = 2\pi \cdot 5.0\,\text{MHz}$. In the following table all the relevant parameters are listed.

		TEM_{00} with dust	TEM_{00} before	TEM_{01}
Max. coupl. $\|F=3\rangle \rightarrow \|F'=4\rangle$	$g^{max}/2\pi$	7.9 MHz	7.9 MHz	6.7 MHz
Max coupl. $\|F=2\rangle \rightarrow \|F'=3\rangle$	$g^{max}/2\pi$	5.3 MHz	5.3 MHz	4.5 MHz
Average coupling:				
$D_2 : 5^2S_{1/2} \rightarrow 5^2P_{3/2}$	$\overline{g}/2\pi$	5.1 MHz	5.1 MHz	4.4 MHz
Cavity decay	$\kappa/2\pi$	5.0 MHz	2.4 MHz	2.4 MHz
Aver. coop.	$\overline{C}$	0.87	1.8	1.3
Finesse	$\mathcal{F}$	30000	62000	62000

For the photon generation experiments in chapter 5 the $|F=2\rangle \rightarrow |F'=3\rangle$ is used. The maximum cooperativity (i.e. for the strongest Zeeman transition) for this transition is given by C= 0.94.

2.6.1 The cavity stabilization and detection setup

A major challenge is to stabilize the cavity so that its resonance frequency is stable compared to the linewidth of the atomic resonance and the cavity linewidth. Translating this requirement from the frequency domain into the spatial one, this means that the cavity length needs to be stable within less than a picometer. This is achieved by locking the cavity onto a laser using an optical phase modulation technique pioneered by Pound, Drever and Hall. [For a review see **?**.] In figure 2.7 the laser setup for the cavity is depicted. To avoid that the stabilization laser interacts with the trapped atoms, this laser is stabilized at a detuning of 8 free spectral ranges $\approx 5\,\text{nm}$ to the red in such a way that the cavity is still in resonance with the atom. In a chain of Pound-Drever-Hall locks, first the Ti:sapphire laser is locked to a resonance in the D_2 line of rubidium, then a transfer cavity is locked to this laser, then the 785 nm laser is locked to this transfer cavity, on a transfer cavity mode with a frequency 1.5 THz away from the atomic transition at 780 nm. The cavity is then locked onto the 785 nm laser. If the laser power used for the stabilization laser is kept very low, the interaction with the trapped atoms can be neglected. If the

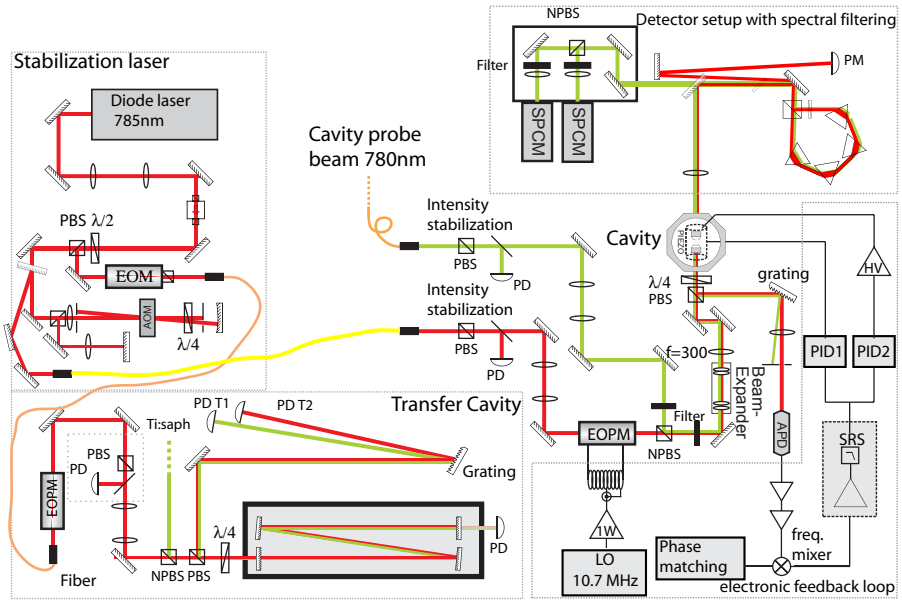

Figure 2.7: **The cavity laser setup.** *The necessity to stabilize the cavity on a laser off-resonant with an atomic transition leads to a chain of locks to stabilize a laser at* 785 *nm which then can be used to stabilize the cavity. The transmitted* 785 *nm is filtered from the* 780 *nm measurement signal by a set of four prisms.*

stabilization laser has a higher intensity it acts as another optical dipole trap, in this case along the cavity axis. Due to the build up of light in a resonant cavity, and the proximity of the 785 nm light with respect to the atomic resonance at 780 nm, only 100 μW of power is needed to create a dipole potential on the order of 30 μK. The combination of this intra-cavity trap with the much deeper transverse trap generates what is called a 2D optical lattice where now the trap is modulated with $\lambda/2$ in two dimensions. The structure of this geometry is discussed in the next section. In the following experiments, the intensity of the stabilization laser was such that it acted as a dipole trap, and it was used to implement a filtering mechanism which will be described in chapter 3.

The transmitted light from the stabilization laser has to be separated from the 780 nm measurement signal. This is achieved by sending the cavity output through 4 prisms, which spatially separate the two different frequencies which are then separated by a mirror with a sharp edge. Due to incoherent scattering, a set of two interference filters is needed to further filter out the 785 nm photons. The light is focussed through a 75 μm pinhole to reduce background before the 780 nm signal output of the cavity is sent on two avalanche photodiodes (Perkin Elmer SPCM AQR-13) with single photon counting capability. The total combined background and darkcount rate is 84 Hz for the detectors, with a 10.5% probability of detecting a 780nm photon that was emitted from the cavity. The first experiments on cavity cooling presented in chapter 3 were done using a different detector setup. Here the light of the stabilization laser was separated from the 780 nm

measurements signal by a holographic grating. The overall probability to detect a photon was 5% and the background count rate was 4 kHz.

2.7 The excitation laser

An atom trapped in the mode of the cavity can be excited by the cavity excitation lasers. The different laser frequencies are delivered to the experiment by the same single mode fiber. The focus of the beam overlapping with the cavity mode has a waist w_0 of 35 μm and the intensity I of the beam is given by $I = 2P/(\pi\, w_0^2)$. The total intensity is then twice that due to the reflection of the beam by a mirror to balance radiation pressure. In order to calculate the corresponding Rabi frequency one uses [**?**]:

$$\Omega_{ij} = \sqrt{\frac{3\lambda^3\, I}{4\pi^2 c\hbar}} \cdot \sqrt{C_{ij}/3780} \tag{2.10}$$

with C_{ij} the relative transition strengths found in appendix A. In chapter 3, a total excitation power of 4μW of incident $|F = 3\rangle \rightarrow |F' = 4\rangle$ light, corresponding to a Rabi frequency of $\Omega_P = 2\pi \cdot 30$MHz, averaged over all Zeeman states was used. The Rabi frequency of the repumping light is $\simeq 2\pi \cdot 10$MHz for all cooling experiments.

2.8 System dimensions

In order to get a feeling for the complexity of the dipole potential in combination with the resonant cavity mode in the interaction region, the potential landscape is plotted in figure 2.8. In contrast to the artistic view presented before, there are quite a few anti-nodes, i.e. potential sites to trap an atom in the interaction region, with every site having a different g and Δ_s. It is therefore remarkable, as will be shown in the next chapters, that the observed single atom signals are very much the same from shot to shot. Because the wavelength of the cavity stabilization laser is slightly larger than that of the resonant mode, the resonant mode of the cavity will beat with the mode of the stabilization laser, thereby creating regions where there is a good overlap for the anti-nodes of both modes and regions where this is not the case. The period of this beat is 60 μm, which is a bit larger than the waist of 16 μm of the steep dipole trap. If the atom is to be trapped in an antinode of the 2D optical lattice, this node needs overlap with the resonant cavity mode in order for the atom to be observed and cooled by cavity-mediated forces. The alignment of the dipole trap and the excitation laser with respect to the cavity mode is therefore of critical importance and requires a precision of several μm at most. Drifts in the alignment on this scale unfortunately are common, which means that after a couple of days the alignment needs to be redone.

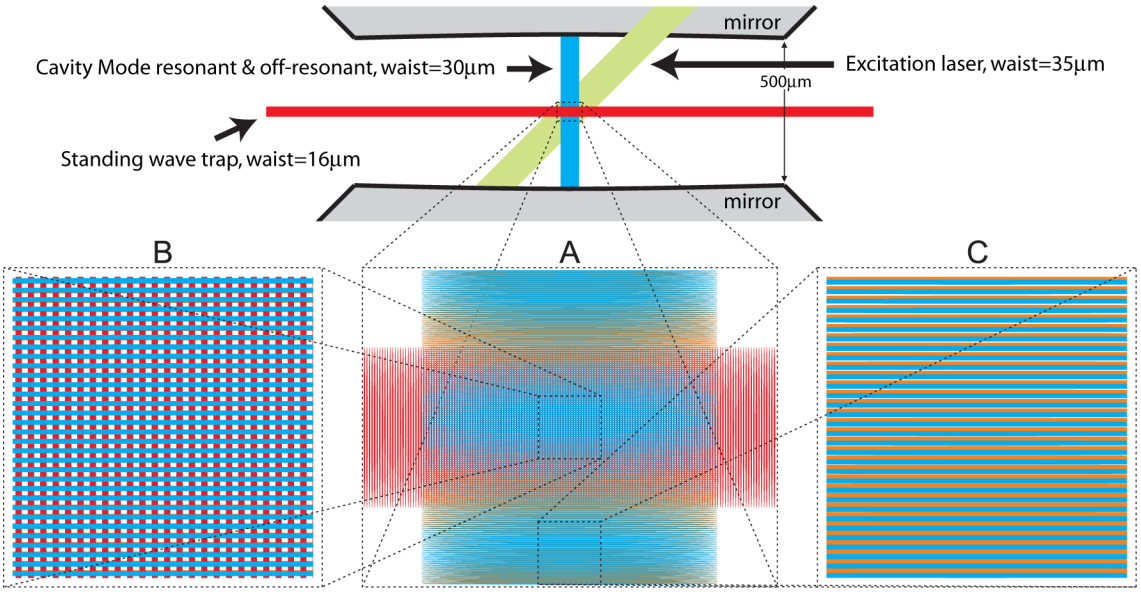

Figure 2.8: **Illustration of the mode structure** *in the atom-cavity interaction region. In this region the potential landscape is very complex due to the strong modulation of the Stark shift from both the dipole laser and the intra-cavity dipole trap, as well as the modulation of the coupling strength g of the resonant mode.* **A.** *Zoom of the interaction region.* **B.** *region where the resonant cavity mode overlaps with the antinodes of the* 785 *nm intracavity dipole laser.* **C.** *region where this is not the case, if the atom is sitting deep in the potential it will not couple to the resonant cavity mode.*

2.9 Observing single atoms with a CCD camera

In the next chapters it will be shown that it is possible to trap and cool one or more atoms in an optical dipole trap and let them interact with the mode of a high-finesse cavity. The implementation of a photon-generation scheme will show that controlled manipulations of the internal degrees of freedom of the atom is possible. The question arises what other kind of experiments are possible with the system at hand. Over the last decade there have been many theoretical proposals to use a string of atoms as a quantum register, i.e. use atoms to store a quantum bit in the internal degrees of freedom, and use the cavity interaction to couple two of these atoms deterministically in such a way that their internal states become entangled or the already entangled state is for example rotated. Such an operation is called a two-qubit quantum gate, and it has been shown that if one can perform a one-qubit phase gate and a two-qubit quantum gate, any operation on n qubits can be decomposed into the sequential application of one- and two-qubit gates, they form a complete set. [**?**] For this to work, addressability of a single qubit stored in an atom is necessary. This can be achieved via the cavity, but there are several limitations. First, as will be shown in chapter 4, if one wants to couple only one atom, it is not possible to couple two, unless one uses a higher order mode of the cavity, which has a lower coupling strength.

Second, the tunability of the cavity is limited, only one transition can be addressed at a time. As an alternative to the cavity, a high-resolution imaging system could be used to observe the fluorescence of the trapped atoms from a direction perpendicular to the cavity axis. By focussing a laser beam through the same objective, the individual qubits could be addressed.

With this in mind, the construction of such an imaging system was started, and the first results are presented in this section

2.9.1 Design and construction of the imaging system

The crucial part of observing the fluorescence of a single atom is to collect as much light from the atom as possible. Because the optical access to the cavity is limited, and the cavity sits in a vacuum chamber this sets constraints on the solid angle that can be covered by a lens, as well as a minimum distance the lens can be brought to the atom. The distance from the cavity center to the surface of the viewport is 22 mm, and the maximally observable solid angle is limited to an numerical aperture of $n \cdot sin\alpha = 0.43,\ \alpha = 25.4°$ by the size of the hole in the piezoceramic tube that is used as a spacer for the cavity mirrors. The numerical aperture in combination with the large working distance of the lens requires the use of singlet lenses with a large clear aperture, which leads to larger lens aberrations. To achieve a high resolution these errors need to be compensated. To fullfill all the requirements it was therefore necessary to design and construct a multi-element lens. The design takes the 8mm thick viewport into account and was optimized and toleranced using the commercially available software ZEMAX. The five custom lens elements were produced by Rodenstock in Munich, and the lens mount was machined in the mechanical workshop at the MPQ. The specifications of the singlet lenses can be found in appendix B. The lens was designed such that its resolution would be diffraction-limited, this limit is $\Delta x_{min} = 1.22\lambda\ (2 \cdot NA) = 1.1\mu m$ for a numerical aperture of 0.43. The actual resolution of the lens was determined to be 1.3 μm, the difference is attributed to small errors in the production process of both lenses and mount. The lens is designed to collect the light from the atom and collimate it. To image the atom the collimated light is then focussed onto a CCD camera by a singlet lens with 700mm focal length. With the focal length of the collimating lens being 25 mm, the magnification factor of the imaging system then becomes 28x. The CCD-camera that is used is an Ixon DV887 from Andortech. The sensor has an array of 512x512 pixels, where each pixel has an area of $16 \times 16\,\mu\text{m}^2$, every pixel therefore represents $0.6 \times 0.6\,\mu\text{m}^2$ in the object plane. A special on-chip electron multiplication gain amplifies the collected signal before analog-digital conversion takes place, thereby increasing the signal-to-noise ratio by a factor of up to a 1000. The entire imaging system is mounted on translation stages to be able to find the atoms, because their position is mainly determined by the dipole trap.

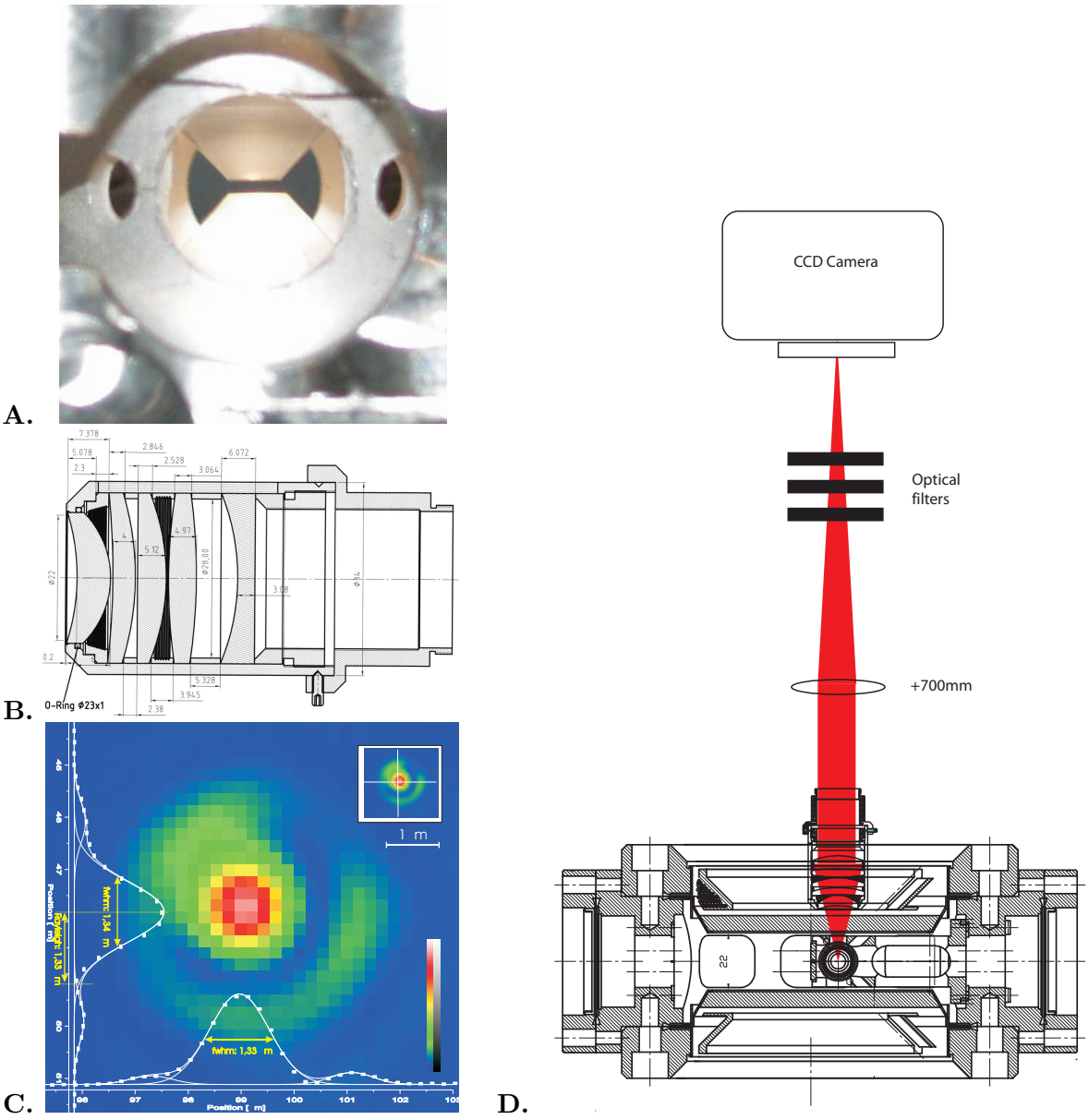

Figure 2.9: **The imaging system.** **A.** *The observable solid angle by the imaging system is limited by the opening in the piezo-ceramic spacer tube.* **B.** *A CAD-drawing of the multi-element lens. The light first passes through three meniscus lenses, a biconvex lens and a plano-concave lens. The design minimizes spherical aberrations.* **C.** *Determination of the resolving power of* $1.3\,\mu m$ *by imaging a* $1\,\mu m$ *pinhole* **D.** *After the light is collimated by the multi-element lens it is then focussed onto a CCD camera by a 700mm singlet lens.*

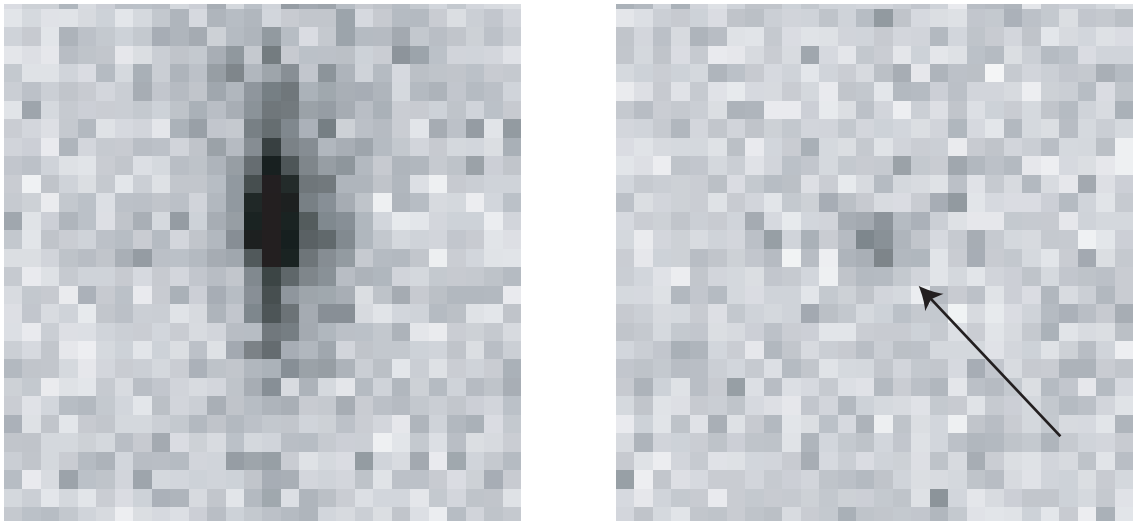

Figure 2.10: **First single atom signals.** *The left image shows the fluorescence collected by the objective when a few atoms were trapped in the cavity mode region. The elongated shape is aligned with the standing wave dipole trap. The image on the right is that of a single atom, which was verified by monitoring the cavity output signal. Light was collected for* 8.5 *s for both images and a* 4×4 *binning was applied. Although these first images do not show a large contrast, there is room for improvement.*

2.9.2 Detecting a single atom

In figure 2.10 two CCD-images are plotted. The left image is taken from a few atoms trapped in the cavity. The right image is that of a single atom. The atom was observed for 8.5 s during which the atom was cooled on the $|F = 2\rangle \rightarrow |F' = 3\rangle$ transition using the cooling forces described in chapter 3. A 4x4 binning was applied for more contrast. The signal is rather weak but it should be possible to increase it by adjusting the position of the objective. Using the $|F = 3\rangle \rightarrow |F' = 4\rangle$ transition could also be helpfull because its overall scattering rate has been observed to be higher. Also, it should be noted that no special effort is made to make the atom visible, the camera only collects light that is emitted anyway and thus forms an additional detection method, not only an alternative one.

Chapter 3

Cooling a single atom in a cavity

3.1 Three-dimensional cavity cooling

3.1.1 Introduction to cavity cooling

From the early experiments with neutral atoms and high-finesse optical cavities, where one used thermal atomic beams that were directed through the cavity to the present experiments, including the ones presented here, an ongoing effort was made to increase the interaction time of an individual atom with the cavity. From the 400 ns interaction time in thermal beam experiments [**?**], $30 - 100\,\mu$s for experiments where the cold atoms produced by a magneto-optical trap were dropped above a cavity [**???**], $\sim 100\,\mu$s when cold atoms were launched with an optical fountain [**?**], this interaction time increased to $400\,\mu$s using an intra-cavity dipole trap with active feedback [**?**]. As people started trapping atoms in optical dipole traps to keep atoms trapped inside a cavity, it turned out that the lifetime of an atom in such a dipole potential was not limited by collisions with molecules from the background gas that kick out the atom. Instead the atom was lost much faster because of heating effects either due to fluctuations in the intensity of the trapping laser or due to fluctuations in the cavity field. It was therefore necessary to implement the possibility to cool the atom while in the dipole trap. In **?** cooling was implemented using forces that originated from the cavity itself, so called cavity cooling. The interaction time was increased to 60 ms, limited, again, by dipole and cavity field fluctuations. In **?** a different approach was pursued. In this case the wavelength of the laser used for the optical dipole trap was such that the ground and excited state were subject to the same dynamical Stark shift. In this way the atom experiences no ac-Stark shift. In combination with Doppler cooling this led to trapping times of 2-3 seconds. As the results on the present experiment will show, using a dipole trap perpendicular to the cavity together with a unique combination of cavity and Sisyphus cooling forces now have made trapping times up to a minute possible, where this trapping time is limited by technical issues. These results were first published in **?** and can also be found in the PhD thesis of Stefan **?**. A theoretical description of the cavity cooling forces based on

a two-level atom interacting with a cavity was developed by Karim Murr, and published in **??**. The main theoretical concepts will now be briefly discussed, for a more rigorous description the reader is referred to the last two articles.

A two-level atom interacting with a cavity and a pump laser can be described in the interaction picture by the following Hamiltonian:

$$\begin{aligned} H/\hbar = \quad & \Delta_a(\boldsymbol{r})|e\rangle\langle e| + \Delta_C \hat{a}^\dagger \hat{a} + g(\boldsymbol{r})(\hat{a}|e\rangle\langle g| + \hat{a}^\dagger|g\rangle\langle e|) \\ - \quad & \eta(\boldsymbol{r})|e\rangle\langle g| - \eta^*(\boldsymbol{r})|g\rangle\langle e| \\ + \quad & U(\boldsymbol{r}) \end{aligned} \tag{3.1}$$

The first line describes the atom-cavity system by the Jaynes-Cummings model, with $\hat{a}, \hat{a}^\dagger$ the annihilation and creation operators of the cavity mode, $\Delta_a(\vec{r}) = \omega_a - \omega L + \Delta_s(\vec{r})$ the detuning of the pump laser to the atomic resonance and $\Delta_C = \omega_C - \omega_L$ the detuning of the cavity with respect to the laser frequency. The second line describes the pump beam with $2|\eta(\boldsymbol{r})|$ its Rabi frequency. $U(\boldsymbol{r})$ is the dipole potential from the trapping laser:

$$U(\boldsymbol{r}) = -\frac{\hbar\Gamma^2}{8\Delta_{as}} \frac{I(\boldsymbol{r})}{I_{sat}} \tag{3.2}$$

with $\Delta_{as} = \omega_a - \omega_s$ the detuning of the trapping laser with respect to the atomic frequency. The Master equation describing the evolution of the system must include the losses by atom and cavity decay, because it is this dissipation of energy from the system that leads to cooling forces. It reads:

$$\dot{\rho} = -\frac{i}{\hbar}[H, \rho] + \kappa \mathcal{L}_{cavity}\rho + \gamma \mathcal{L}_{spontaneous}\rho\,, \tag{3.3}$$

with Lindblad operators $\mathcal{L}_{cavity}$ and $\mathcal{L}_{spontaneous}$:

$$\mathcal{L}_{cavity}\rho = 2a\rho a^\dagger - \rho a^\dagger a - a^\dagger a \rho\,, \tag{3.4}$$

$$\mathcal{L}_{spontaneous}\rho = 2\int d^2\hat{\boldsymbol{k}} N(\hat{\boldsymbol{k}}) \mathrm{e}^{-i\boldsymbol{k}\cdot\boldsymbol{r}}|g\rangle\langle e|\rho|e\rangle\langle g|\mathrm{e}^{+i\boldsymbol{k}\cdot\boldsymbol{r}} - \rho|e\rangle\langle e| - |g\rangle\langle g|\rho \tag{3.5}$$

with $N(\hat{\boldsymbol{k}})$ the (dipole) angular distribution of spontaneously emitted photons with direction $\hat{\boldsymbol{k}} = \boldsymbol{k}/|\boldsymbol{k}|$. ($\int d^2\hat{\boldsymbol{k}} N(\hat{\boldsymbol{k}}) = 1$). The time evolution of any operator is now given by $\langle \dot{O}(t) \rangle = tr\left(O\dot{\rho}(t)\right)$

To find expressions for the light forces one uses the Heisenberg equation of motion:

$$\boldsymbol{F} = \frac{d\hat{\boldsymbol{p}}}{dt} = \frac{i}{\hbar}[H, \hat{\boldsymbol{p}}] = -\nabla H \tag{3.6}$$

where $\hat{\boldsymbol{p}} = -i\hbar\nabla$ is the momentum operator. To find an expression for the mean force $F = \langle \boldsymbol{F} \rangle$, first the steady state expectation values of the operators acting on cavity and atom are calculated using the Master equation formalism and approximating the atomic system by an harmonic oscillator. This is valid in the limit of low saturation. These expressions are then substituted into the equations describing the mean force, and one arrives at several general expressions for the forces along different directions.[**?**] By expanding the force up to first order in the velocity one finds the friction force, that can

either cool or heat. A tedious, more general calculation beyond the limit of low saturation shows that the description is still valid outside the low-saturation limit. In addition, however, a Sisyphus-like force on the same order of magnitude and independent of the cavity is found, which turns out to be important for the experiment. The cavity-dependent forces will cool the motion of the atom if the cavity is blue detuned with respect to the pump laser, i.e. $\Delta_C > 0$, as will be explained below. The four identified forces are given by:

$$\boldsymbol{F}_P = -4\hbar \boldsymbol{k}_P (\boldsymbol{k}_P \cdot \boldsymbol{v}) \frac{\kappa \Delta_C}{(\Delta_C^2 + \kappa^2)^2} g^2 P_E \tag{3.7a}$$

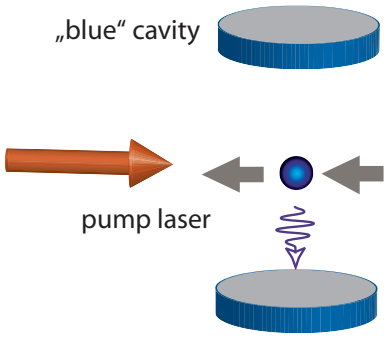

This force acts along the axis of the pump beam, counteracting the motion of the atom which is depicted in the figure by the grey arrows. The atom and cavity are in resonance when the atom moves towards the pump beam. $P_E \approx |\eta(\boldsymbol{r})|^2/\Delta_s^2$ is the excitation probability. The atom absorbs a photon with momentum $\hbar\vec{k}_P$ from the pump beam and emits a photon into the cavity. The motional energy in the pump direction is therefore reduced. Because the pump beam is retro-reflected the same process happens if the atom moves in the other direction along the pump beam. Due to the Doppler shift the atom will be more resonant to the laser in which direction the atom moves.

$$\boldsymbol{F}_C = -4\hbar \nabla g (\nabla g \cdot \boldsymbol{v}) \frac{\kappa \Delta_C}{(\Delta_C^2 + \kappa^2)^2} P_E \tag{3.7b}$$

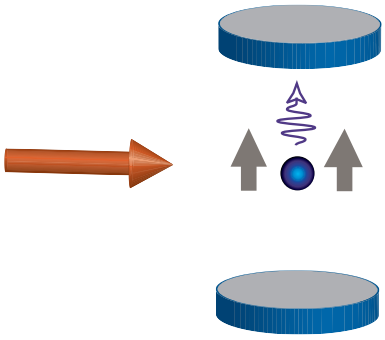

This force acts along the cavity axis. In contrast to the previous force, where the cooling arises from an increased absorption probability if the atom moves in a certain direction, this force is the effect of a preferred emission of the photon into the cavity if the atom moves along the cavity axis. The atom is Dopper shifted into resonance with one of the two counter-propagating cavity modes. This picture of two counter-propagating cavity modes is valid if one averages the force over $\lambda/2$ and thus neglects the interference pattern of the cavity mode. The atom will emit in the direction of motion. As a result of the momentum kick from the emission of the photon, the atom experiences a friction force.

$$\boldsymbol{F}_S^{Cav} = -4\hbar\nabla\Delta_S(\nabla\Delta_S\cdot\boldsymbol{v})\frac{\kappa\Delta_C}{(\Delta_C^2+\kappa^2)^2}\frac{g^2P_E}{\Delta_A^2+\gamma^2} \tag{3.7c}$$

There is no easy visualization to understand this cooling force along the standing wave trap axis. The friction arises from the fact that the cavity field is slow to adapt to fluctuations in the atom-cavity coupling due to motion of the atom.

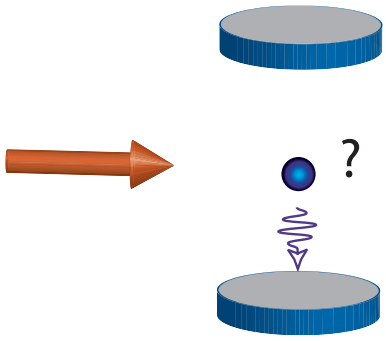

$$\boldsymbol{F}_S^{Sis} = -4\hbar\nabla\Delta_S(\nabla\Delta_S\cdot\boldsymbol{v})\frac{\Delta_A}{2\gamma(\Delta_A^2+\gamma^2)}P_E^2 \tag{3.7d}$$

The configuration of trapping and cooling lasers give rise to another cooling force along the standing wave dipole trap, independent of the cavity. In essence the description is that of Sisyphus cooling with a blue detuned laser [**??**], with the difference that now trapping and optical pumping is done by two separate lasers. Depending on the position of the atom in the trap, the atom experiences a dynamical Stark shift $\Delta_s(\vec{r})$, which detunes the atom out of resonance with the pumping laser. As is depicted, the excitation probability is highest if the atom is near a node. The atom in the excited state moves a little before decaying. If it has moved away from the node, its potential energy will have increased, leading to the emission of a photon with a slightly higher energy. Thus with every cycle, kinetic energy is taken from the system.

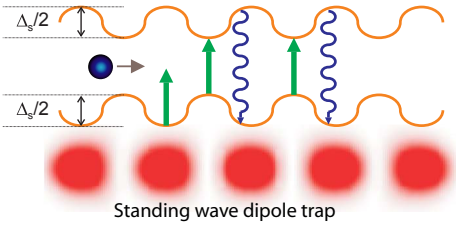

3.1.2 Experimental implementation and results

As described in chapter 2, ^{85}Rb atoms are loaded from a magneto-optical trap (MOT) into a running wave dipole trap which transports the atoms to the cavity, where they are loaded into a deeper standing wave trap. In the cavity interaction region the atoms are subject to a pump laser. Initially this was done to be able to monitor whether atoms were present in the cavity or not. After scanning the frequency and amplitude of the pump laser as well as the depth of the trapping potential, a regime was found where the atoms could be cooled, which resulted in longer trapping times. In what follows, the main results that will be presented were published in **?**.

The frequency of the pump laser as well as the cavity were chosen to be near-resonant with the $|F=3\rangle \rightarrow |F'=4\rangle$ transition, which is the same closed transition for cooling the atoms in the MOT. As with the MOT, a repump laser on the $|F=2\rangle \rightarrow |F'=3\rangle$ transition is necessary. The dynamic Stark shift Δ_s, induced by the trapping laser, shifts

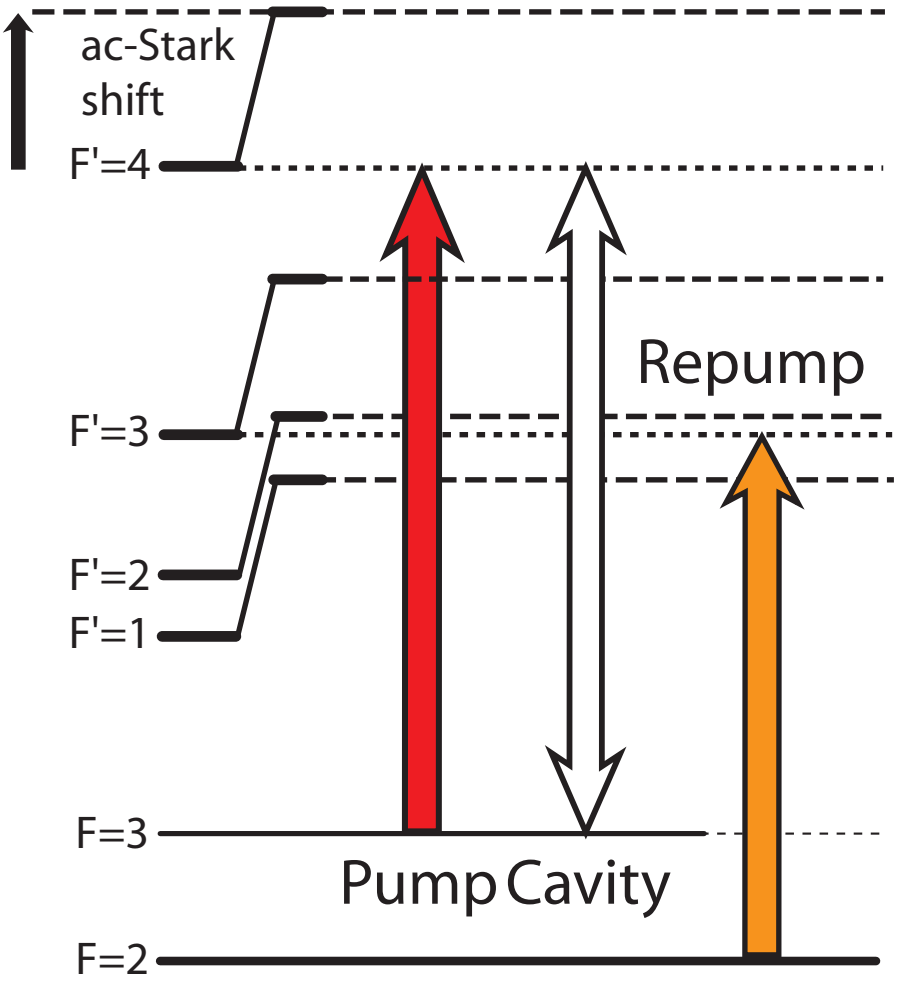

Figure 3.1: **The laser scheme** *used for cavity cooling. The cavity and pump laser used for cooling are resonant or detuned by a few MHz to the unperturbed* $|F = 3\rangle \rightarrow |F' = 4\rangle$ *transition. In addition a repumper is resonant with the* $|F = 2\rangle \rightarrow |F' = 3\rangle$ *transition. Due to the Stark-shift* ($2\pi \simeq 70\,MHz$) *induced by the dipole laser the actual atomic resonances are shifted out of resonance with the lasers.*

the lasers out of resonance with the atom. In Fig. 3.1 a Stark shift of $\simeq 2\pi \cdot 70\,\mathrm{MHz}$ is depicted, this is the shift the atom experiences if the atom is at rest at an antinode. The Stark shift is position dependent, the average shift depends on its motion, i.e. its temperature, and can therefore in principal be anywhere between $0 - 70\,\mathrm{MHz}$.

In figure 3.2 the cavity output is plotted versus time for a single atom trapped for 20 s (upper plot) and an atom trapped for 12 s (lower plot). The stream of photons emitted by the atom into the cavity is very constant on a millisecond timescale. As one can see in the lower graph, the loss of an atom leads to an abrupt change in the rate the atom scatters photons into the cavity. A detailed analysis revealed that the rate a single atom

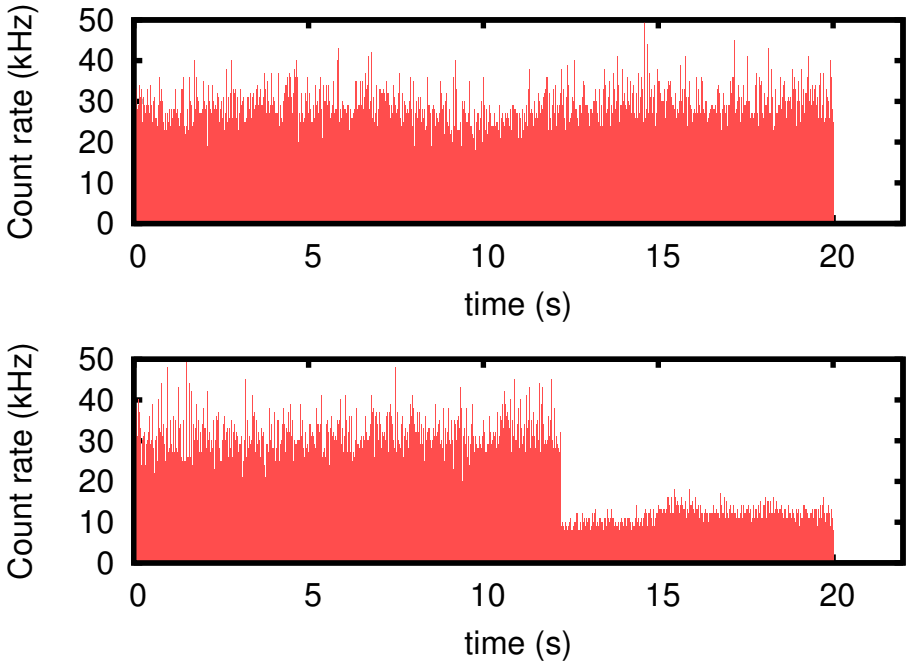

Figure 3.2: **Single atom traces.** *The trapped atom can be monitored by recording the photon signal leaking out of the cavity. In the upper trace this very constant signal is depicted for a single atom that remained for more than 20 s in the cavity. In the lower graph the atom is lost after 12 s, showing an abrupt drop in the count rate. The remaining background signal is originating from the 785 nm stabilization laser.*

emits photons is constant enough from atom to atom so that it is possible to distinguish between one or two atoms by merely looking at the scattering rate into the cavity. The theoretical prediction for this scattering rate is given by:

$$R_{scat} \simeq 2\kappa \, \frac{g^2}{\Delta_C^2 + \kappa^2} \cdot \frac{|\eta(\boldsymbol{r})|^2}{\Delta_a^2 + \gamma^2} \tag{3.8}$$

The Rabi frequency $2|\eta(\boldsymbol{r})|$ is given by $2\pi \times 30\,\mathrm{MHz}$. For $\Delta_C = 0\,\mathrm{MHz}$, $\Delta_s = 2\pi \cdot 70\,\mathrm{MHz}$, a scattering rate of $1.8 \times 10^3\,\mathrm{kHz}$ is thus predicted, of which we detect 5%. In the experiment the measured average scattering rate is $14 \pm 2\,\mathrm{kHz}$, less than the predicted 90kHz. One must however take into account that the atom can occupy the $|F = 2\rangle$ state and needs to be repumped to $|F = 3\rangle$ before a next photon can be scattered. It is estimated that photons are scattered only 1/6 of the time.

For a dataset of 50 traces with the pump laser on continuously the lifetime was found to be 17 s, whereas the lifetime of an atom in the dipole trap without being excited by the pump laser was determined to be 3s. This dark lifetime is mainly limited by residual

intensity fluctuations in the laser beams that create the dipole potential, which lead to heating.

To investigate the role of the cavity on the lifetime of the atom in the trap, both the cavity and the pump laser were scanned in frequency, as can be seen in figure 3.3, where the lifetime of the atom in the trap is plotted as a function of the cavity detuning Δ_C. One has to take a large number of atom traces to calculate the lifetime for a single detuning. At the same time long term drifts in the alignment of trapping and pumping laser with respect to the cavity mode will strongly affect the lifetime of the trapped atom. In order to be able to do the scan presented in figure 3.3 in a sufficiently small amount of time, an additional heating rate was introduced in the system that decreased the lifetime of a trapped atom from 3 s to 22 ms. This was done by modulating the intensity of the trapping laser by 30% at a frequency of 7 kHz. The results show that regardless of the detuning Δ_C one can expect an increased lifetime (~ 100 ms) when pumping the atom continuously, as is exemplified by the data point taken at $\Delta_C = 2\pi \cdot 50$ MHz, where the cavity does not play a role. The same increase is found for $\Delta_C = 0$ MHz , where the cavity forces have no net effect, as can be seen from the accompanying friction coefficients $\beta_{P,C}$ plotted in the upper part of the graph. The 4-fold increase is therefore attributed to the Sisyphus-like force F_S^{sis} with friction coefficient β_S . For $\Delta_C > 0$ MHz, i.e. a blue detuned cavity, the lifetime is enhanced even further, whereas for a red detuned cavity ($\Delta_C < 0$ MHz) the lifetime is reduced. The cavity cooling forces can thus increase or decrease the lifetime by another factor of 4 depending on the sign of the detuning. The two experimental curves reflect the two ways one can vary the detuning Δ_C, either by leaving the pump frequency $\omega_P = \omega_A$ fixed and scan the cavity detuning (•), or vice versa(□). The atomic resonance is detuned by the much larger ac-Stark shift $\Delta_s \approx 2\pi \cdot 70$ MHz, so both scanning methods give the same results.

3.1.3 The filter phase: selecting a single atom.

The traces presented in figure 3.2 show single trapped atoms. The atom loading mechanism, however, is not deterministic in the sense that it is not possible to load an exact number of atoms from the MOT, transport them to the cavity and load them into the standing wave trap. Instead a small amount of atoms are transported from the MOT and end up randomly distributed in the standing wave trap. To make sure one and only one atom is trapped, a trick is applied to get rid of the other atoms. This filtering phase makes use of the cooling forces. In figure 3.4 the sequence is visualized. Some of the atoms are immediately trapped in the standing wave potential after it was switched on, others move freely along the standing wave, and due to the cooling forces are preferentially trapped in the intersection with the cavity mode. Next, the dipole trap and the cooling lasers are turned off for 10 ms. Only very cold atoms positioned in the center of the cavity will be trapped in the remaining weak intra-cavity dipole trap formed by the cavity stabilization laser at 785 nm. The depth of this trap is 30 μK in an antinode. The other atoms will be no longer trapped and move out of the cavity interaction region. Subsequently, the dipole trap and pump lasers are turned on again. In almost 50% of the experimental runs it is a single atom that survives the filter phase, and with a very high probability no atoms enter

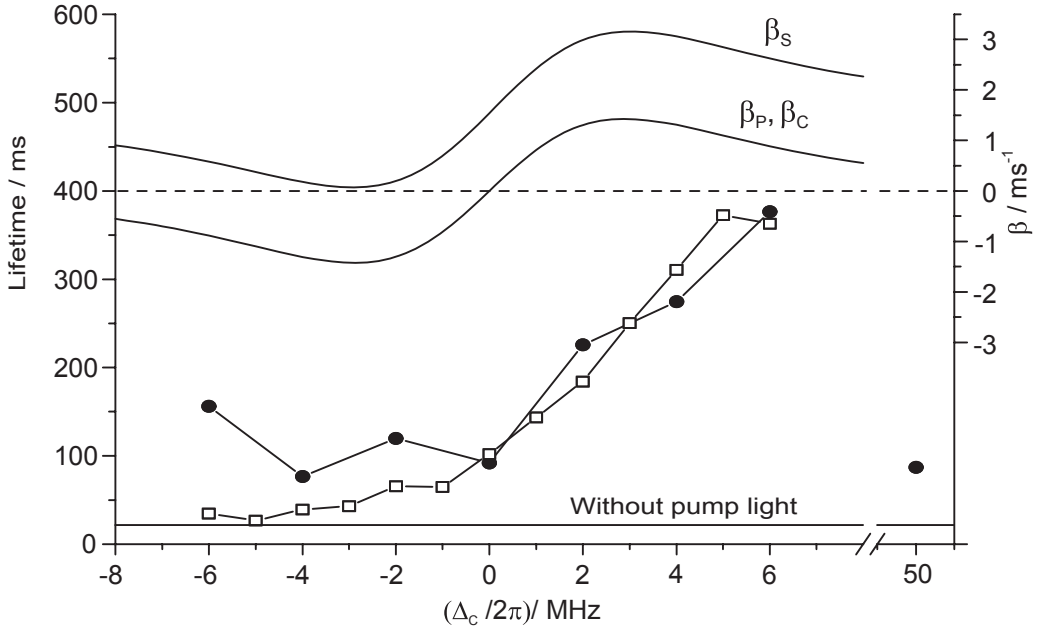

Figure 3.3: **Trapping time and friction forces** *as a function of the cavity detuning. For this scan the lifetime for an atom in the trap was reduced to* 22 *ms by parametric heating. A fourfold increase in lifetime is attributed to the Sisyphus-like force, independent of the cavity detuning. A blue detuned cavity increases the lifetime by another factor of four.*

the trap at a later stage. Using the procedure described above, it is thus possible to trap one and only one atom with a high success rate.

3.1.4 Estimation of the temperature of the cooled atom.

The theoretical lower limit for the equilibrium temperature is given by $T = \hbar\kappa/2k_b \simeq 120\,\mu$K, in analogy to the free space Doppler cooling limit, with γ replaced by κ. [**?**] In free space Doppler cooling much lower temperatures than the theoretical limit have been achieved [**?**], and this effect was explained by **?**. Their mechanism, called polarization gradient cooling, took into account the fact that atoms have a multilevel structure, with magnetic sub-levels. The polarization of the lasers used to excite the atom is integral to this description. In the configuration used for cavity cooling the pump beam is retro-reflected to balance the radiation pressure. To avoid a standing wave geometry, the linear polarization of the pump beam is rotated by 90°, usually denoted as $lin \perp lin$. It is therefore reasonable to expect sub-Doppler effects similar to those in free space Doppler

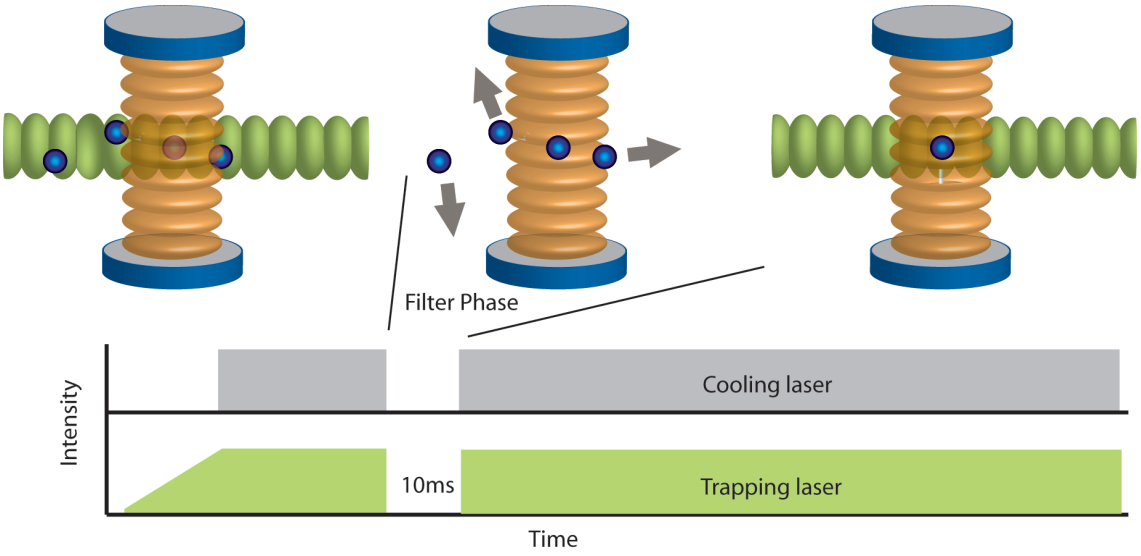

Figure 3.4: **The filter phase** *is used to deterministically select a single atom in the cavity. First, a few atoms are loaded into the dipole trap. Atoms are preferentially cooled down in the center of the cavity mode due to the cooling forces. Second, for* 10 *ms the trapping laser and cooling laser are switched off and only atoms cold enough to be trapped in the dipole trap created by the stabilization laser remain trapped. Third and last, The dipole trap is switched back on and a single atom is well-coupled to the cavity.*

cooling. Although the temperature of the single trapped atom was not measured directly, several independent estimations lead to the notion that the temperature of the trapped atom is very low. First of all, a periodic modulation corresponding to the trap frequency along the cavity axis is found in the autocorrelation function of the emitted photon stream. This means the atom oscillates in a single antinode. The trap depth of the weak intra-cavity dipole trap being $k_B \cdot 30\,\mu$K, which at the same time is the upper limit of the atomic energy, the mean kinetic energy cannot be more than 50% of this value, leading to a temperature estimate of $15\,\mu$K. If one assumes that the distribution in the scattering rate from atom to atom is an effect of a distribution in the cavity coupling $g(\vec{r})$, this leads to a distribution of $\pm 9\,\mu$m along the standing wave. The origin of this spread lies in the filtering phase, where the standing wave dipole trap is turned off. The atoms oscillate in the intra-cavity trap until the orthogonal trap is switched back on and are thus redistributed. The measured distribution leads to a temperature estimation of $6\,\mu$K for the atoms during the filtering phase. An interesting question is whether the atom is cooled down into its motional groundstate. The estimated $15\,\mu$K corresponds to a mean vibrational quantum number $\tilde{n} = 0.13$ for the motion along the standing wave dipole trap, the atom thus mainly occupies the groundstate.

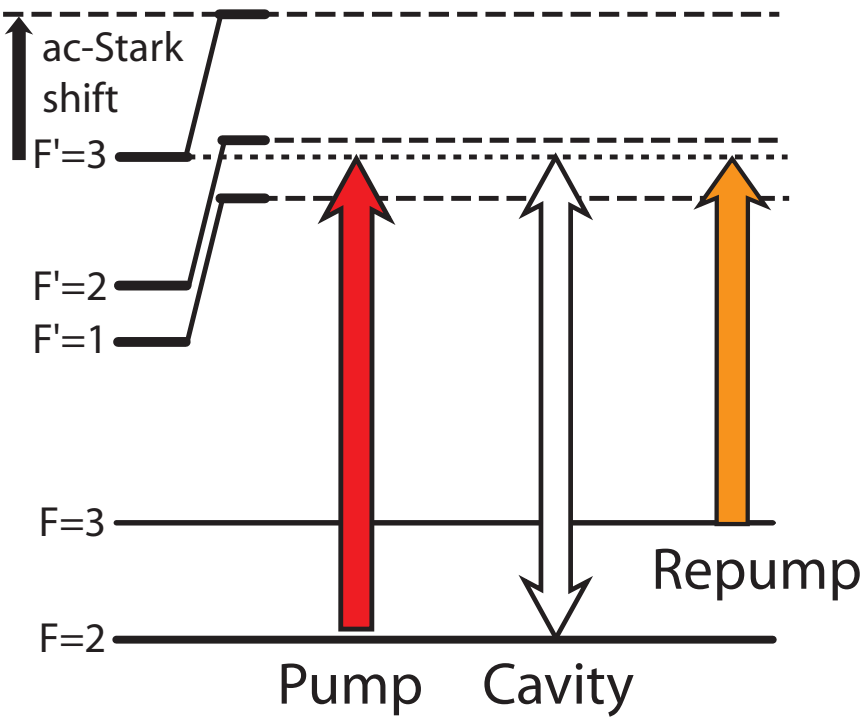

Figure 3.5: **The new laser scheme** *that operates with the cavity on a transition suitable for single-photon production. The cavity and the Pump laser used for cooling are now resonant with the unperturbed* $|F = 2\rangle \rightarrow |F' = 3\rangle$ *transition, the repumping laser is now on the unperturbed* $|F = 3\rangle \rightarrow |F' = 3\rangle$ *transition.*

3.2 Combining cavity cooling with single photon production

The increase in trapping time achieved with cavity cooling finds an application in the use of the atom as a single photon server, as will be discussed in chapter 5. Such a server cannot make use of the $|F = 3\rangle \rightarrow |F' = 4\rangle$ transition because an excited state that couples to two separate ground states is necessary. The excited $|F' = 4\rangle$ state only couples to the $|F = 3\rangle$ ground state, and is therefore not suitable. Unfortunately, as the cavity is needed for both cooling and single-photon generation, it is not possible to combine both when the cavity is needed to be resonant with different transitions. Although in principal it is possible to cool on one transition, then shift the frequency of the cavity, and generate single-photons on another one, this is not desirable for technical reasons. First, as the cavity would have to be shifted while simultaneously being stabilized, the minimum shift of 121 MHz (for the cavity to be resonant with $|F = 3\rangle \rightarrow |F' = 3\rangle$) is very hard to realize with the current setup. Second, shifting the cavity takes time, several 10's of milliseconds for 121 MHz. Cooling between subsequent single-photon pulses would be out of the question.

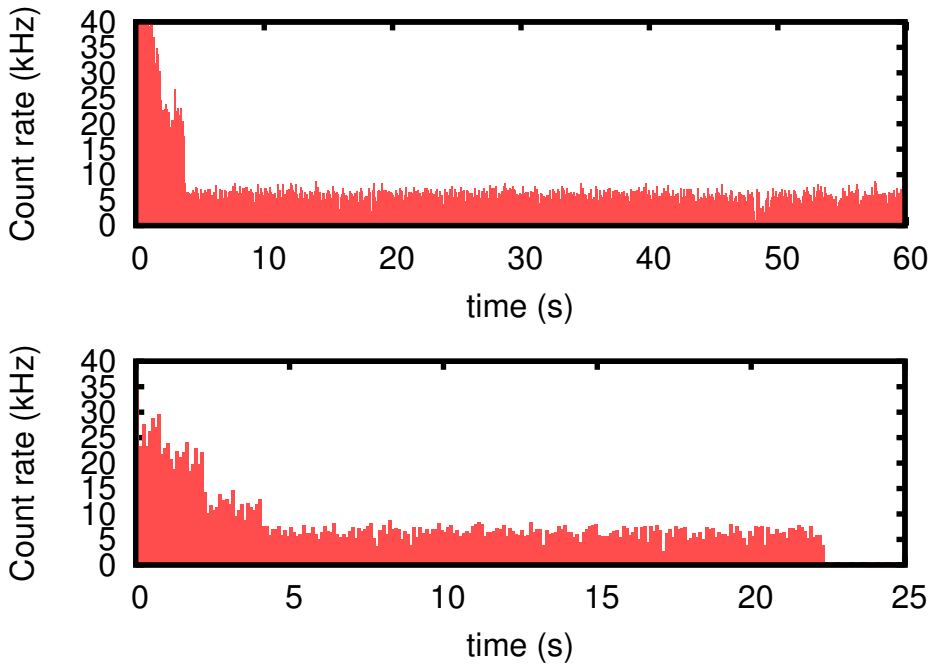

Figure 3.6: **Single-atom traces** *that show that long trapping times can be achieved with cavity cooling on the* $|F = 2\rangle \rightarrow |F' = 3\rangle$ *transition. Compared to the data taken in Figure 3.2 the background count rate has been reduced to an almost negligible* 84 *Hz.*

As was discussed at the beginning of this chapter, the cooling forces were predicted in the general framework of a two-level atom interacting with a cavity. For this reason an attempt was made to use the $|F = 2\rangle \rightarrow |F' = 3\rangle$ transition for cooling purposes. The scheme is depicted in figure 3.5. The cavity and the cooling laser are near-resonant with the unperturbed transition. Because the hyperfine splitting between $|F' = 2\rangle$ and $|F' = 3\rangle$ is 63 MHz and the induced ac-Stark shift can be $\sim 2\pi \cdot 70$ MHz, they are actually closer to the $|F = 2\rangle \rightarrow |F' = 2\rangle$ transition. A laser resonant with $|F = 3\rangle \rightarrow |F' = 3\rangle$ is acting as a repumper. As shown in example traces in figure 3.6, cooling works very well on this transition. Surprisingly, the optimal parameters regarding laser frequency and intensity of the pump beam as well as the depth of the dipole trap are almost identical to the ones used on the old transition. ($\mathrm{P}_{dipoletrap} = 2\,\mathrm{W}$, $2|\eta(\boldsymbol{r})| = 2\pi \times 26\,\mathrm{MHz}$). This leads to the observation that effective cooling in our configuration is strongly dependent on a few key parameters independent of the cavity, where this dependency is not predicted by the developed theory.

With trapping times of up to 60 s it should be possible to generate a large number of photons from the same atom. Results on such an experiment are discussed in chapter 5.

Chapter 4

Deterministic control of atom-cavity coupling

In this chapter, results are presented on a method to control the strength of the interaction of a single atom with a high-finesse cavity. The basic ingredients are formed by a single atom trapped in an antinode of a standing wave dipole potential aligned perpendicular to the mode of a high-finesse cavity. The cavity coupling strength $g(\vec{r})$ has a Gaussian dependence of the distance from the cavity axis in its normal plane. As the $29\,\mu$m waist of the cavity mode is large compared to the $\ll \lambda/2 \approx 0.5\,\mu$m confinement of an atom trapped in the standing wave, the average coupling strength can be adjusted by moving the atom further in or out of the cavity. A large part of the following results have been published in **?** and were also discussed in **?**.

4.1 Controlling the position of an atom in the cavity

In the experiment, as the atoms are trapped in an antinode of the standing wave trap, the atoms can be moved around by moving the anti-nodes of the trap. The anti-nodes, i.e. the interference pattern created by the two counter-propagating laser beams, can be moved if the relative phase of the beams is changed. This can be done by temporarily shifting the frequency of one of the beams, as was shown by **?**. Another method, which is applied here, can be used if the standing wave is created by retro-reflecting an incoming beam, simply by moving the mirror along the propagation axis. Because the field has to be zero at the reflecting surface, this sets a boundary condition for the standing wave. Here, instead of moving the mirror directly, the optical path length between the cavity and the mirror can be changed by tilting a 3.1 mm thick, transparent glass slab mounted on a galvo-scanner in the beam line, see figure 4.1. The position of the atom becomes a function of the angle α of the slab with the laser beam. With $500\,\mu$m being the largest possible displacement, this is large compared to the cavity waist. It is thus possible to move one or more atoms completely in and out of the cavity. The angular repeatability of the closed-loop galvo-

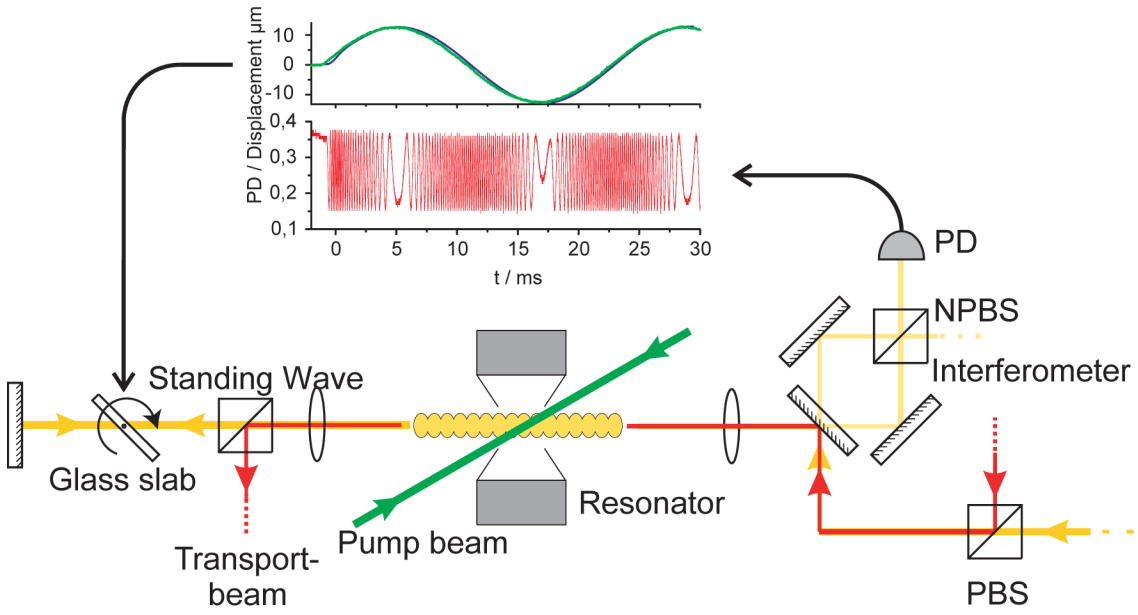

Figure 4.1: **Controlled positioning of a single atom** *can be achieved by moving the interference pattern of the dipole trap, with an atom trapped in one of its anti-nodes. Tilting a glass slab in the beam line will change the optical path length of the trapping laser, thereby shifting the interference pattern. The small amount of light transmitted through the last mirror before focusing into the vacuum chamber of both the incoming and reflected beam can be used to create a Mach-Zehnder interferometer. By counting the fringes observed by a photodiode, the displacement created by the glass slab can be calibrated.*

scanner(Model: General Scanning M3-H) leads to a 15 nm accuracy in the position of the standing wave pattern. As can be seen in the right part of figure 4.1, a very small part of the incoming and reflected laser light is transmitted through the last mirror before the vacuum chamber, and is observed with a Mach-Zehnder interferometer. The galvo-scanner can be calibrated by counting the number of fringes that can be observed during an oscillation of the glass slab.

4.2 Results

In figure 4.2 the photon stream out of the cavity is plotted as a function of time. In the lowest plot, the relative displacement from the starting position of the anti-nodes is shown, which is periodically modulated. A clear modulation in the scattering rate for one (top graph) or two (middle graph) atoms is visible. As was described in chapter 3 the scattering depends directly on the cavity coupling the atom experiences. The earlier mentioned Gaussian dependence is clearly visible in the scattering rate. Due to the cooling

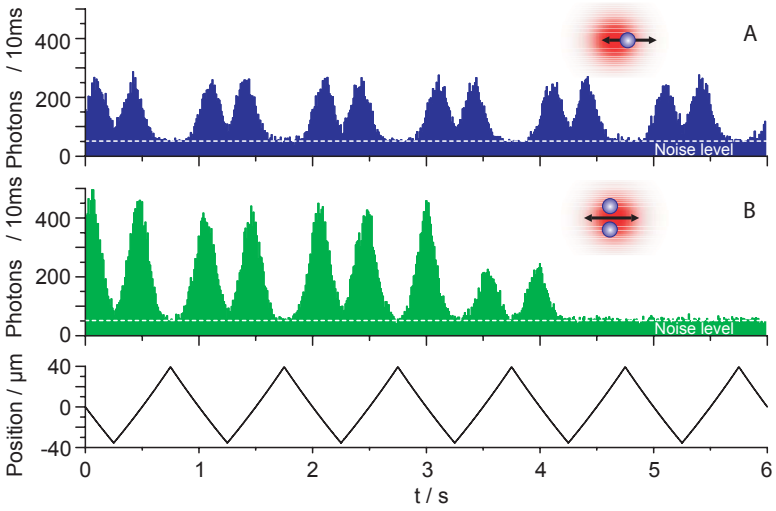

Figure 4.2: **Deterministic control of atom-cavity coupling** *is illustrated here by moving one (***A***) or two (***B***) atoms through the cavity mode. As can be clearly seen, the scattering rate into the cavity varies with the displacement of the atom from the cavity center (***C***)*

forces and the filter phase, the initial position of the trapped atom is in the center of the cavity mode, which is why the peaks in the scattering rate are centered around $0\,\mu$m displacement. To quantify the accuracy with which the atom can be positioned, the following measurement was done, see figure 4.3. After an initial 100 milliseconds where

the atom is at rest after the filter phase, the standing wave pattern is moved for 500 ms, with an oscillation frequency of 20 Hz leading to 10 oscillations. The amplitude is 25 μm. Afterwards the atom at rest is observed for another 100 ms. What is being investigated is the spread in the peak positions as a function of the number of transits, relative to the position of the peak from the first passage through the cavity. As depicted in Fig. 4.3C this distribution increases with the number of transits. With an uncertainty of 2 μm in the determination of the center of a peak being dominant in the first few transits, the distribution width steadily increases with 135 nm for every transit later on. From transit to transit, the accuracy to return the atom to the same position is therefore given by this 135 nm, which is very small compared to the waist of 29 μm of the cavity mode. From the same dataset, it is also possible to estimate the initial distribution of the atom. As can be seen in Fig. 4.3A;B, a different initial position manifests itself in a different scattering rate. Because the atom is subsequently moved through the cavity, it is possible to determine how large this scattering rate is with respect to the maximum scattering rate. In this way, the global atom to atom fluctuations in the scattering rate do not play a role anymore. It thus becomes possible to assign an initial displacement from the cavity center for every atom. The atomic positions are found to be distributed $\pm 7.7\,\mu$m along the standing wave.

The filter phase, as was shown, is very effective in selecting well-centered cold atoms. In an attempt to extend our deterministic atom-cavity coupling scheme to more than one atom, which would enable experiments in which by successively coupling atoms to a cavity, entanglement swapping and quantum gate experiments can be performed, see for instance **?**, it was tried to repeat the previous single atom experiments without the filter phase, in order to have several atoms distributed over the standing wave potential. In figure 4.4 results are presented on such an experiment. In the upper graph, a single atom after the filter phase is moved repeatedly through the cavity, and a clear periodic signal is visible. In the lower three graphs, the filter phase was not part of the initialization. At first instance, the data show peaks periodic with the movement of the glass slab. From oscillation to oscillation however, some peaks vanish or are at a different position. Also some of the peaks seem to bunch together in one larger peak.

An explanation for this is that now atoms are being moved around that during preparation were not trapped in the cavity mode, and hence were not cooled. Due to their higher temperature, it has become more probable that they do not move along with the standing wave all the time, but instead hop to different anti-nodes. It must be concluded that the atom must be very cold in order to do deterministic cavity coupling experiments, a situation that in the present configuration can only be achieved by atoms trapped initially in the cavity mode. Experiments using a string of trapped atoms, whereby moving the string to couple a single atom sequentially to a cavity, will therefore be challenging. One example on how to do this will be presented in the next section.

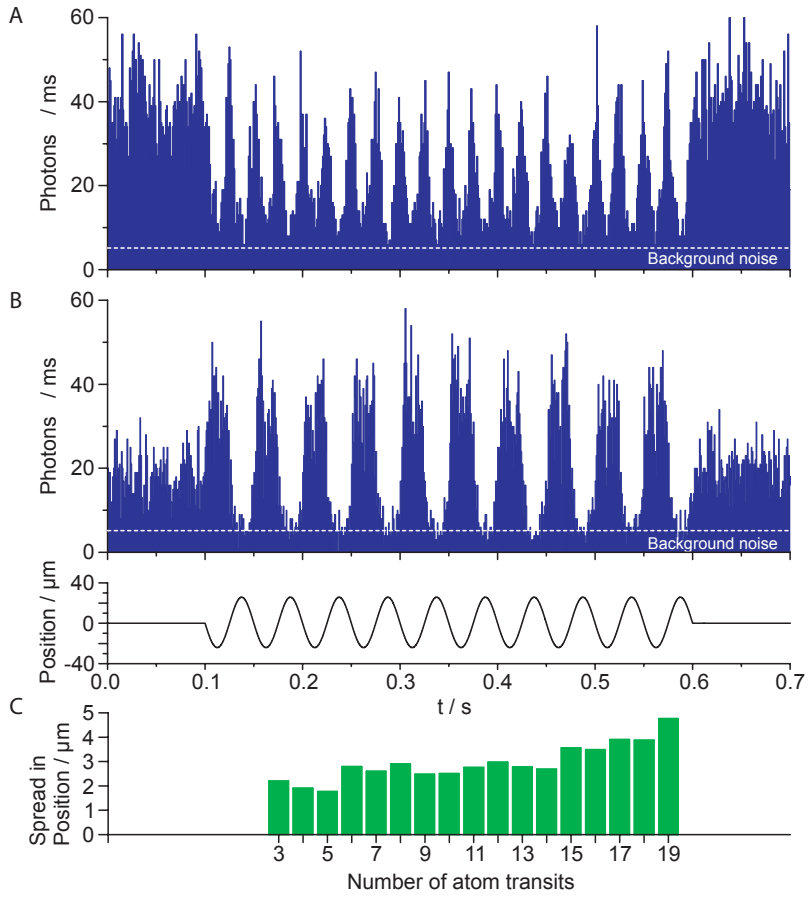

Figure 4.3: **Analysis of the repeatability of positioning. A.** *An initially well-coupled atom displays the same scattering rate after having been moved in and out of the cavity 19 times.* **B.** *The same holds for an atom trapped off-center.* **C.** *Statistical analysis of the peak positions from transit to transit for 71 traces reveals that the spread in atomic position increases by* 135 *nm after every oscillation. The initial* 2 μ*m spread in the atomic position is due to noise in the detection.*

4.3 Sequential coupling of two atoms by use of the TEM_{01} mode

As was discussed in the last section, cooling is necessary for deterministic cavity coupling. The cavity cooling only takes place in the cavity mode, but if one uses the TEM_{01} mode of the cavity instead of the TEM_{00}, an atom can be trapped in both maxima of the mode. As the spacing between these maxima is 42 μm it is possible to move one atom to a position in the cavity where it is maximally coupled to the cavity, whereas the other atom is not coupled at all. Such a measurement is depicted in figure 4.5. In the upper part, only one

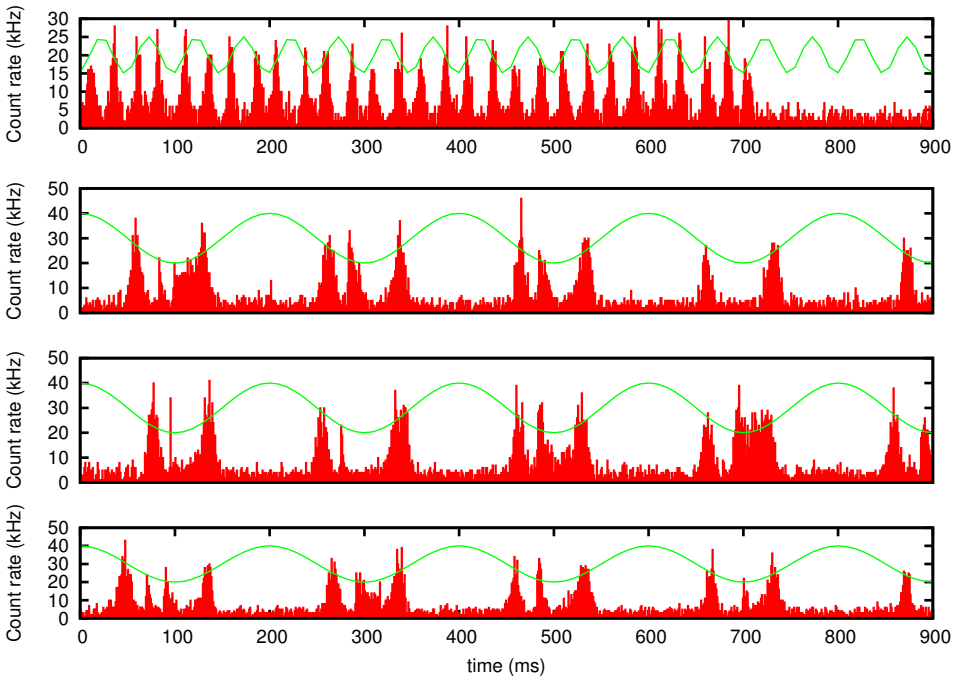

Figure 4.4: **Moving more than one atom.** *High repeatability requires atoms that are so cold cold that they are trapped deep in the dipole potential. When loading more than one atom (by leaving out the filter phase) distributed over the potential, the lack of cooling manifests itself in atoms that disappear or bunch during transits, Repeatability is therefore lost. The upper trace is a control trace with a single atom which displays a good repeatability.*

atom is trapped, and one identifies two peaks on every transit, belonging to the maxima. In the middle trace, two atoms are trapped. And because they are subject to a filter phase, they were each trapped in one of the maxima. If these atoms are now moved through the trap, three peaks occur with every transit. The left peak is when only the right atom is coupled. The middle peak is when both atoms are coupled, and is therefore larger. The last peak is when only the left atom is coupled.

Using the TEM_{01}, it is possible to couple either one of the atoms or both. With this level of control, it should therefore be possible to start experiments in the direction of quantum computation.

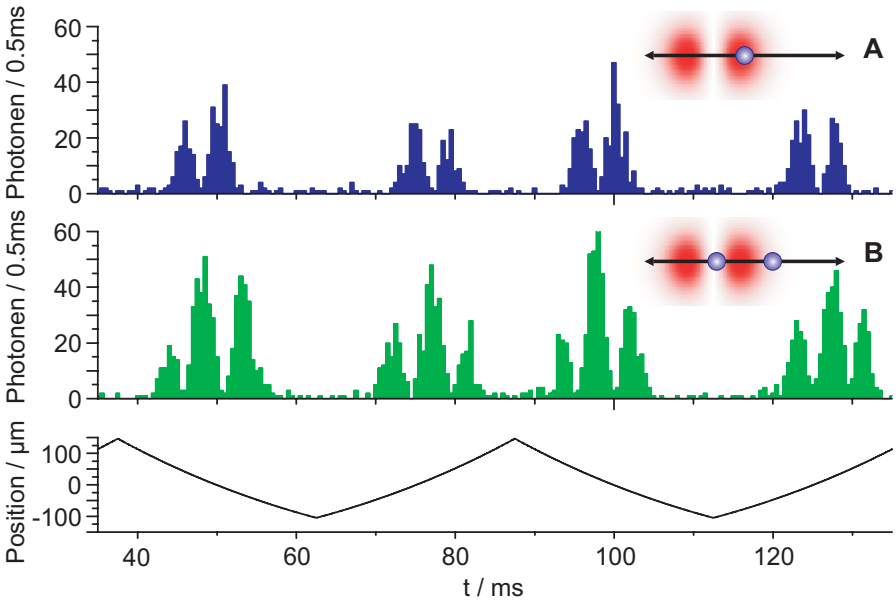

Figure 4.5: **Controlled coupling to the TEM_{01} mode** *for one (***A.***) or two atoms (***B.***) Because the two atoms were cooled down in the mode their separation enables the coupling of either one of the atoms or both. This manifests itself in three peaks in the scattering rate when the atom transit the cavity, the middle peak being larger because there two atoms scatter into the cavity.*

Chapter 5

Single photons from a single atom in a cavity

5.1 Single photon generation: Introduction and Theory

In this chapter, results are presented on the generation of single photons from a neutral atom quasi-permanently coupled to a high-finesse cavity. The work in sections 5.4 and 5.5 has been published in **?**. The single photons were generated via a method called vacuum-stimulated Raman adiabatic passage, which is a STIRAP(stimulated Raman adiabatic passage)-like technique where one of the lasers is replaced by the cavity. [**?**] An important property of this method is that three atomic levels are involved, which has the advantage that after the emission of a single photon into the cavity the atom is in a state different from the initial state. In this way it is guaranteed that no additional photons are produced within the pulse after the production of the first photon. Before a theoretical description is given, the general idea of the adiabatic passage is illustrated in figure 5.1. An atom in the ground state $|u,0\rangle$ is excited by a laser pulse with Rabi frequency $\Omega_P(t)$, detuned by $\Delta_P = \omega_{eu} - \omega_P$ from the $|e,0\rangle$ state. This excited state is coupled to another electronic ground state $|g,1\rangle$ via the cavity, the coupling strength being $2g$. The cavity detuning $\Delta_C = \omega_{eg} - \omega_C$ is now defined with respect to the $|g\rangle \rightarrow |e\rangle$ transition, and no longer to the laser frequency as was the case in the description of cavity cooling in chapter 3. For simplicity Raman resonance, $\Delta = \omega_{eu} - \omega_P = \omega_{eg} - \omega_{cav}$, is assumed. If the atom falls back from $|e,0\rangle$ to $|g\rangle$ a photon is emitted into the cavity, $|0\rangle \rightarrow |1\rangle$. If one takes the Hamiltonian of this system and calculates the eigenfrequencies and eigenstates, one finds that there is an eigenstate that does not contain the excited state $|e,0\rangle$. Furthermore, the relative contribution of both ground states to this so-called "Dark" state is a function of the Rabi frequency Ω_P of the pumping laser. By applying a laser pulse with a linear ramp in the Rabi frequency, an atom in the $|u,0\rangle$ state can be transferred into $|g,1\rangle$ without populating the excited state $|e,0\rangle$. The $|g,1\rangle$ state decays to $|g,0\rangle$ and a single photon is emitted from the cavity. If the Rabi frequency Ω_P changes slow enough so that the system follows the dark eigenstate, i.e. the transfer is adiabatic, the transfer efficiency

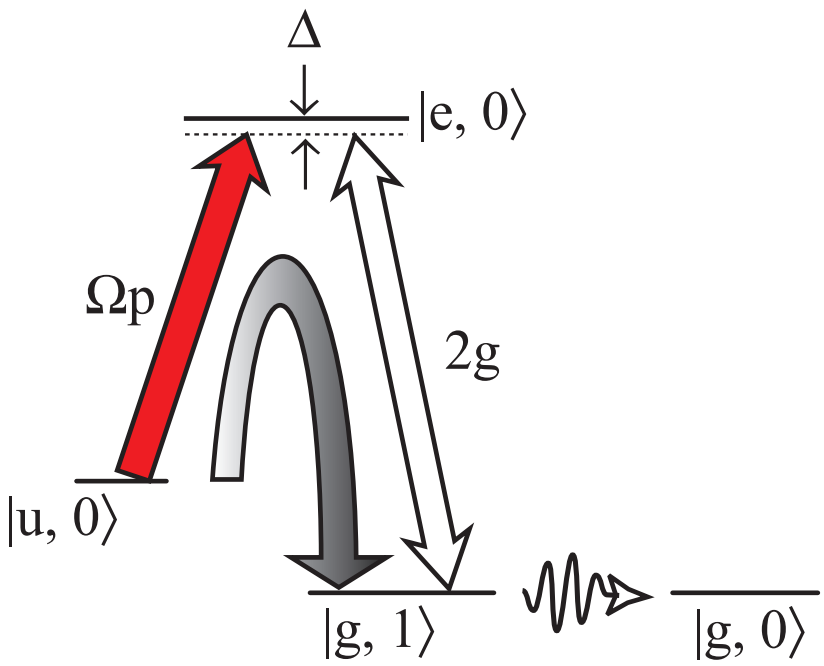

Figure 5.1: **The single-photon generation scheme.** *The three-level system consists of two ground states* $|u,0\rangle$,$|g,1\rangle$ *and an excited state* $|e,0\rangle$*. The cavity couples the* $|g,1\rangle$ *state with* $|e,0\rangle$ *state. A trigger laser with Rabi frequency* Ω_P *couples the* $|u,0\rangle$ *state to the* $|e,0\rangle$ *state. An atom initially in the* $|u,0\rangle$ *state can be adiabatically transfered into the* $|g,1\rangle$ *state by slowly increasing the intensity of the trigger laser. The* $|g,1\rangle$ *state decays to* $|g,0\rangle$ *and a single photon is emitted from the cavity.*

can be near unity for a three-level system. As soon as the $|g,1\rangle$ state decays, there no longer is a real dark state and the excited state is mixed in, which can lead to losses by spontaneous emission. In view of these two issues, one finds that the adiabatic passage requires a strong coupling of the atom with the cavity, and a slowly changing mixing angle Θ of the dark state:

$$\frac{g^2}{\gamma} \gg \frac{d\Theta}{dt} + \frac{\kappa}{2} \tag{5.1}$$

The Hamiltonians of the atom and the cavity read:

$$\hat{H}_A = \hbar\left[\omega_g|g\rangle\langle g| + \omega_e|e\rangle\langle e| + \omega_u|u\rangle\langle u|\right] \tag{5.2}$$

$$\hat{H}_C = \hbar\omega_C\left(\hat{a}^\dagger\hat{a} + \frac{1}{2}\right) \tag{5.3}$$

The description of the (lossless) cavity mode is analog to that of a harmonic oscillator, where in this case $\hat{a}^\dagger$ and $\hat{a}$ are creation and annihilation operators of the photons in the cavity. The pump laser and cavity interactions are described by the Hamiltonians:

$$\hat{H}_{ue} = \frac{\hbar}{2}\left(\frac{\mu_{eg}E_P(t)}{\hbar}\right)\left[|e\rangle\langle u| + |u\rangle\langle e|\right] \tag{5.4}$$

$$\hat{H}_{ge} = \frac{\hbar}{2}(2g)\left[|e\rangle\langle g|\hat{a} + \hat{a}^\dagger|g\rangle\langle e|\right] \tag{5.5}$$

μ_{eg} is the transition dipole moment and $g = \sqrt{\frac{\mu_{eg}^2\omega_C}{2\hbar\epsilon_0 V}}$ the cavity coupling. Using the Hamiltonian $\hat{H} = \hat{H}_C + \hat{H}_A + \hat{H}_{ge} + \hat{H}_{ue}$ one can now calculate the new eigenfrequencies and eigenstates of the complete three-level atom-cavity system. First the system is translated into a reference frame rotating with laser frequency ω_P, then a rotating-wave approximation (RWA) is performed. This means that terms rotating at twice the optical frequency ω_i are neglected. In addition, it is assumed that the pump laser cannot excite the $|g\rangle \rightarrow |e\rangle$ transition, i.e. terms rotating with $\omega_{ge} - \omega_{ue}$ are neglected. After the RWA the Hamiltonian of the three-level system in the interaction picture reads:

$$\hat{H}_{int} = \frac{\hbar}{2}\left[-2\Delta|u\rangle\langle u| - 2\Delta\hat{a}^\dagger\hat{a} - 2g\left(|e\rangle\langle g|\hat{a} + \hat{a}^\dagger|g\rangle\langle e|\right) - \Omega_P\left(|e\rangle\langle u| + |u\rangle\langle e|\right)\right] \tag{5.6}$$

Solving $det|\hat{H}_{int} - \hbar\omega\hat{1}| = 0$ leads to the following eigenfrequencies:

$$\begin{aligned} \omega^0 &= -\Delta, \\ \omega^\pm &= \frac{1}{2}\left(-\Delta \pm \sqrt{4g^2 + \Omega_P^2 + \Delta^2}\right) \end{aligned} \tag{5.7}$$

with the accompanying eigenstates:

$$\begin{aligned} |\phi^0\rangle &= \cos\Theta|u,0\rangle - \sin\Theta|g,1\rangle, \\ |\phi^+\rangle &= \sin\Phi\sin\Theta|u,0\rangle - \cos\Phi|e,0\rangle + \sin\Phi\cos\Theta|g,1\rangle, \\ |\phi^-\rangle &= \cos\Phi\sin\Theta|u,0\rangle + \sin\Phi|e,0\rangle + \cos\Phi\cos\Theta|g,1\rangle \end{aligned} \tag{5.8}$$

where the mixing angles Θ and Φ are given by:

$$\tan\Theta = \frac{\Omega_P}{2g} \quad \text{and} \quad \tan\Phi = \frac{\sqrt{4g^2 + \Omega_P^2}}{\sqrt{4g^2 + \Omega_P^2 + \Delta^2} + \Delta} \tag{5.9}$$

One immediately notices that the eigenstate $|\phi^0\rangle$ does not contain the state $|e,0\rangle$. A system prepared in this state is therefore robust against decay by spontaneous emission from the atom, and without other decay processes will remain in it indefinitely. Without the pump laser, $\Omega_P = 0$, the dark state $|\phi^0\rangle$ is identical to the $|u,0\rangle$ state. If one now applies the pump laser, the $|g,1\rangle$ state is mixed in. In the limit $\Omega_P \gg 2g$, $|\phi^0\rangle \approx |g,1\rangle$. In a real system, the cavity decays with decay rate κ, thus the $|g,1\rangle$ state will decay into the $|g,0\rangle$ state, thereby emitting a photon from the cavity. It is this sequence of events that is used to produce single photons in our setup.

So far, the cavity decay κ and the spontaneous decay rate γ from the excited state $|e,0\rangle$ were excluded from the description. Inclusion of these processes leads to the following Master equation. [**?**, chapter15.4]

$$\frac{d}{dt}\hat{\rho} = -\frac{i}{\hbar}[\hat{H_{int}}, \hat{\rho}] + \hat{\mathcal{L}}[\hat{\rho}] \tag{5.10}$$

with $\hat{H_{int}}$ the lossless three-level atom-cavity system Hamiltonian from 5.6 and $\hat{\mathcal{L}}$ the Liouville operator describing the non-hermitian time evolution due to losses. In Lindblad form it can be written as:

$$\begin{aligned}\hat{\mathcal{L}}[\hat{\rho}] = &\gamma_{eu}((2|u\rangle\langle e|\hat{\rho}|e\rangle\langle u| - |e\rangle\langle e|\hat{\rho} - \hat{\rho}|e\rangle\langle e|)\\ &+ \gamma_{eg}(2|g\rangle\langle e|\hat{\rho}|e\rangle\langle g| - |e\rangle\langle e|\hat{\rho} - \hat{\rho}|e\rangle\langle e|)\\ &+ \kappa(2\hat{a}\hat{\rho}\hat{a}^\dagger - \hat{a}^\dagger\hat{a}\hat{\rho} - \hat{\rho}\hat{a}^\dagger\hat{a})\end{aligned} \tag{5.11}$$

The last line describes the process of cavity decay with rate κ, whereas the first two lines describe the spontaneous decay to $|u\rangle$ and $|g\rangle$ with rates γ_{eu} and γ_{eg}. Including these processes sets restraints on the magnitude of the couplings $\Omega_P, g, \kappa, \gamma$ with respect to each other if the system is to remain in the dark eigenstate $|\phi_n^0\rangle$ while increasing Ω_P to transfer from $|u,0\rangle$ to $|g,1\rangle$. A detailed analysis can for instance be found in **???**. Using the density matrix formalism the temporal evolution can be investigated by integrating 5.10 numerically.

The adiabaticity condition is met if $d\Theta/dt$ is much smaller than g^2/γ. Also, only if the decay processes κ and γ can be seen as small perturbations to the system described by the Hamiltonian in 5.6, the dark state $|\phi_n^0\rangle$ remains an eigenstate of the system. This is the case if $\kappa \ll \frac{2g^2}{\gamma}$. The adiabatic passage therefore requires the system to be in the strong coupling regime $g \gg (\kappa, \gamma)$, and in addition the mixing angle Θ should only slowly change compared to the cavity decay time. These constraints were already summarized in equation 5.1.

5.1.1 Implications for the experimental realization

The next sections describe the various approaches taken in the implementation of the single-photon production scheme. The cavity decay rate $\kappa = 2\pi \cdot 5\,\mathrm{MHz}$ is a fixed property of the cavity, whereas $\gamma = 2\pi \cdot 3\,\mathrm{MHz}$ is fixed by the choice of atomic transition in ^{85}Rb. The cavity coupling $g = 2\pi \cdot 5\,\mathrm{MHz}$ is both dependent on the atomic transition and the cavity mode volume. Only Ω_P is a freely accessible experimental parameter. With $g^2/2\kappa\gamma = 0.94$ the atom-cavity system does not find itself in the limit of strong coupling. As a consequence, because of the adiabaticity criterion stated in the previous section, the dark state $|\phi^0\rangle$ does not longer completely overlap with one of the eigenstates of the Hamiltonian in 5.6, and hence decay processes will decrease the efficiency of the transfer. In the bad cavity limit the following relation can be derived for the emission probability:

$$P_{emit} = (1 + \frac{\kappa\gamma_{eg}}{g^2})^{-1} \tag{5.12}$$

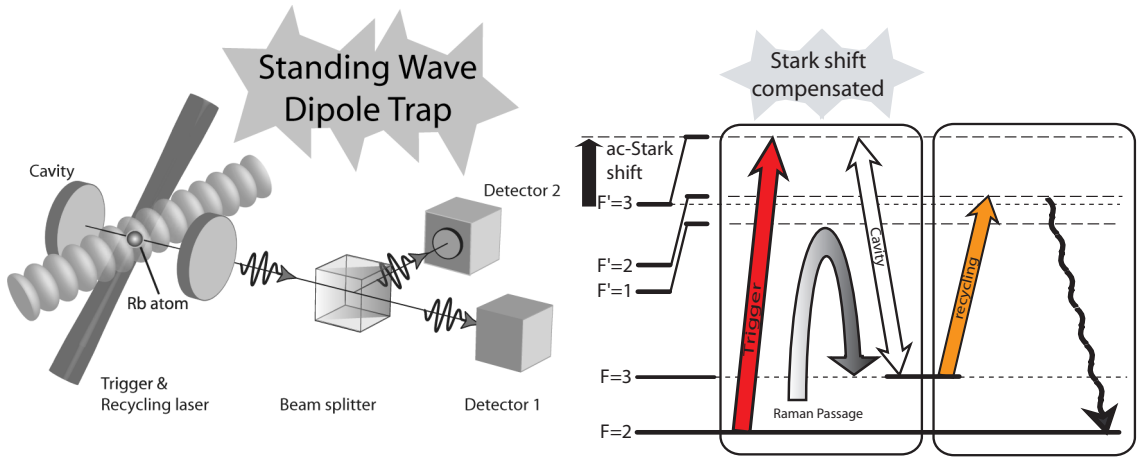

Figure 5.2: **Implementation of the photon generation scheme** *with the cavity on the Stark-shifted* $|F = 3\rangle \rightarrow |F' = 3\rangle$ *transition. The atom is prepared in the standing wave with cooling on* $|F = 3\rangle \rightarrow |F' = 4\rangle$*. The cavity and the trigger laser are subsequently shifted in resonance with the Stark-shifted* $|F = 3\rangle \rightarrow |F' = 3\rangle$ *and* $|F = 2\rangle \rightarrow |F' = 3\rangle$ *transition respectively. The repumping laser is scanned over* 70 *MHz to look for the perturbed* $|F = 3\rangle \rightarrow F' = 3\rangle$ *resonance.*

It was shown in **?** that this relation also holds outside this limit by comparison with a number of numerical simulations with different parameter sets. For the parameters of the system one expects a maximum emission probability $P_{emit} = 79\%$. It should be mentioned that this is an upper limit because in the experiment the coupling g varies with the position of the atom with respect to the cavity mode. It is also dependent on the Zeeman sublevel involved in the transition. Furthermore, as the atom moves in the trap it experiences a dynamical Stark shift. This means that Δ also varies with the position of the atom.

5.2 First attempts to implement single photon production, measurement of the Stark shift

In a first attempt to produce single photons, it was tried to use a three-level scheme with the cavity resonant with the atomic $|5S_{1/2}\ F = 3\rangle \rightarrow |5P_{3/2}\ F' = 3\rangle$ transition, as is depicted in figure 5.2. A single atom was prepared in the cavity using the cooling forces presented in chapter 3. Sub-sequentially the cavity was shifted in to resonance with the $|F = 3\rangle \rightarrow |F' = 3\rangle$ transition. Due to technical limitations, it was not possible to shift the cavity more than 50 MHz without losing the cavity lock. To bridge the necessary 121 MHz, one has to consider that the atom is Stark-shifted by 100 MHz, calculated from the laser intensity used. By scanning the $|F = 3\rangle \rightarrow |F' = 3\rangle$ repumping laser in the pulsed photon generation experiment, a spectroscopy was performed to analyze the feasibility of the proposed scheme. The result is depicted in figure 5.3. The experimental sequence is depicted in the inset. First atoms are trapped in the cavity and cooled using the configuration described in the previous chapter, then the cavity is detuned by -40 MHz

(+), −50 MHz (x) or −60 MHz (*) and the $|F = 2\rangle \rightarrow |F' = 3\rangle$ trigger laser is tuned into Raman resonance with the cavity. For 100 ms trigger pulses followed by recycling pulses are exciting the trapped atoms, with a repetition rate of 140 kHz. Afterwards the cavity is shifted back to the normal cooling configuration, to check for the presence of the atom. As can be seen from the inset, the photon signal during pulsing decays rapidly, so that almost no atoms survive the 100 ms. The highest number of photons were produced with the recycling-laser detuning at $70 - 80$ MHz as can be seen from the three curves with different detunings of cavity and trigger laser. The data shown in the inset was taken with these parameters and the conclusion is that due to the short lifetime of the atom during photon generation in combination with the overall weak signal, it is not possible to record a sufficient signal to see an antibunching in the photon statistics, which would prove that single-photons are being generated, let alone that the photons could be used for practical purposes. A different approach is needed, which will be discussed in the next sections. Another thing one can learn from these measurements is that based on the efficiency of the recycling laser that probes the atomic transition, the average Stark-shift the atom experiences in the trap is on the the order of $70 - 80$ MHz, whereas 100 MHz was predicted based upon the used dipole laser intensity. The difference could for instance be explained by non-perfect alignment of the two counter-propagating dipole laser beams that together form the standing wave potential.

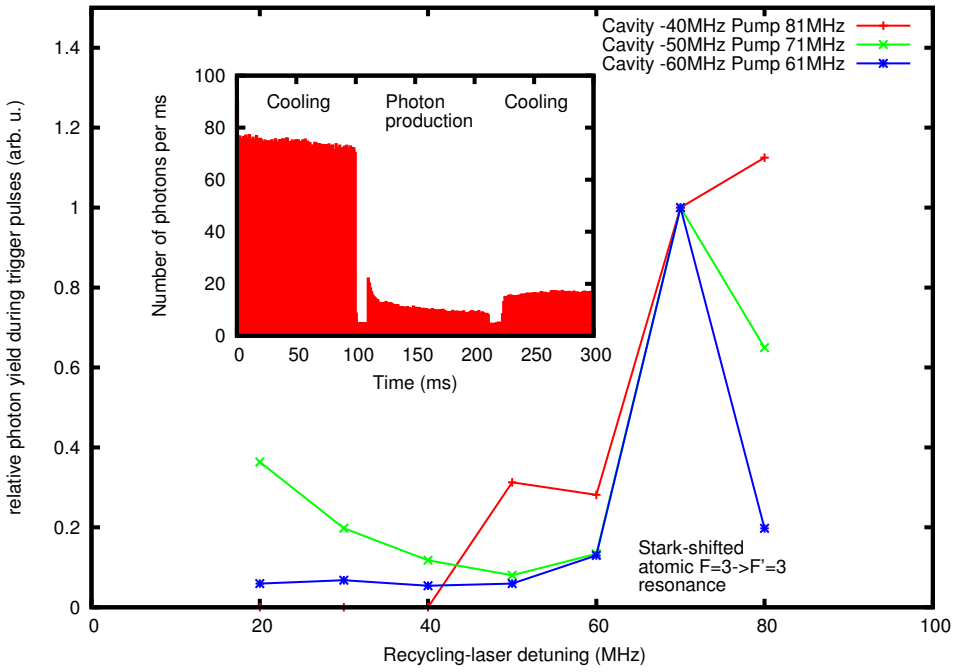

Figure 5.3: **Frequency scan of the repumping laser.** *Plotted is the relative photon yield during the trigger pulses as a function of the frequency of the recycling laser for various cavity detunings with accompanying trigger laser detunings to maintain the Raman resonance. A clear resonance occurs around a detuning of* 70 *MHz, which shows that the atom is ac-Stark shifted by this amount. The inset shows the measurement procedure. First the single atom is cooled, then the single photons generation pulses are applied for 100ms, after which the possibly remaining atom is cooled again. As can be seen from this averaged data, the single-photon production is not very efficient and the lifetime of the atom during photon production is very short, resulting in a much lower signal from the cavity in the second cooling interval.*

5.3 Single photons from an atom flying through the cavity

After the first experiments on photon production from a single trapped atom were not successful, it was decided to test the experimental setup by repeating experiments previously done with atoms falling through a cavity, see **?**. In a similar fashion,the atoms here will now move through the cavity while being guided in a transport optical dipole trap, but because the dynamic ac-Stark shift is small ($\sim 3\,$MHz) compared to the hyperfine-splitting the atom behaves as if it is freely moving through the cavity. The situation is sketched in figure 5.4.

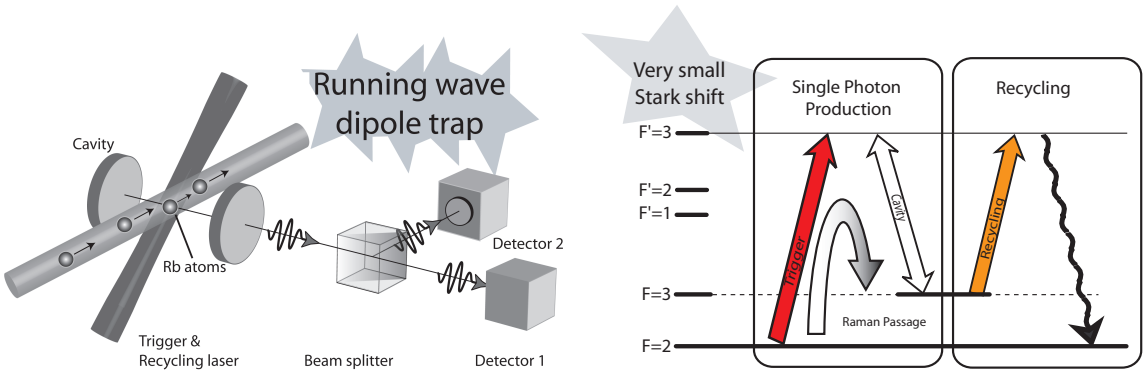

Figure 5.4: **Single photons from atoms flying through the cavity.** *Atoms are guided by the running wave dipole trap into the cavity. During their presence in the cavity mode, the atoms are subject to laser pulses, which stimulate the emission of single photons into the cavity. After escaping from the cavity, these photons are then recorded by detectors in a Hanbury-Brown and Twiss setup. With a negligible ac-Stark shift from the guiding dipole trap, the cavity and the recycler are resonant with the* $|F = 3\rangle \rightarrow |F' = 3\rangle$ *transition, and the trigger laser is resonant with the* $|F = 2\rangle \rightarrow |F' = 3\rangle$ *transition.*

A guided atom interacts for about 0.25 ms with the cavity before leaving the cavity mode again. If one now applies pulses with a rate of 140 kHz, a number of single-photon emissions from the atom can be induced. Because a dilute cloud of atoms is sent through the cavity, the small signal of a single atom can add up to a signal that after evaluation shows a clear antibunching, that is, if it has been possible to eliminate the major sources of noise that can mask the antibunching. As was mentioned earlier the use of three atomic levels is required to be able to generate single photons. In order to reproduce the results in **?** a different approach was now needed to couple the necessary three-level system with the lasers and cavity, because the Stark shift no longer plays a role. The scheme is shown in figure 5.4. The cavity, up to now stabilized so that it was resonant to the $|F = 3\rangle \rightarrow |F' = 4\rangle$, now had to be stabilized to the $|F = 3\rangle \rightarrow |F' = 3\rangle$ transition. The trigger laser is now resonant with the $|F = 2\rangle \rightarrow |F' = 3\rangle$, and the atom is recycled by a laser resonant with the $|F = 3\rangle \rightarrow |F' = 3\rangle$ transition. In figure 5.5 the cross-correlation of the photons detected on both detectors is depicted. The data displayed was taken during an experimental run of 599 atom cloud launches, with a 100 ms recording interval per cycle. On average 38 ± 19 photons were detected per launched MOT. The rather large distribution in this number is probably a result of fluctuations in the number of atoms loaded into the MOT, which is hard to control when a low number of atoms is required. The probability to produce a photon can be estimated by finding the number of times a photon is recorded in the next pulse after the first photon is detected. The data contains 175 of these pairs. If we divide the number of pairs by the number of single photon detections, 22352, we obtain this probability. We thus find that in 0.8% of the pulses a photon is detected. If we take into account the transmission loss of 89%, the production efficiency is 8%. On the left hand side of figure 5.5 one clearly sees a Gaussian-shaped peak in the correlations around $\Delta\tau = 0$. The interaction time of the atom with the cavity is given by 0.27 ± 0.02 ms,

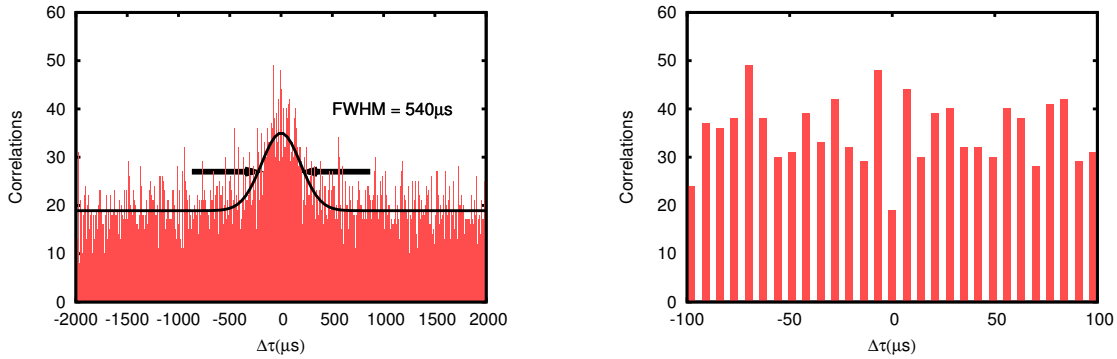

Figure 5.5: **Photon emission statistics** *for an experimental run where 599 atomic clouds were transported into the cavity. The half-width half-maximum of 270μs of the Gaussian shaped increase in the number of correlations in the left graph is a measure of the average interaction time with the cavity of a single atom upon transit. The drop in correlations at $\Delta\tau = 0$ in the right graph indicates that single photons are produced.*

half the width of the Gaussian. This means an atom is coupled during 38 pulses. With 8.0% efficiency this means one expects approximately 4 photons per atom. On average 38 photons are detected per launch. If one takes into account that only 10.5% of the photons escaping the cavity are detected, it can be concluded that approximately 100 atoms pass through the cavity mode per atom cloud. If one zooms in on the region around $\Delta\tau = 0$, as is done in the figure on the right hand side, one sees a clear drop in the number of correlations for $\Delta\tau = 0$. This antibunching tells one that photons are emitted one at a time. In an ideal situation there would be no correlations for $\Delta\tau = 0$ at all, but as we send several atoms into the cavity, we can not guarantee that sometimes more than one atom is present in the cavity, which could lead to a simultaneous emission of two photons. Also one cannot distinguish between correlations between two photons or correlations between background clicks and a photon. Of the 19 correlations at $\Delta\tau = 0$, two are attributed to dark clicks. The remaining 17 correlations can be explained by a model where a single atom is present during 27.3% of the pulses and during 6.2% of the pulses a second atom is present in the cavity.

With these results on single-photon production with a dilute cloud of atoms moving through the cavity, the earlier experiments by **?** were reproduced. By guiding the atoms through the cavity with a dipole trap instead of dropping the atoms from above the cavity, the interaction time of the single atoms with the cavity was increased nine-fold. Unfortunately, one can not guarantee that only one photon is produced per pulse, because fluctuations in the number of atoms interacting with the cavity exist due to the nature of the loading mechanism. A reduction of the atom flux can improve the antibunching, but only at the cost of a lower photon emission rate. It can be concluded, however, that the system is operating at a noise level where anti-bunching from a single atom can be observed. The next logical step is to apply single-photon production on a single atom trapped in the standing-wave dipole trap. For this to work, cooling of the atom is necessary.

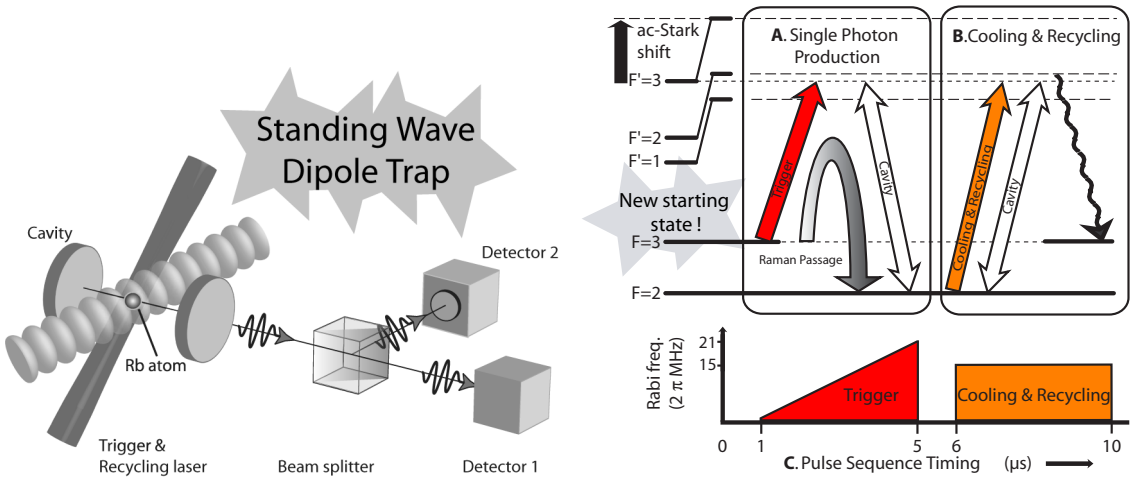

Figure 5.6: **The single-photon generation scheme with a trapped atom.** *The standing wave trapping configuration is depicted on the left. The scheme is depicted on the right. The cavity is now resonant with the unperturbed $|F = 2\rangle \rightarrow |F' = 3\rangle$ transition. However, the standing wave dipole trap shifts the atom out of resonance with lasers and cavity. The pulsing sequence starts with the atom in the $|F = 3\rangle$ state. The standing wave dipole trap shifts the atom out of resonance with lasers and cavity. After the triangular shaped photon generation pulse the atom is recycled by a rectangular pulse. The recycling laser also cools the atom, see chapter 3.*

5.4 Single photons from a single trapped atom

Cooling of the atom with the cavity on the $|F = 2\rangle \rightarrow |F' = 3\rangle$ transition was established, see chapter 3. A photon generation scheme was subsequently implemented, in figure 5.6 the configuration is depicted. On the right hand side the pulse scheme is shown. After a single atom is trapped and cooled into the standing wave dipole trap, the atom, in the $|F = 3\rangle$ state, is excited by a laser pulse increasing linearly in the Rabi frequency. The atom undergoes a Raman adiabatic passage stimulated by the cavity into the $|F = 2\rangle$ state. In the process a single photon is emitted into the cavity. Prior to the next trigger pulse, the atom needs to be recycled back to the $|F = 3\rangle$ state. This is achieved by exciting the atom with a laser pulse resonant with the cavity. The atom can cycle a few times, thereby emitting photons into the cavity, before it falls into the $|F = 3\rangle$ state. During the recycling phase the atom is cooled because the laser frequency used is the same as for the cooling scheme. The only difference here is that the atom is only cooled as long as it has not fallen into the $|F' = 3\rangle$ state. During continuous cooling this is prevented by an additional repumping laser. In figure 5.7 the cavity output is plotted as a function of time after the single-photon production has begun. For this particular trace, more than one atom is trapped in the beginning. After about 2.7 s only one atom remains, and it stays there for the next 30 s. The signal that is plotted here contains both the photons produced during the trigger interval as well as the recycling interval. Clearly, it is possible to combine single-photon production with atom cooling, as the atom stays much longer

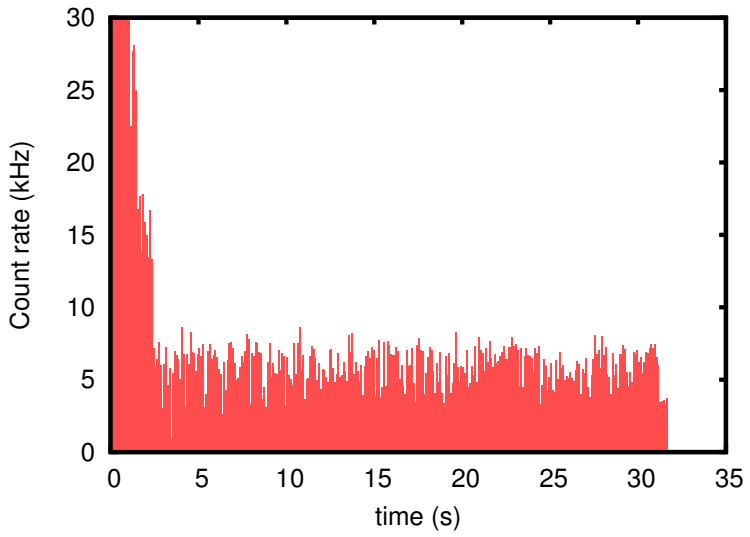

Figure 5.7: **Cavity output signal as a function of time during a photon generation run.** *A few atoms have been loaded into the standing wave dipole trap and quickly leave the cavity until one is left, which remains for another* 30 *s during which single photons are produced during the trigger pulses.*

than its lifetime in the trap when it would not be illuminated (5 s). From a dataset of 526 experimental runs the lifetime of an atom in the trap during photon production is determined to be 10.3(1) s. This lifetimes reduces to 8.3(2) s with the requirement that only one atom is trapped. The dataset contains 4397 s of single-photon production, in which 4.2×10^6 photons were detected. With a repetition rate of 100 kHz one calculates that in 0.93% of the pulses a photon is detected. 10.5% of the generated photons can be detected. This means that the photon-generation probability is 9%. The photon signal depicted in figure 5.7 can be decomposed into a histogram of the arrival time of the photon during the photon generation cycle. In the beginning of the trigger pulses the number of photons detected increases along with the linearly increasing Rabi frequency of the trigger laser but levels off near the end of the 4 μs long pulse. The rate of photons scattered during the square 4 μs-long recycling pulse is high from the start but decreases as the atom is more likely to have fallen into the $|F = 3\rangle$ state. Approximately five times more photons are detected during the recycling pulses than during trigger pulses. This ratio of 5:1 can be interpreted such that on average five photons are scattered in the cavity before the atom falls into the $|F = 3\rangle$ state. These photons do not have to have been emitted during the same pulse. If the recycling is not successful during the pulse, no single photon will be generated in the the next trigger pulse until the atom is recycled. The cooling experiments on $|F = 2\rangle \rightarrow |F' = 3\rangle$ in chapter 3 showed an average scattering rate of 5 kHz. As was mentioned the recycling phase is just a pulsed version of this, without a repumper. It does therefore not seem likely that the scattering rate during recycling is limited by an inefficient adiabatic passage during the trigger pulse, because it is not higher if a repumping laser

would be on continuously. Under the assumption of an efficient adiabatic passage, one arrives at the conclusion that the inefficiency in recycling is responsible for limiting the single photon generation efficiency to 9%. However, because the recycling is not efficient, enough photons are scattered to enable atom cooling during the recycling pulse, leading to long trapping times of an atom, leading to more single photons from the same atom. If one on the other hand does assume an efficient adiabatic passage, this would mean that either all the single photons will be generated before the end of the pulse or, in case the trigger pulse intensity is weak, the number of generated photons would still increase towards the end of the pulse. Because here the number of photons generated per time bin levels off towards the end of the pulse the assumption of an efficient adiabatic passage is not supported by the data. Both the adiabatic passage and the recycling thus play a role in the limited efficiency of the photon generation. A possible explanation is the residual motion of the atom in the dipole trap leads to time- and position-dependent shifts in both the cavity coupling g and the ac-Stark shift Δ_s. These shifts can decrease the efficiency of both photon-generation and recycling processes. To improve the efficiency in future experiments one can think about adding a third pulse after the current recycling pulse to the pulsing sequence, in which two lasers recycle the atom more efficiently via a Raman transition. In this way both long trapping times and a higher efficiency might be achieved.

In figure 5.9 the average correlation function of a trapped atom is shown. The antibunching visibility is 94%. The remaining correlations at $\Delta\tau = 0$ can be accounted for by a simple model of correlations between detected photons and background clicks.

In figure 5.10 the efficiency of photon production was investigated as a function of frequency and intensity of both trigger and recycling laser pulses. The upper left graph shows the Gaussian-shaped dependency of the photons detected during recycling on the frequency of the recycling laser. With a full width half maximum of 12 MHz this is very close to the width of the cavity resonance. One finds the same behavior for the photons in the trigger intervals, see the upper right graph. Again a Gaussian-shaped dependency on the frequency of the trigger laser is found. In the lower left graph the amount of photons in the recycling intervals is plotted as a function of the Rabi frequency of both the trigger laser and the recycling laser. In the lower right graph the same is plotted for the photons detected in the trigger interval. The shape of the plots in the lower graphs are very similar. The reason becomes clear if one remembers that photon production and recycling are directly linked in the pulsing scheme. Fewer photons during recycling leads to fewer photons during trigger pulses. From the graphs we find that we produce the most photons in the trigger interval as well as in the recycling interval if the Rabi frequency of the incoming trigger laser is chosen to be $2\pi \times 22$ MHz. Together with the reflected beam the overall Rabi frequency becomes $2\pi \times$ 32MHz. The Rabi frequency of the recycling laser is chosen to be $2\pi \times 15$ MHz which together with its reflection gives a Rabi frequency of $2\pi \times 22$ MHz. It is with these Rabi frequencies that the dataset depicted in figure 5.9 was taken.

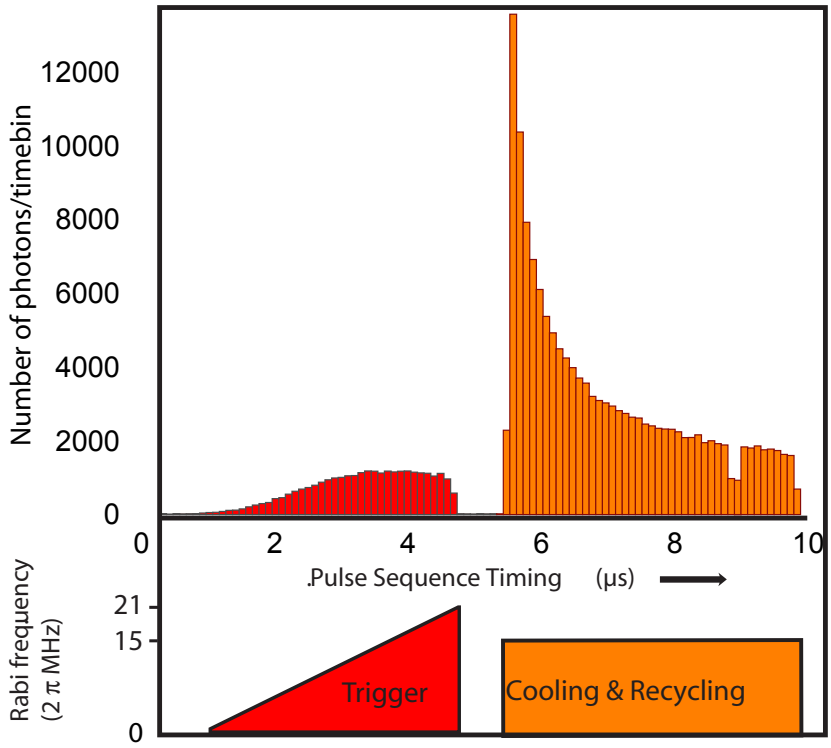

Figure 5.8: **Histogram of the arrival time of the detected photons relative to the pulse timing.** *From this plot information can be retrieved on the average response of the trapped atom on the pulses. The single photons generated during the trigger pulse can be separated from those generated during the recycling pulse. As the trigger pulse increases linearly in the Rabi frequency, this is mimicked in the increasing number of photons during the pulse interval. This increase however saturates after approximately half the* $4\,\mu s$ *pulse duration. The square recycling pulse immediately induces scattering into the cavity. The decrease in the number of scattered photons is the result of the atom falling into the* $|F = 3\rangle$ *state. Each time bin in the plot is* $0.1\,\mu s$ *long*

5.5 A Single-Photon Server with Just One Atom

A single atom trapped in a cavity can produce single photons for an extended period of time, as was shown in the previous section. The next thing to consider is how to distribute these photons for experiments. If one wants to send single photons to a user, two requirements need to be fulfilled: First, the user must be notified that single photons are available. In this case this means we need to know exactly when a single atom is trapped. Second, one must guarantee that single photons are distributed. The way to implement the two requirements is the following: After a few atoms are trapped and cooled into the dipole trap, one waits a short period while monitoring the cavity output. As soon as the output level drops to that of a single atom, the next 1.5 s the photons are used to calculate a

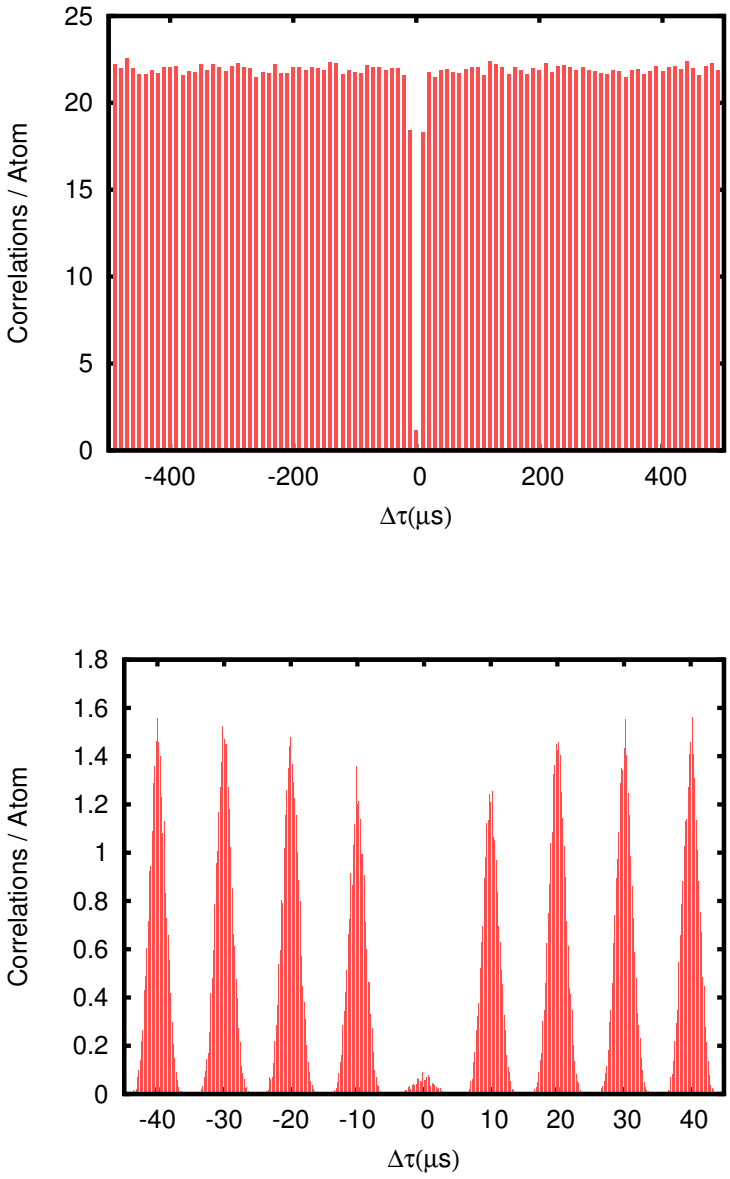

Figure 5.9: **Single atom correlation function.** *Plotted are the correlations for 454 single-atom traces between clicks of both detectors during trigger pulses as a function of the time difference between the two detections. For a single-photon emitter, no coincident detections are expected and indeed there are very few correlations for* $\Delta\tau = 0$*. Compared to the number of correlations for* $\Delta\tau \neq 0$ *the visibility of the antibunching is 94.6%, limited only by correlations with background detections. The lower graph shows the same correlation function but with a higher time resolution of* 200 *ns. The comb-like structure is the result of the pulsed nature of the experiment.*

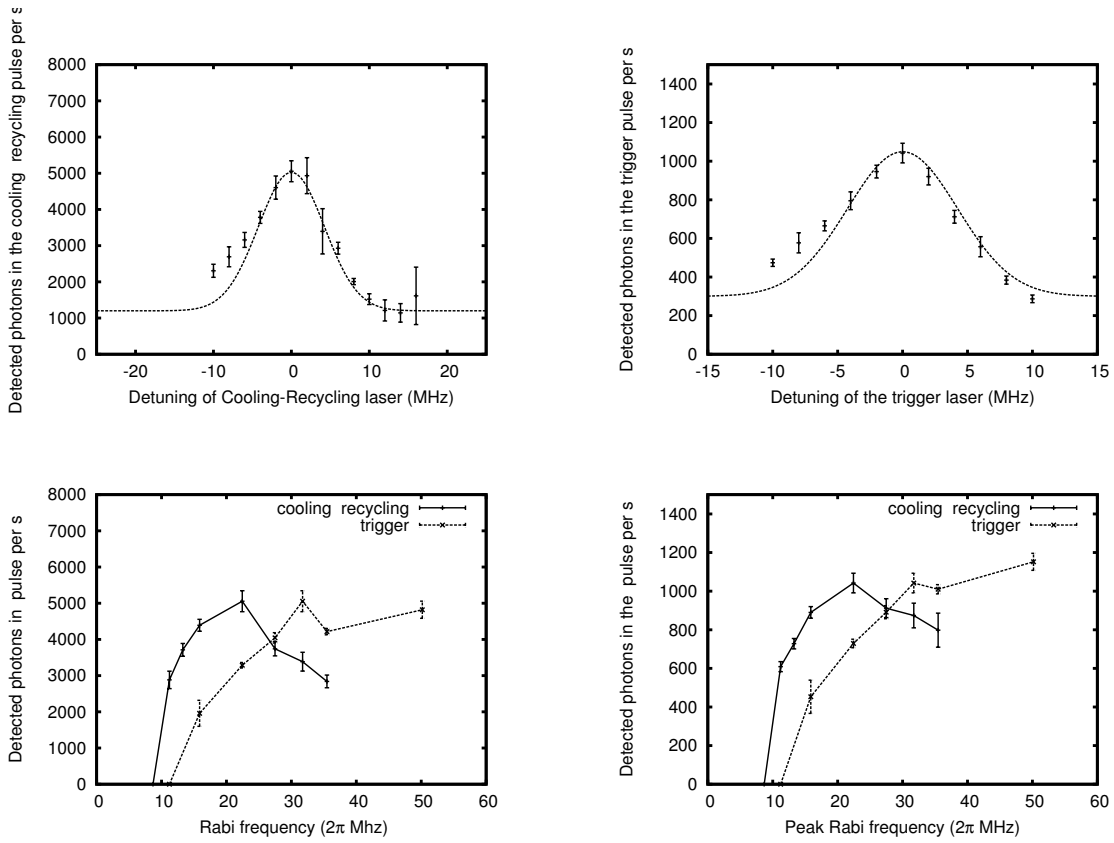

Figure 5.10: **Scan of laser frequencies and intensities.** *In the upper two graphs the frequency of the recycling laser (left) and the trigger laser (right) is scanned. Plotted in the left graph is the average number of detected photons per second during the recycling pulses as a function of the detuning of the recycling laser with respect to the cavity. On the right the same is plotted for detection during the trigger pulse as a function of the detuning of the trigger laser. In both plots a resonance with a FWHM of* $\simeq 2\kappa = 12\,MHz$ *is visible. This resonance is ascribed to the cavity. The photon yield is highest if both laser are resonant with the cavity. In the lower graphs the (peak) intensity of the recycling laser and the trigger laser is varied. Both the photons detected during the trigger pulse (right) and the recycling pulse (left) are plotted as a function of Rabi frequency. The optimal parameters are found to be a Rabi frequency of* $2\pi{\cdot}15\,MHz$ *for the recycling laser, corresponding to* $2\pi{\cdot}22\,MHz$ *in the plots due to the reflection of the beam, and a peak intensity of* $2\pi \cdot 21\,MHz$ *for the trigger pulse, corresponding to* $2\pi \cdot 30\,MHz$ *in the plots.*

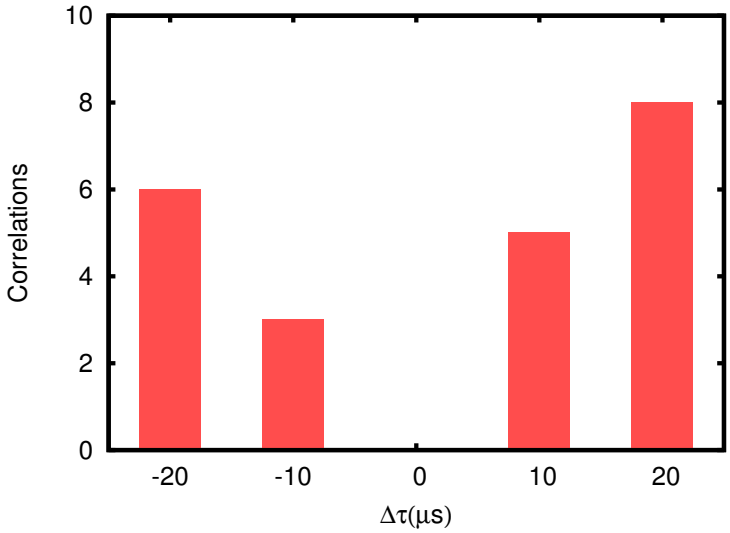

Figure 5.11: **Coincidence test after 1.5 seconds.** *The data is tested against the selection rule that after* 1.5 *s the average number of correlations for non-zero time difference must exceed 1.5, to make sure that there is a trapped atom. The correlations at* $\Delta\tau = 0$ *may not exceed 30% of this average to make sure that not more than one atom is trapped.*

correlation function as in figure 5.11, calculated from the trace in figure 5.7. If the average number of correlations for non-zero time difference is higher than 1.5 and the number of correlations at $\Delta\tau = 0$ is less than 30% of this average, the coincidence test proves that a single atom is present, and single photons are produced. For the remaining time the cavity output can be redirected to a user during trigger intervals, this redirection could for instance be implemented using an acousto-optic modulator. The photons detected during recycling can be used to check whether the atom is still there. The loss of an atom from the cavity can be detected within ~ 30 ms with 98% probability. In figure 5.12 the correlation function of the photons from the experimental run in figure 5.7 that would have been distributed is displayed. As far as is known, the results presented here are the first observation of antibunching in the light emitted by one and the same neutral atom. In other experiments one had to average over many single-atom observation intervals to collect enough data to observe the antibunching.[**???**] The observation of antibunching is a direct manifestation of the quantization of the electromagnetic field, and thus in some sense, the presented data can be considered to result from the first experiment in quantum optics with just one neutral atom.

An impression of the proposed protocol to operate the system as a single-photon server, delivering up to 300000 photons from one and the same atom, is depicted in figure 5.13. Reloading an atom after the loss is detected takes about 1.5 s. One then has to wait for $10.3 - 8.3 = 2.0$ s on average before a coincidence test can be performed. The single

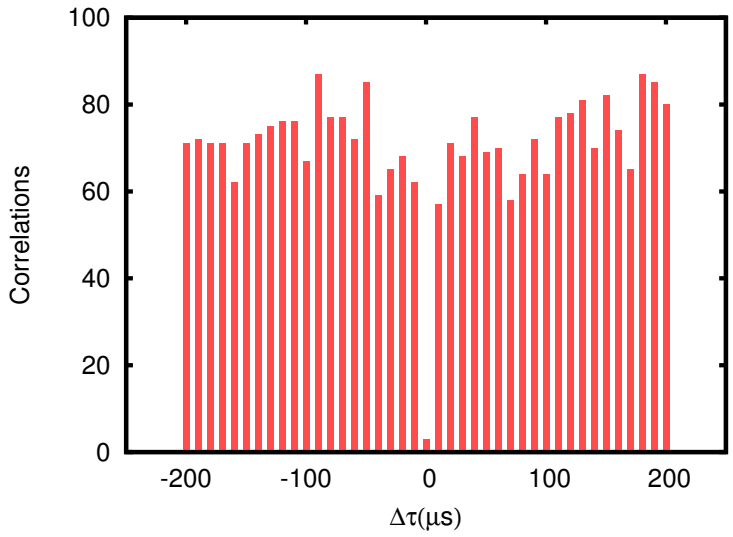

Figure 5.12: **The correlation function of 2.8×10^4 detected photons produced by one and the same atom.** *The antibunching visibility is 95.8%.*

atom is available on average after the test for $8.3 - 1.5 = 6.8\,\mathrm{s}$. A duty cycle of 58% is therefore expected for the server. Trapping times of up to 30 s have routinely been achieved, a further increase in the average trapping times is feasible with optimization of the alignment of the system, and would lead to even higher duty cycles. Of the 9×10^3 photons that are produced per second, 2×10^3 of them will be available for distribution after separation of the single photons from the 785 nm light from the cavity stabilization laser. Taking into account that a single atom is available for photon production for 58% of the time, this means that photons can be distributed at a rate of 1.2 kHz on average.

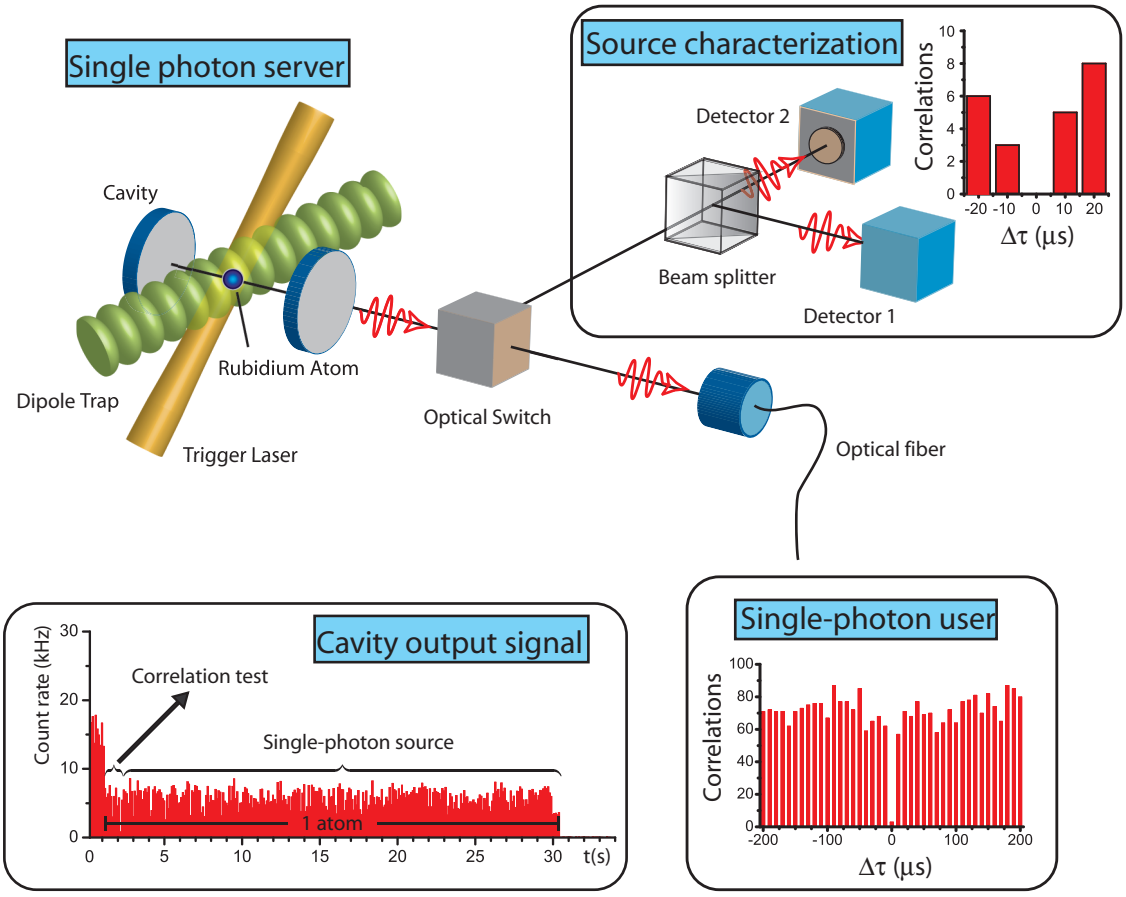

Figure 5.13: **Operation as a single-photon server.** *A few atoms are trapped and cooled in the mode of the cavity. Then, laser pulses are applied to the atoms and the photons emitted from the cavity are sent to a characterization setup. As soon as the cavity output signal drops to that of a single atom, the next* 1.5 *s of signal is used to check for coincidences between the two detectors. Only if these are not found will the cavity signal during trigger pulses be directed into a fiber for distribution of single photons to a user. The signal during recycling pulses will be sent to the characterization setup, where the loss of an atom can be detected in* 30 *ms with 98% probability. The reloading of atoms into the cavity can then be started.*

Chapter 6

Outlook

With the the presented experimental setup, a large stream of single photons can be generated from the same single atom. Experiments can now be performed that were previously performed with single photons from other sources. One of these applications is *quantum key distribution*, which relies on the fact that any measurement on a quantum system will disturb the same system. The parties that exchange the key will thus be able to detect whether eavesdropping takes place or not. Such an experiment was for instance performed with a diamond vacancy-center source. [**?**] Photons generated with an atom-cavity system have a very narrow bandwidth and the photon wave packet is expected to be Fourier-limited, making the photons highly indistinguishable. Quantum information processing experiments using single photons and linear optics rely on the interference of two photons impinging simultaneously on a beam splitter. This interference occurs if the photons are indistinguishable. Earlier experiments with single photons generated by an atom-cavity system have shown a very good visibility of this two-photon interference. [**?**] To assess the suitability of the present source, such a two-photon interference experiment could then be performed. This interference was also realized with photons from a quantum dot embedded in a semiconductor microcavity. [**?**]. The next step could then be to teleport a quantum state encoded in the paths a photon can take or create entanglement of the polarization state of the photons and test the Bell's inequalities. [**??**] These experiments would form the precursor to the implementation of quantum computing with single photons and linear optics. [**?**] Further optimization of photon production efficiency and total number of photons from the same atom will also motivate future experiments with the current system, but perhaps the real challenging and potentially rewarding experiments are those that go beyond the use of the apparatus as a single-photon generator. The results presented in this thesis constitute considerable advances in the ability to control the interaction of a single atom with the high-finesse cavity. This control is essential in the realization of schemes for entanglement of distant atoms [**?????**] or the quantum teleportation of atomic states. [**???**] In comparison to earlier experiments in our group [**???**] the new capabilities can be summarized as follows:

Long interaction times: As was demonstrated in chapter 3 the interaction time of a single atom with a cavity was increased by several orders of magnitude by trapping the atom in an independent dipole trap. Cavity cooling forces were exploited and led to trapping times of up to a minute.

Quantum protocol implementation without reducing lifetime: The application of the atom-cavity system as a single photon server in chapter 5 showcased the successful implementation of a quantum protocol in the internal states of an atom while maintaining atom-cavity interaction times longer than without excitation of the atom.

Deterministic control of atom-cavity coupling: By controlling the position of a trapped atom with a repeatability of 135 nm with respect to the cavity mode, as was done in chapter 4, the atom-cavity coupling strength could be deterministically controlled.

Individual addressability of an atom independent of the cavity: Although not fully implemented yet, the CCD images taken of single atoms and presented in section 2.8 show that the resolution of the imaging system is such that it should be possible to address a single atom by a laser beam focused through this system. With laser pulses it should then be possible to manipulate the internal atomic state of an atom without the involvement of the cavity.

Let us now have a closer look at the schemes that are suitable for implementation with the present apparatus. The first step is to entangle the internal state of an atom with the polarization state of a photon. Experiments of these kind were recently performed, using a single trapped ion [**?**], a single atom trapped in a dipole trap [**?**] and in the Rempe group with an atom falling through a cavity [**?**]. The scheme used in this last experiment is identical to the one described in figure 6.1. The entanglement scheme centers on the use of the $|F = 1\rangle \rightarrow |F' = 1\rangle$ transition to create entanglement between atom and photon. For this reason it is necessary to switch to the use of ^{87}Rb atoms. It should be possible to cool atoms with the cavity on the $|F = 2\rangle \rightarrow |F' = 3\rangle$ transition. This is the closed transition used for the magneto-optical trap with ^{87}Rb, and cavity cooling is thus expected to be similar to cavity cooling on $|F = 3\rangle \rightarrow |F' = 4\rangle$ in ^{85}Rb. The scheme starts with the preparation of an atom in the state $|F = 2, m_F = 0\rangle$. The atom is transferred into the $|F = 1\rangle$ state in a vacuum-stimulated Raman adiabatic passage by a π-polarized laser beam which is resonant with the transition $|F = 2\rangle \rightarrow |F' = 1\rangle$, and incident perpendicular to the cavity axis. The cavity only couples to transitions with Δm=$\pm$1, the atom decays either into the $m_F = -1$ state by emitting a σ^+-photon or by emitting a σ^--photon and decaying into the $m_F = +1$ state. In this way the emitted photon is entangled with the atomic state. The entangled state can be probed by a measurement on the photon and on the internal state of the atom. If now two atom-cavity systems, referred to as Alice and Bob, independently generate an entangled atom-photon pair, Alice and Bob's atoms can be entangled by a projective measurement on both photons. This is successful in 50% of the cases. This state can then be probed by measuring the internal state of both atoms. A slight change in the entanglement protocol allows for the teleportation of a quantum state , see the lower left box [**?**]: The main difference is that now Alice maps her atomic quantum state $|\Phi\rangle = \alpha|\mathrm{F}{=}1,\mathrm{m}_f = 1\rangle + \beta|\mathrm{F}{=}1,\mathrm{m}_f = -1\rangle$ onto the polarization state of a photon

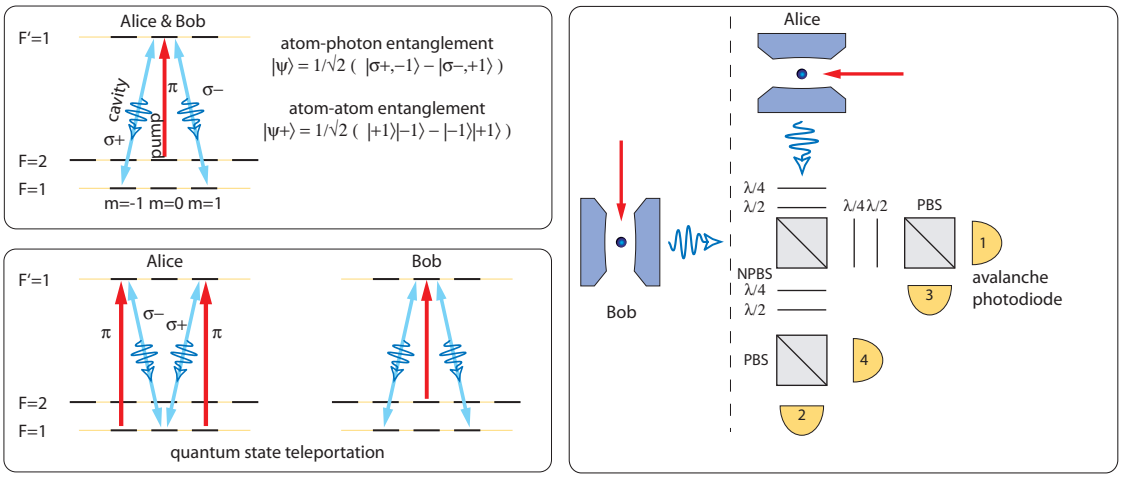

Figure 6.1: **Schemes for atom-atom entanglement and quantum state teleportation.** *The upper left box depicts the energy levels of* ^{87}*Rb involved in the entanglement scheme. First the atoms in Alice and Bob's cavities are entangled with the polarization state of a photon. By detecting the photons by 4 avalanche photodiodes in the configuration as shown in the right box, the two atoms can be entangled. The lower left box shows a similar scheme for the teleportation of a quantum state. Here Alice maps the internal state of the atom onto a photon. By overlapping this photon with a photon which is maximally entangled with Bob's atom, Bob's atom collapses into Alice's original state upon proper detection of both photons. In some of the cases Bob needs to perform a unitary operation on the atom based on the outcome of the photon detection. This information is sent to him via a classical channel.*

by applying a π-polarized laser pulse resonant with $|F = 1\rangle \rightarrow |F' = 1\rangle$. Bob creates a maximally entangled atom-photon pair in the same manner as in the entanglement scheme. Correlations in the photon detections signal the collapse of Bob's atom into the state Alice began with. In 50% of the attempts, teleportation is successful, where in half of those successful attempts a local unitary operation on Bob's atom is necessary to arrive at the correct state. The necessity of this operation depends on which detectors detected a photon. This information is sent to Bob via a classical channel.

The presented atom-atom entanglement scheme as well as the teleportation scheme both require two cavity systems. A second cavity system is now being constructed in the group of Professor Rempe at the MPQ. Its design is based on the apparatus with which the experiments in this thesis were performed. The schemes require the simultaneous emission of a photon from each cavity. A high success rate for these experiments therefore depends on the efficiency with which the atom-photon interface works as well as on the availability of an atom in both setups at the same time. It is here that the above-listed improved capabilities come into play. The long interaction time increases the probability that atoms are present simultaneously in both cavities. If one assumes that photons that are entangled with the internal state of the atom can be produced with the same rate

with which photons are currently, both systems would distribute these photons at a rate of 1.2 kHz, see section 5.5. With the probability of 1.2% to have a photon in a pulse at a repetition rate of 100 kHz, this would lead to 14 pulses per second where two photons arrive at the beam splitter simultaneously. (Neglecting any further propagation losses) In 50% of these, entanglement between the atoms is created. The number of coincidences can be increased substantially if the photon generation efficiency can be improved. Through the addressability of the atom by controlling its position with respect to the cavity or by manipulating and detecting the internal state through the imaging system, the local operations on the atoms that are required by the schemes can be performed.

It is just a matter of time and hard work before the photon-mediated entanglement of two massive particles separated over a macroscopic distance can be observed for the first time.

Appendix A

Rb transition strengths

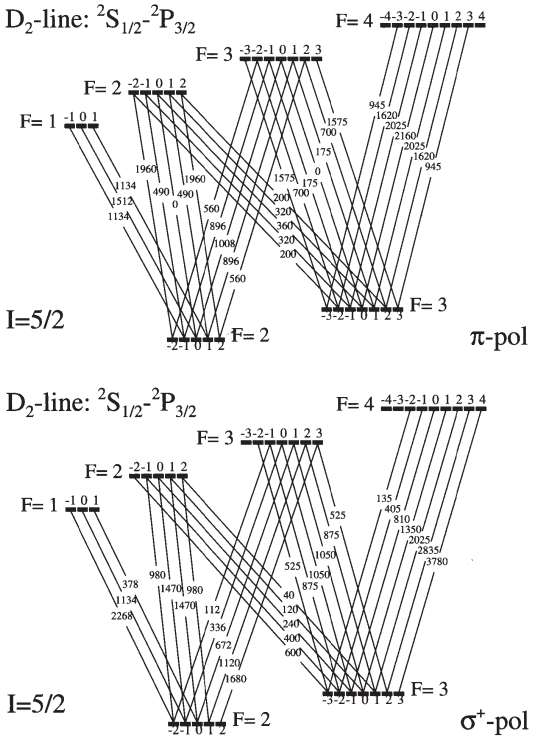

Figure A.1: *The relative transition strengths of the D_2-line of ^{85}Rb. The figure is taken from the book* Laser cooling and trapping **?**

The dipole matrix element is given by $\mu_{ij}^2 = \mathrm{C}_{ij} \times 1,67 \cdot 10^{-61}\mathrm{C}^2\mathrm{m}^2$, with C_{ij} the relative strength of the transition taken from the diagram.

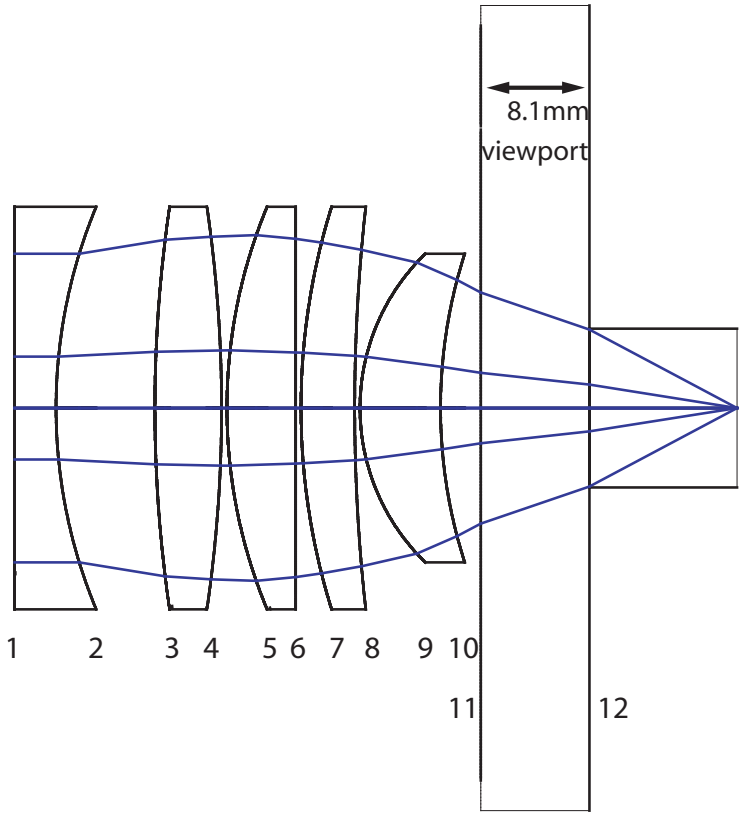
8.1mm
viewport
1
2
3
4
5
6
7
8
9
10
11
12

Appendix B

Lens data

Plane	Type	Radius [mm]	Thickness[mm]
1	plane-	∞	3.08
2	concave(BK7)	39.1018	7.37
3	bi-	103.29	4.97
4	convex (BK7)	-103.29	0.40
5	convex-	39.1018	5.12
6	plane (BK7)	∞	0.40
7	convex-	50.4863	4.00
8	concave (BK7)	136.752	0.40
9	convex-	16.0241	6.00
10	concav (BK7)	37.579	2.99
11	View-	∞	8.1
12	port (Fused Silica)	∞	

Bibliography

R. Alléaume, F. Treussart, G. Messin, Y. Dumeige, J-F. Roch, A. Beveratos, R. Brouri-Tualle, J-P. Poizat, and P. Grangier. Experimental open-air quantum key distribution with a single-photon source. *New Journal of Physics*, **6**, 92 (2004).

A. Ashkin. Trapping of atoms by resonance radiation pressure. *Phys. Rev. Lett.*, **40**, 729 (1978).

Eric D. Black. An introduction to pound-drever-hall laser frequency stabilization. *American Journal of Physics*, **69**, 79–87 (2001).

B. B. Blinov, D. L. Moehring, L.-M. Duan, and C. Monroe. Observation of entanglement between a single trapped atom and a single photon. *Nature*, **428**, 153–157 (2004).

N. Bloembergen and R.V. Pound. Radiative damping in magnetic resonance experiments. *Phys. Rev.*, **95**, 8 – 12 (1954).

S. Bose, P. L. Knight, M. B. Plenio, and V. Vedral. Proposal for Teleportation of an Atomic State Via Cavity Decay. *Phys. Rev. Lett.*, **83**, 5158–5161 (1999).

Jaeyoon Cho and Hai-Woong Lee. Quantum teleportation with atoms trapped in cavities. *Phys. Rev. A*, **70**, 034305 (2004).

J. I. Cirac and P. Zoller. Quantum Computations with Cold Trapped Ions. *Phys. Rev. Lett.*, **74**, 4091 (1995).

J. I. Cirac, P. Zoller, H. J. Kimble, and H. Mabuchi. Quantum state transfer and entanglement distribution among distant nodes in a quantum network. *Phys. Rev. Lett.*, **78**, 3221–3224 (1997).

J. Dalibard and C. Cohen-Tannoudji. Dressed-Atom Approach to Atomic Motion in Laser Light: The Dipole Force Revisited. *J. Opt. Soc. Am. B*, **2**, 1707 (1985).

J. Dalibard and C. Cohen-Tannoudji. Laser cooling below the Doppler limit by polarization gradients: simple theoretical models. *J. Opt. Soc. Am. B*, **6**, 2023–2045 (1989).

B. Darquié, M. P. A. Jones, J. Dingjan, J. Beugnon, S. Bergamini, Y. Sortais, G. Messin, A. Browaeys, and P. Grangier. Controlled single-photon emission from a single trapped two-level atom. *Science*, **309**, 454–456 (2005).

D. P. DiVincenzo. The Physical Implementation of Quantum Computation. *Fortschr. Phys.*, **48**, 771 (2000).

L.-M. Duan, A. Kuzmich, and H. J. Kimble. Cavity qed and quantum-information processing with "hot" trapped atoms. *Physical Review A (Atomic, Molecular, and Optical Physics)*, **67**, 032305 (2003).

Einstein. On the quantum theory of radiation. *Physikalische Zeitschrift*, **18**, 121–128 (1917).

P.M. Farrell and W. R. MacGillivray. On the consistency of rabi frequency calculations. *J. Phys. A*, **28**, 209–221 (1995).

D. Fattal, E. Diamanti, K. Inoue, and Y. Yamamoto. Quantum teleportation with a quantum dot single photon source. *Phys. Rev. Lett.*, **92**, 037904 (2004a).

D. Fattal, K. Inoue, J. Vučković, G. S. Solomon, and Y. Yamamoto. Entanglement formation and violation of Bells inequality with a semiconductor single photon source. *Phys. Rev. Lett.*, **92**, 037903 (2004b).

X.-L. Feng, Z.-M. Zhang, X.-D. Li, S.-Q. Gong, and Z.-Z. Xu. Entangling distant atoms by interference of polarized photons. *Phys. Rev. Lett.*, **90**, 217902 (2003).

T. Fischer, P. Maunz, P. W. H. Pinkse, T. Puppe, and G. Rempe. Feedback on the motion of a single atom in an optical cavity. *Phys. Rev. Lett.*, **88**, 163002 (2002).

M. Fleischhauer, S.F. Yelin, and M.D. Lukin. How to trap photons? Storing single-photon quantum states in collective atomic excitations. *Opt. Comm.*, **179**, 395–410 (2000).

J.P. Gordon, H.J. Zeigler, and C.H. Townes. Molecular Microwave Oscillator and New Hyperfine Structure in the Microwave Spectrum of NH3. *Phys. Rev.*, **95**, 282 (1954).

R. Grimm, M. Weidemuller, and Y. B. Ovchinnikov. Optical dipole traps for neutral atoms. *Adv. At. Mol. Opt. Phys.*, **42**, 95–170 (2000).

M. Hennrich. *Kontrollierte Erzeugung einzelner Photonen in einem optischen Resonator hoher Finesse*. Dissertation, Max-Planck-Institut für Quantenoptik und Technische Universität München (2003).

M. Hennrich, T. Legero, A. Kuhn, and G. Rempe. Vacuum-Stimulated Raman Scattering Based on Adiabatic Passage in a High-Finesse Optical Cavity. *Phys. Rev. Lett.*, **85**, 4872–4875 (2000).

M. Hijlkema, B. Weber, H.P. Specht, S.C. Webster, A. Kuhn, and G. Rempe. A single-photon server with just one atom. *Nature Physics*, **3**, 253–255 (2007).

E.A. Hinds. pertubative cavity quantum electrodynamics. In P. Berman, editor, *Supplement 2 to Advances in Atomic, Molecular and Optical Physics*, pages 1–56. New York: academic (1994).

J. Hong and H.-W. Lee. Quasideterministic generation of entangled atoms in cavities. *Phys. Rev. Lett.*, **89**, 237901 (2002).

C. J. Hood, M. S. Chapman, T. W. Lynn, and H. J. Kimble. Real-time cavity QED with single atoms. *Phys. Rev. Lett.*, **80**, 4157 (1998).

C. J. Hood and H. J. Kimble. Characterization of high-finesse mirrors: Loss, phase shifts, and mode structure in an optical cavity. *Phys. Rev. A*, **64**, 033804 (2001).

E. T. Jaynes and F. W. Cummings. Comparison of Quantum and Semiclassical Radiation Theories with Application to the Beam Maser. *Proc. IEEE*, **51**, 89–109 (1963).

M. Keller, B. Lange, K. Hayasaka, W. Lange, and H. Walther. Continuous generation of single photons with controlled waveform in an ion-trap cavity system. *Nature*, **431**, 1075–1078 (2004).

H. J. Kimble, M. Dagenais, and L. Mandel. Photon Antibunching in Resonance Fluorescence. *Phys. Rev. Lett.*, **39**, 691 – 695 (1977).

C. Klempt, T. van Zoest, T. Henninger, O. Topic, E. Rasel, W. Ertmer, and J. Arlt. Ultraviolet light-induced atom desorption for large rubidium and potassium magneto-optical traps. *Phys. Rev. A*, **73**, 013410 (2006).

E. Knill, R. Laflamme, and G. J. Milburn. A scheme for efficient quantum computing with linear optics. *Nature*, **409**, 46–52 (2001).

A. Kuhn, M. Hennrich, T. Bondo, and G. Rempe. Controlled generation of single photons from a strongly coupled atom-cavity system. *Appl. Phys. B*, **69**, 373–377 (1999).

A. Kuhn, M. Hennrich, and G. Rempe. Deterministic single-photon source for distributed quantum networking. *Phys. Rev. Lett.*, **89**, 067901 (2002).

A. Kuhn and G. Rempe. Optical Cavity QED: Fundamentals and application as a Single-Photon Light Source. *Proceedings of the Varenna School on 'Experimental Quantum Information'* (2001).

S. Kuhr, W. Alt, D. Schrader, M. Müller, V. Gomer, and D. Meschede. Deterministic Delivery of a Single Atom. *Science*, **293**, 278–280 (2001).

T. Legero, T. Wilk, M. Hennrich, G. Rempe, and A. Kuhn. Quantum beat of two single photons. *Phys. Rev. Lett.*, **93**, 070503 (2004).

H. Mabuchi, Q. A. Turchette, M. S. Chapman, and H. J. Kimble. Real-Time Detection of Individual Atoms Falling Through a High-Finesse Optical Cavity. *Optics Lett.*, **21**, 1393 (1996).

C. Marr, A. Beige, and G. Rempe. Entangled state preparation via dissipation-assisted adiabatic passages. *Phys. Rev. A*, **68**, 033817 (2003).

P. Maunz, T. Puppe, I. Schuster, N. Syassen, P. W. H. Pinkse, and G. Rempe. Cavity cooling of a single atom. *Nature*, **428**, 50–52 (2004).

J. McKeever, A. Boca, A. D. Boozer, R. Miller, J. R. Buck, A. Kuzmich, and H. J. Kimble. Deterministic generation of single photons from one atom trapped in a cavity. *Science*, **303**, 1992 – 1994 (2004).

J. McKeever, J. R. Buck, A. D. Boozer, A. Kuzmich, H.-C. Nagerl, D. M. Stamper-Kurn, and H. J. Kimble. State-insensitive cooling and trapping of single atoms in an optical cavity. *Phys. Rev. Lett.*, **90**, 133602 (2003).

H. J. Metcalf and P. van der Straten. *Laser Cooling and Trapping*. Springer, New York (1999).

P. Meystre and M. Sargent. *Elements of Quantum Optics*. Springer, third edition (1999).

T. W. Mossberg, M. Lewenstein, and D. J. Gauthier. Trapping and cooling of atoms in a vacuum perturbed in a frequency-dependent manner. *Phys. Rev. Lett.*, **67**, 1723–1726 (1991).

P. Münstermann, T. Fischer, P. Maunz, P. W. H. Pinkse, and G. Rempe. Dynamics of Single-Atom Motion Observed in a High-Finesse Cavity. *Phys. Rev. Lett.*, **82**, 3791–3794 (1999).

K. Murr. Large velocity capture range and low temperatures with cavities. *Phys. Rev. Lett.*, **96**, 253001 (2006).

K. Murr, S. Nußmann, T. Puppe, M. Hijlkema, B. Weber, S. C. Webster, A. Kuhn, and G. Rempe. Three-dimensional cavity cooling and trapping in an optical lattice. *Phys. Rev. A.*, **73**, 063415 (2006).

S. Nußmann, M. Hijlkema, B. Weber, F. Rohde, G. Rempe, and A. Kuhn. Submicron positioning of single atoms in a microcavity. *Phys. Rev. Lett.*, **95**, 173602 (2005a).

S. Nußmann, K. Murr, M. Hijlkema, B. Weber, A. Kuhn, and G. Rempe. Vacuum-stimulated cooling of single atoms in three dimensions. *Nature Physics*, **1**, 122–125 (2005b).

Stefan Nußmann. *Kühlen und Positionieren eines Atoms in einem Resonator*. Dissertation, Technische Universität München (2006).

T. Pellizzari, S. A. Gardiner, J. I. Cirac, and P. Zoller. Decoherence, Continuous Observation, and Quantum Computing: A Cavity QED Model. *Phys. Rev. Lett.*, **75**, 3788–3791 (1995).

P. W. H. Pinkse, T. Fischer, P. Maunz, and G. Rempe. Trapping an Atom with Single Photons. *Nature*, **404**, 365–368 (2000).

M. B. Plenio, S. F. Huelga, A. Beige, and P. Knight. Cavity-loss-induced generation of entangled atoms. *Phys. Rev. A*, **59**, 2468–2575 (1999).

E. M. Purcell. Spontaneous Emission Probabilities at Radio Frequencies. *Phys. Rev.*, **69**, 681 (1946).

E. Raab, M. Prentiss, A. Cable, S. Chu, and D. E. Pritchard. Trapping of Neutral Sodium Atoms with Radiation Pressure. *Phys. Rev. Lett.*, **59**, 2631 (1987).

G. Rempe, R. J. Thompson, R. J. Brecha, W. D. Lee, and H. J. Kimble. Optical Bistability and Photon Statistics in Cavity Quantum Electrodynamics. *Phys. Rev. Lett.*, **67**, 1727–1730 (1991).

F. Rohde. *Ein optischer Resonator hoher Finesse als Atomdetektor*. Diplomathesis, Max-Planck-Institut für Quantenoptik und Technische Universität München (2003).

C. Santori, D. Fattal, J. Vučković, G. S. Solomon, and Y. Yamamoto. Indistinguishable photons from a single-photon device. *Nature*, **419**, 594 – 597 (2002).

A. S. Sorensen and K. Molmer. Probabilistic generation of entanglement in optical cavities. *Phys. Rev. Lett.*, **90**, 127903 (2003).

R. Taïeb, R. Dum, J. I. Cirac, P. Marte, and P. Zoller. Cooling and localization of atoms in laser-induced potential wells. *Phys. Rev. A*, **49**, 4876–4887 (1994).

J. Volz, M. Weber, D. Schlenk, W. Rosenfeld, J.Vrana, K. Saucke, C. Kurtsiefer, and H. Weinfurter. Observation of entanglement of a single photon with a trapped atom. *Physical Review Letters*, **96**, 030404 (2006).

H. Walther, B.T.H. Varcoe, B. Englert, and T Becker. Cavity quantum electrodynamics. *Rep. Prog. Phys.*, **69**, 325 – 5382 (2006).

B. Weber. *Transport von Atomen in einer optischen Dipolfalle*. Diplomathesis, Max-Planck-Institut für Quantenoptik und Technische Universität München (2002).

T. Wilk, S. C. Webster, A. Kuhn, and G. Rempe. *Private Communication* (2007a).

T. Wilk, S. C. Webster, H. P. Specht, A. Kuhn, and G. Rempe. Polarization-controlled single photons. *Phys. Rev. Lett.*, **98**, 063601 (2007b).

Publications

- M. Hijlkema, B. Weber, H.P. Specht, S.C. Webster, A. Kuhn and G. Rempe,
  A Single-Photon Server with Just One Atom,
  Nature Physics **3** 253-255 (2007).

- K. Murr, S. Nußmann, T. Puppe, M. Hijlkema, B. Weber, S.C. Webster, A. Kuhn, and G. Rempe,
  Three-dimensional cavity cooling and trapping in an optical lattice. *Phys. Rev. A.*, **73**, 063415 (2006).

- S. Nußmann, K. Murr, M. Hijlkema, B. Weber, A. Kuhn and G. Rempe,
  Vacuum-stimulated cooling of single atoms in three dimensions,
  Nature Physics **1**, 122-125 (2005).

- S. Nußmann, M. Hijlkema, B. Weber, F. Rohde , G. Rempe and A. Kuhn,
  Submicron Positioning of Single Atoms in a Microcavity,
  Physical Review Letters, **95**, 173602 (2005).

Acknowledgments

The thesis in front of you is the result of more than five years spent at the Max-Planck-institute of quantum optics. I've enjoyed the close-knitted friendly atmosphere in the group, which has been one of its main attractions from the day I started my PhD. I am much indebted to all my past and present colleagues for teaching me so many things and creating a stimulating environment to work in. I would like to start by thanking Gerhard Rempe for giving me the opportunity to do my PhD-research in his group. Thanks for letting us do our own thing while at the same time making sure we were still on the right track. I would like to thank Axel Kuhn for his supervision of our experiment. A visit to your office was always useful if I had a problem or a question.

The complexity of the experiments I was involved in always required solid teamwork to pull it off. I was therefore lucky to have such great team members. Even before I started, Stefan Nußmann had already designed the experimental apparatus. I would like to thank you for making the right choices, leading to a very successful setup. Your guidance helped me learn all about experimental quantum optics, and your perseverance set an example for me to follow. Bernard Weber also has been my colleague from day one. I thank you for your advice on many things and your valuable work in the laboratory. I envy your ability to summarize difficult issues in just a few sentences. Holger Specht joined the team later, and he brought a curiosity for technology with him that was very inspiring. Thank you for your invigorating enthusiasm. Felix Rohde built the heart of our experiment during his diploma thesis. Thank you for assembling the cavity and for the laughs we had. I would also like to thank Simon Webster for his contributions in the lab and Tobias Müeller for proof-reading this thesis. Karim Murr always showed a great interest in my work and he made a vital contribution to our understanding of cavity cooling. Thank you for your opinion on all kinds of matters, Karim.

As we started our experiment we learned a lot from the Pistoleros, our sister-experiment. I am very grateful to Markus Hennrich, Thomas legero, Tatiana Wilk, Stefan Kudera and Patrizia Krok. Also I'd like to thank Jörg Bochman, Gunnar Langfahl,Christoph Erbel and Martin Mücke of the new Pistoleros generation who are setting up the new experiment.

The Molekülis, Tobias Junglen, Thomas Rieger, Sadiq Rangwala, Patrick Windpassinger, Michael Motsch, Martin Zeppenfeld, Laurens van Buuren, Markus Schenk, Christian Sommer and Sebastian Pohle deserve thanks for the daily exchange of niceties and not-so-niceties across the curtain that separate our labs.

The Cavies, Peter Maunz, Thomas Puppe, Ingrid Schuster, Alexander Kubanek, Alex Grothe and Johannes Almer were very helpful with their computer wizardry and their expertise on sophisticated measurements.

The coolest place in Germany was as always in the lab of the BEC guys, Johannes Schuster, Andreas Marte, Stephan Dürr, Thomas Volz, Niels Syassen, Dominik Bauer, Sebastian Ernst, Sven Teichmann, Eberhard Hansis, Matthias Lettner and Daniel Dietze. Thank you guys.

The technical support in the Rempe group is world class, and I have Josef Bayerl, Franz Denk, Helmuth Stehbeck and Thomas Wiesmeier to thank for that. Odette Gori was always very helpful with organizational matters.

I would like to thank Pepijn Pinkse, not only for his advice, but also for the 'Dutch connection'. We Dutchmen have to stick together. Thomas Rieger and Stephan Dürr introduced me to the wonderful world of rock climbing, and took me along on many trips, for which I am very grateful. Markus Hennrich and Niels Syassen were always up for running a lap or two, thanks a lot.

And finally, I would like to thank my parents, for all their support these years. Thank you mom and dad.